AIR DISPERSION STUDY
AND AIR QUALITY EVALUATION

LD CELULOSE - INDIANÓPOLIS MG

Consultoria Ambiental Especializada e Laboratório Acreditado ISO/IEC 17.025 CRL 1151

Prepared for:

Prepared in:

18/06/2018

www.lentzmeioambiente.com.br
Fone/Fax: (11) 3853-2138
lentz@lentzmeioambiente.com.br
Rua Álvaro Luís Roberto Assumpção, 431, São Paulo/SP – 04618-020

REVISION	DATA	REVIEW DESCRIPTION	PREPARED BY:	REVIEWED BY:	APPROVED BY:
00	06/18/2018	Original Document	Daniel Zacharias	George Lentz	George Lentz
01	06/25/2018	Reviewed on Celso Tomio Tsutsumi request	George Lentz	George Lentz	George Lentz
02	07/04/2018	Changes in ERT re-simulation figures 1h. Reviewed on request Celso Tomio Tsutsumi	Daniel Zacharias	Daniel Zacharias	George Lentz
03	07/12/2018	Reviewed on Celso Tomio Tsutsumi request	George Lentz	George Lentz	George Lentz

SUMMARY

FIGURE LIST

TABLE LIST

LIST OF ABBREVIATIONS AND SYMBOLS

CO: Carbon monoxide

CONAMA: National Council for the Environment

ERT: Reduced total súlfur

NO_2: Nitrogen dioxide

NO_X: Nitrogen oxides, expressed in terms of NO_2

PTS: Total Suspended Particles

SO_2: Sulfur dioxide

SO_X: Oxides of sulfur, expressed in terms of SO_2

1 OBJECTIVE

The objective of this Atmospheric Dispersion Study - EDA is to predict the changes in air quality caused by the air pollutants emitted by the LD Celulose unit to be installed in the city of Indianópolis and Araguari, MG.

The present study was prepared according to the requirements of the technical note: "TECHNICAL GUIDELINES FOR THE PREPARATION OF AN ATMOSPHERIC DISPERSION STUDY", elaborated by FEAM (State Foundation for the Environment).

The results of the simulations were compared with the respective standards determined in CONAMA Resolution 03/1990.

2 INTRODUCTION

The Atmospheric Dispersion Study (EDA) has great importance in air quality assessment, simulating the emissions of the enterprise and allowing to identify the size of the affected area.

The study allows the understanding of atmospheric conditions in each treated scenario, to assist in the establishment of preventive and / or mitigation actions when necessary, besides complying with the requirements of the legislation demonstrating commitment with respect to the environmental aspects.

2.1 Atmospheric Dispersion Computational Model

Mathematical modeling is an important tool to evaluate the concentration of pollutants in the atmosphere emitted by stationary sources. This model allows the contributions of certain sources to be analyzed in the final result of the air quality.

The model used in this study is one of the tools and / or criteria recommended by the environmental control agencies at national and international level.

In 1991, the American Meteorological Society (AMS) and the U.S. Environmental Protection Agency (EPA) began a formal collaboration aimed at introducing the most current concepts of planetary boundary layer (CLP) in atmospheric dispersion regulatory models. A working group (AMS / EPA Regulatory Improvement Committee, AERMIC) was formed with researchers from both institutions to develop a model that would meet this goal.

The EPA regulatory platform for near field modeling during the previous 25 years remained, with few exceptions, fundamentally unchanged, with ISC3 being the main model used, because of this, the AERMIC's goal was to develop a new model that would completely replace the ISC3.

On April 21, 2000, the EPA proposed the adoption of AERMOD as a replacement for ISC3 in Appendix A of the Guideline on Air Quality Models. The current version of the AERMOD has been revised and incorporated the PRIME algorithms for downwash estimation.

AERMOD (v16216r) is a Gaussian plume model that considers the concentrations obtained for all distances as averages of the time simulations. This type of model presents good results for studies whose objective is to obtain a spatial pollution distribution instead of punctual results in space and time.

In the stable boundary layer (CLE) the concentration distribution is assumed to be Gaussian both horizontally and vertically. In the convective boundary layer (CLC) the horizontal distribution is assumed to be Gaussian, while in the vertical the distribution is described with a bi-Gaussian probability density function.

In general, the AERMOD model is the combination of two cases: A horizontal plume impacting the ground and a plume that accompanies the terrain. For all situations, the total concentration per recipient is the weighted sum of these two situations (Figure 1). These two plumes are separated by a critical current line of height H_C (Figure 2).

The general concentration equation is applied under stable or convective atmospheric conditions and is given by:

$$C_T\{x_r, y_r, z_r\} = f \cdot C_{c,s}\{x_r, y_r, z_r\} + (1 - f) C_{c,s}\{x_r, y_r, z_p\}$$

Where: $C_T\{x_r,y_r,z_r\}$ is the total concentration, $C_{c,s}\{x_r,y_r,z_r\}$ is the contribution of the horizontal plume (c and s refer to the convective and stable conditions, respectively), $C_{c,s}\{x_r,y_r,z_p\}$ is the contribution of the feather that accompanies the terrain, f is the weight of the horizontal plume, {xr, yr, zr} are the coordinates of the receiver (with zr defined relative to the height of the base of the source and zp is the height of the receiver above of the local ground height). It is important to note that calculation of concentration all heights (z) refers to the elevation of the base of the source.

The weight factor of the pen state is given by $f = 0.5 (1 + \varphi_p)$. When the plume concentrates entirely below the HC ($\varphi_p = 1$), the concentration is determined only by the horizontal plume. When it is entirely above the HC ($\varphi_p = 0$), the contribution weight of each of the two states is the same. In flatland simulations, the contribution of each of the two plumes will be the same (Figure 2).

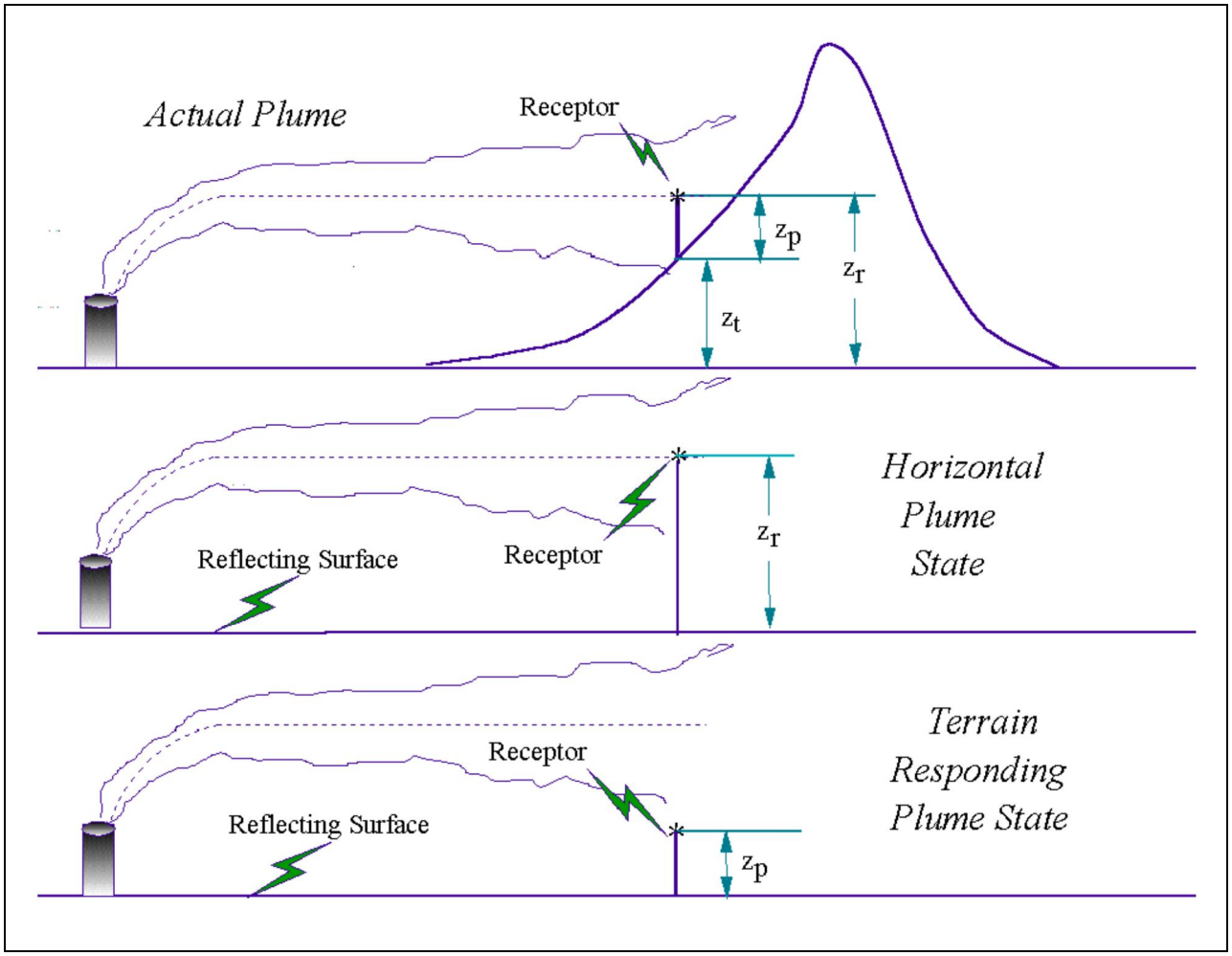

Figure 1: Two-stage analysis system. The total concentration is given by a weighted sum of the two possible extreme states of the boom.

Source: https://www3.epa.gov/ttn/scram/models/aermod/aermod_userguide.pdf (access: 04/11/2018)

The AERMOD simulates five different types of boom depending on the atmospheric stability and the location of the boom in the boundary layer: Direct, Indirect, Penetrated, Injected and Stable.

In convective conditions, the horizontal distribution is Gaussian, and the vertical distribution is the combination of three types of plume: Direct (the plume is within the mixing layer but does not interact with the top of the layer), Indirect (the plume is in of the blend layer, starts to rise and tends to spread close to the top of the blend layer) and Penetrada (the feather escapes from the blend layer, penetrates into a higher stable layer and floats therein). The AERMOD can also simulate in special situations a plume injected directly into the stable layers of the atmosphere by a point source whose

emission height is greater than the height of the blend layer at that time. Injection sources are simulated as feathers under stable conditions, however the influence of turbulence and winds within the blend layer is considered in the calculation of heterogeneity as the passage of the feather through the blend layer until reaching the receivers.

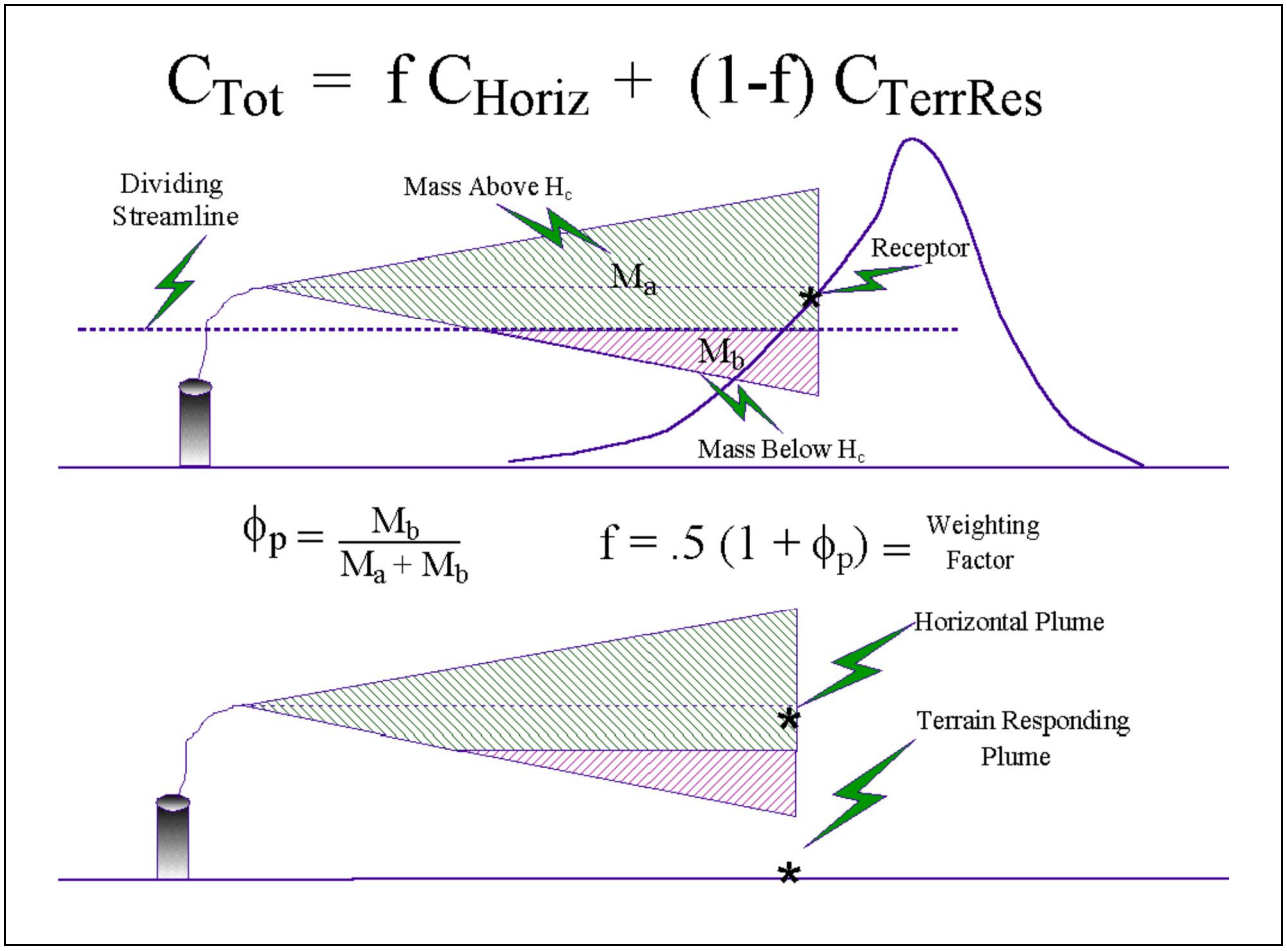

Figure 2: Treatment of the ground in the AERMOD. Determination of the weight factor used in the calculation of the total concentration.

Source: https://www3.epa.gov/ttn/scram/models/aermod/aermod_userguide.pdf (access: 11/04/2018)

In AERMOD, the dispersion formulation for the convective boundary layer (CLC) represents one of the most significant advances in comparison to existing regulatory models. It assumes that sectors of the plume are emitted in sequence and that move according to the wind, traversing a sequence of ascending and descending convective elements (Figure 3).

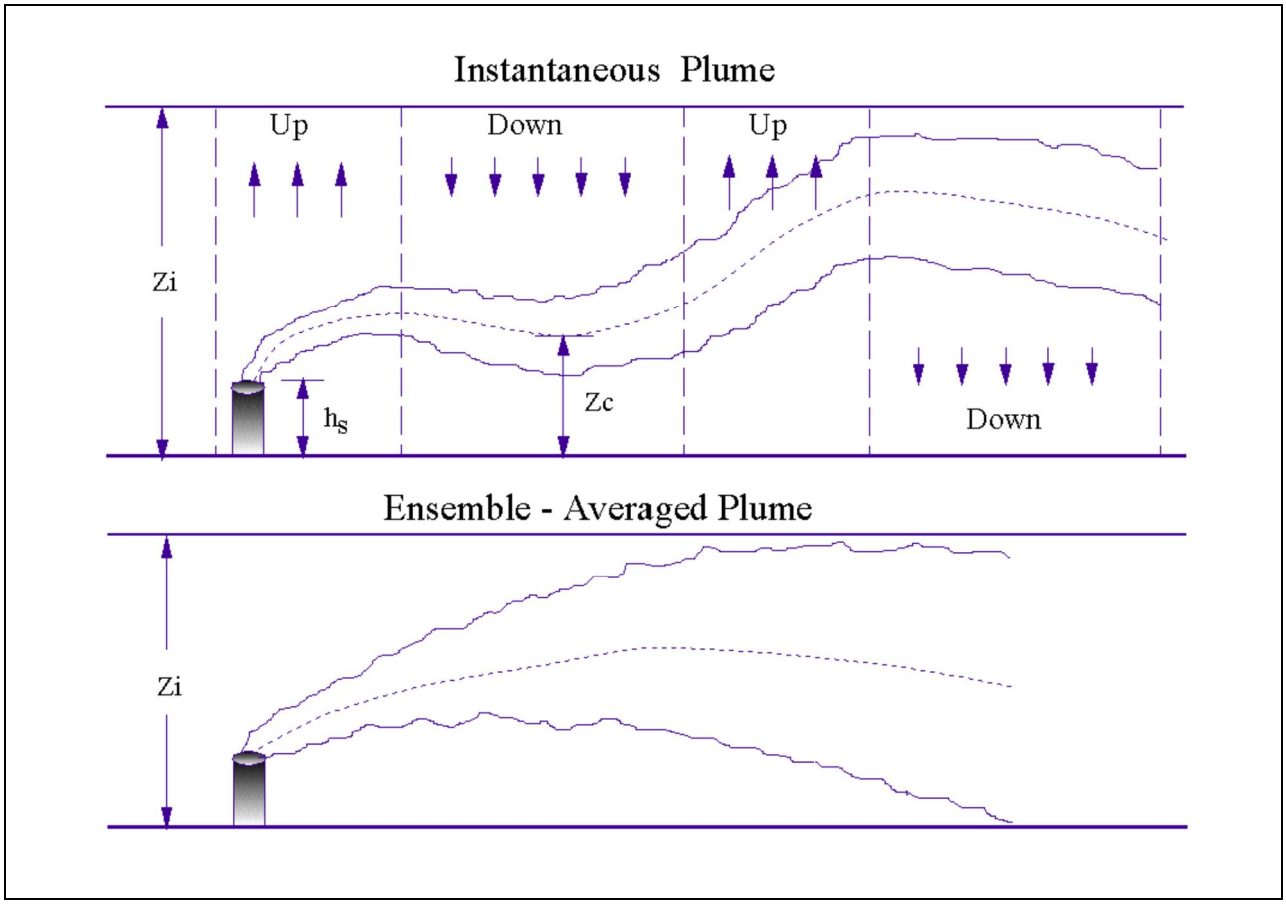

Figure 3: Instant pen and its respective average in the CLC.

Source: https://www3.epa.gov/ttn/scram/models/aermod/aermod_userguide.pdf(access 11/04/2018)

At CLC the probability density function of the vertical velocity (w) has a positive asymmetry coefficient and results in a non-Gaussian distribution of the vertical concentration of the boom. Positive asymmetry is consistent with a greater occurrence of downward movements of the plume than of ascending motions.

In the mathematical treatment used by the AERMOD, the direct plume is the one that first touches the soil and has subsequent reflections between the ground level and the top of the mixing layer. An indirect source is included on the mixing layer to calculate the initial position of the quasi-reflection of the feather material that did not penetrate the layer stable at altitude. This source is called indirect because it is not an image of the true source (as it happens in models like ISC), the pen is not reflected perfectly at the top of the blend layer, so the indirect source treats the portion of the mass of the feather which first touches the top of the mixing layer and its subsequent reflections. The rise of the boom is added to the downward dispersion delay of the top material of the CBL. The

penetrated fountain (or pen) is included in the bill of material that initially penetrated the stable layer at altitude, but was subsequently re-entangled and dispersed by the CBL (Figure 4).

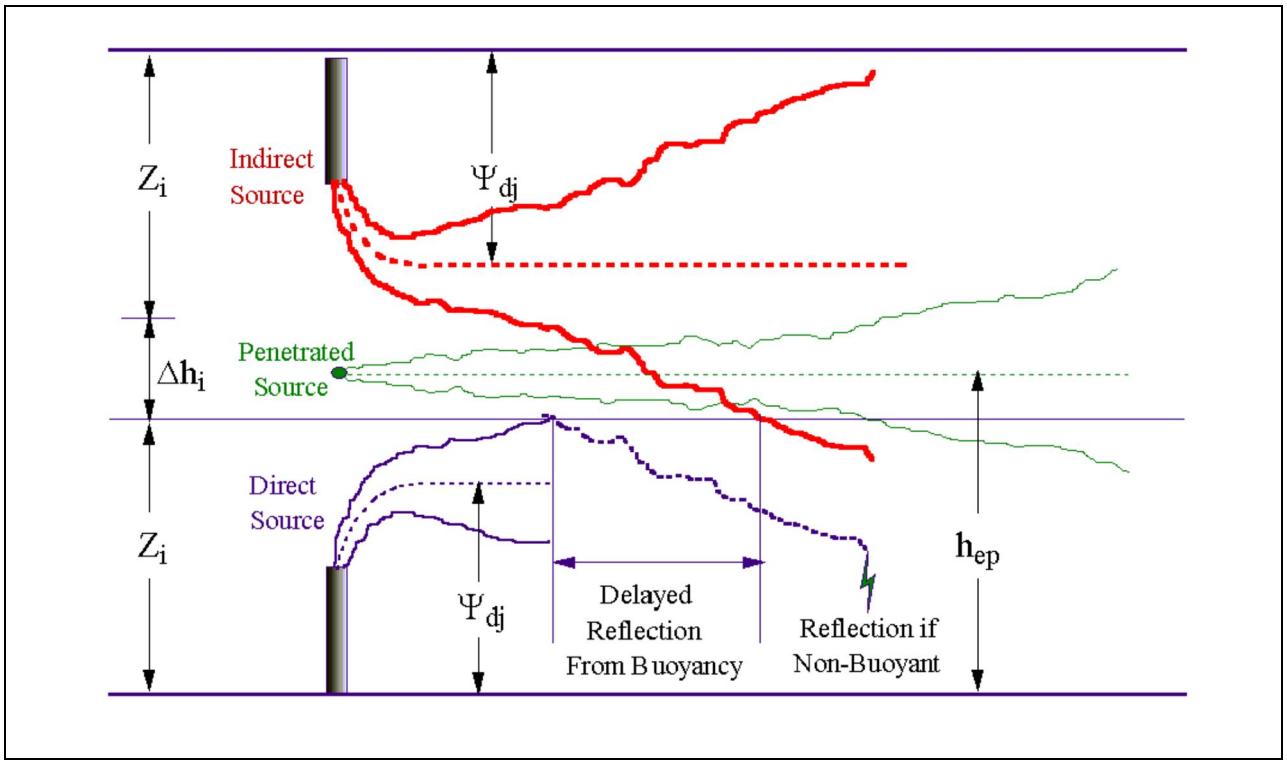

Figure 4: Mathematical treatment used by the AERMOD of the real pen in the CLC.

Source: https://www3.epa.gov/ttn/scram/models/aermod/aermod_userguide.pdf (access: 04/11/2018)

The upward and downward movement of the plume occurs due to atmospheric turbulence and the positive asymmetry coefficient projects a downward final trajectory to the plume, defining the location of the maximum concentration. Concentrations at ground level begin to appear when downward velocities are intense enough that some sections of the plume touch the surface.

A (Figure 5) illustrates the approximation of the asymmetric distribution in the CLC by a bi-Gaussian approach. The figure shows two averages of the trajectory of the plume, one due to the ascending motions of the atmosphere ($\overline{w}_1$) and the other one due to the downward motions ($\overline{w}_2$).

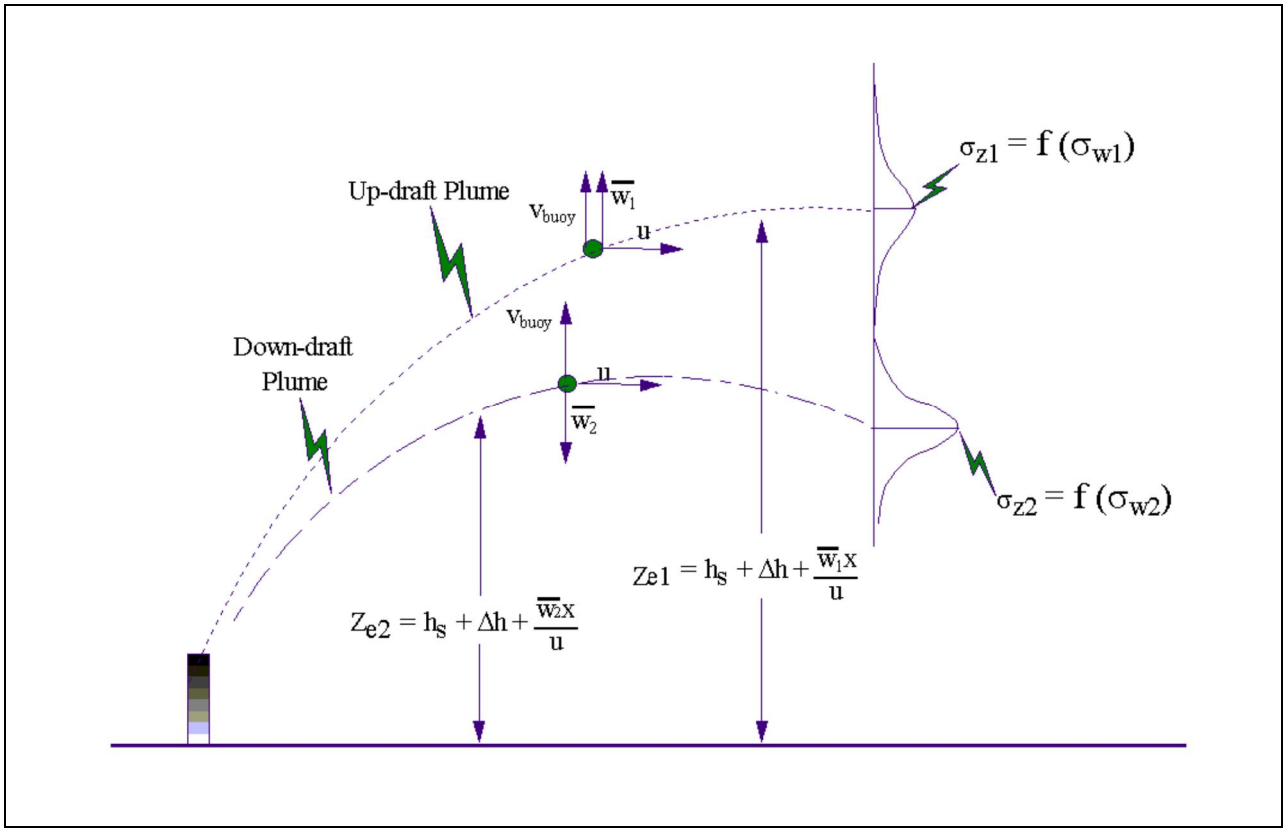

Figure 5: Bi-Gaussian approach of the approximation of an asymmetric distribution by two Gaussian distributions, one for the upward movements and another for the descendants.

Source: https://www3.epa.gov/ttn/scram/models/aermod/aermod_userguide.pdf (access: 11/04/2018)

The meteorological data used by the AERMOD to simulate the atmospheric conditions in which the pollutants are dispersed in a given area are basically divided between surface data and altitude data. Surface data are responsible for the representation of the thermodynamic and turbulent conditions of the atmosphere, and the altitude data represents the transport conditions of the pollutants at different atmospheric levels.

2.2 Mill Location and the Surrounding Municipalities

The pulp mill (Figure 6) will be installed mainly in the municipality of Indianópolis due to some factors, such as: proximity to planting, access roads, via railroad, availability of water resources, and others.

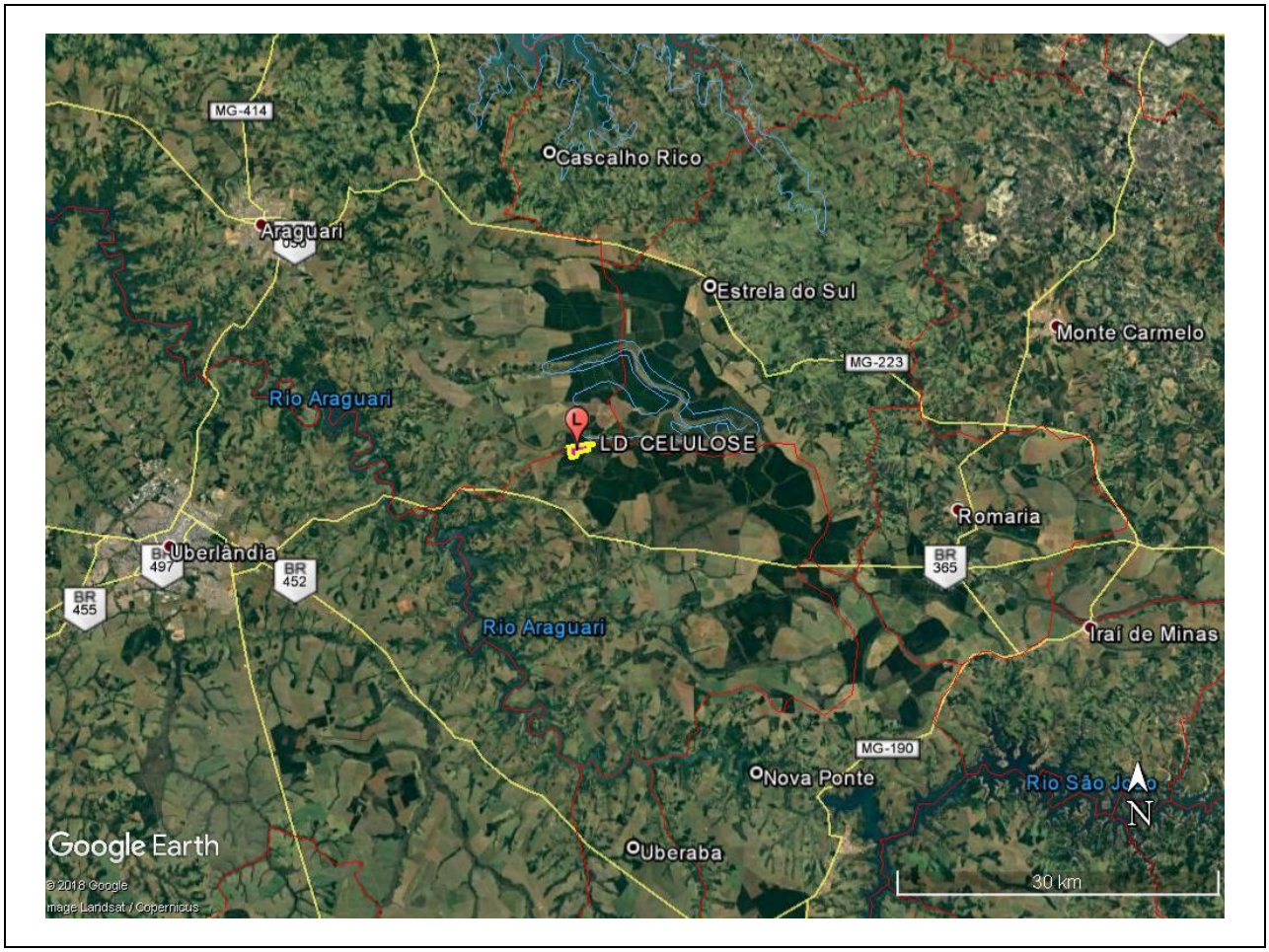

Figure 6: Pulp mil location and surroundings municipalities.

Source: Google Earth.

3 PULP MILL

The unit will be installed in an area of the Farm currently occupied by a tree plantation used for cutting and extracting timber with access by roads to be built during the work (Figure 7).

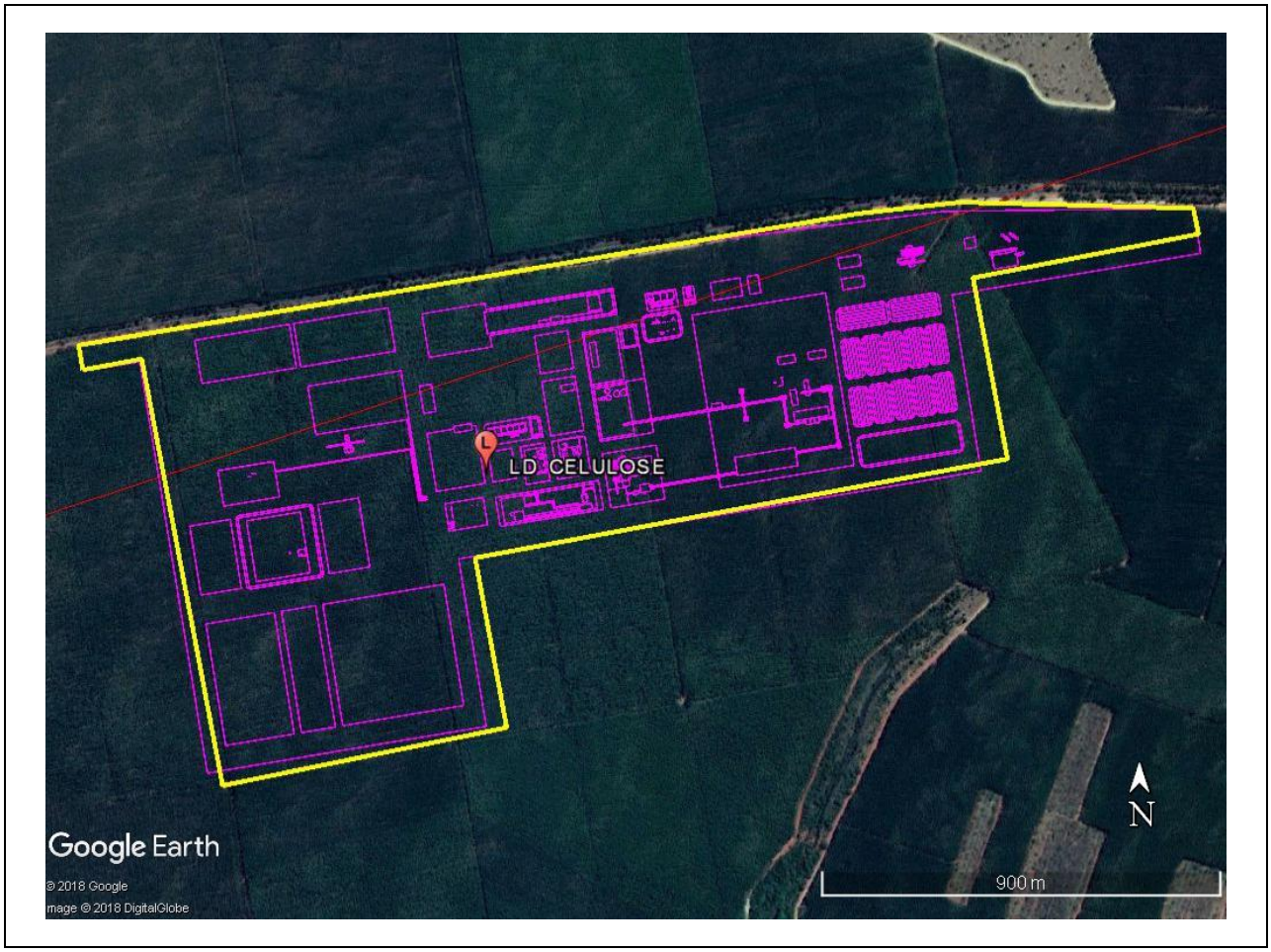

Figure 7: Pulp mil future location.

Source: Google Earth.

Mill plant of the unit inserted in the simulations was obtained from the general layout 10100895200011000M050001c.pdf, provided by the contractor.

4 ATMOSPHERIC DISPERSION STUDY DEVELOPMENT

The processes that generate atmospheric emissions, in this dispersion study, are mainly the processes of pulp production and steam generation.

The mathematical model used in this EDA is AERMOD, being an important tool to evaluate the concentration of pollutants in the atmosphere emitted by stationary sources. This model allows the contributions of certain sources to be analyzed in the final result of the air quality.

The EPA regulatory platform used in this study is based on a Gaussian plume model that considers the concentrations obtained for all distances as averages of the time simulations. This type of model presents good results for studies whose objective is to obtain a spatial distribution of pollution instead of punctual results in space and time.

AERMOD, as well as most of the operational models for pollutant dispersion studies in the atmospheric boundary layer, is based on the Gaussian approximation, since, because they are near-field models, they use the hypothesis that the dispersion occurs in an area of homogeneous horizontal turbulence with variation in the vertical turbulence due to the influence of the relief and the use of the soil. The Gaussian models use simplified turbulence schemes for the near field, parameterized as a function of atmospheric stability.

A well-adjusted computational simulation allows analyzing and quantifying the individual contribution of each of the existing emitting sources in the simulated area and the resulting impact on air quality. The simulations allow greater capacity of management of the industrial units, allowing a more accurate prognosis of the changes in air quality.

4.1 Study Domain

Initially, 12 discrete receivers (Table 1) were determined in the project surroundings in the critical locations and in the air quality monitoring stations, shown in Figure 8.

Table 1: Discrete receptors location

RECEPTORS	DESCRIPTION	UTM E (m)	UTM N (m)	ELEVATION (m)
RECP_01	Road BR-365	189623	7910157	894
RECP_02	Gas station	194298	7907130	961
RECP_03	Duratex Office	195643	7907779	979
RECP_04	Road LMG-748	188397	7913871	939
RECP_05	School near by BR-365	187749	7910803	871
RECP_06	Dolearina	204960	7930177	987

RECEPTORS	DESCRIPTION	UTM E (m)	UTM N (m)	ELEVATION (m)
RECP_07	Estrela do Sul	216219	7925259	763
RECP_08	Duratex Headquarter	198458	7924119	959
RECP_09	Indianópolis	192887	7891741	805
RECP_10	Aragurari	162359	7935846	957
RECP_11	Uberlândia	154938	7907156	868
RECP_12	Nova Ponte	219301	7878211	940

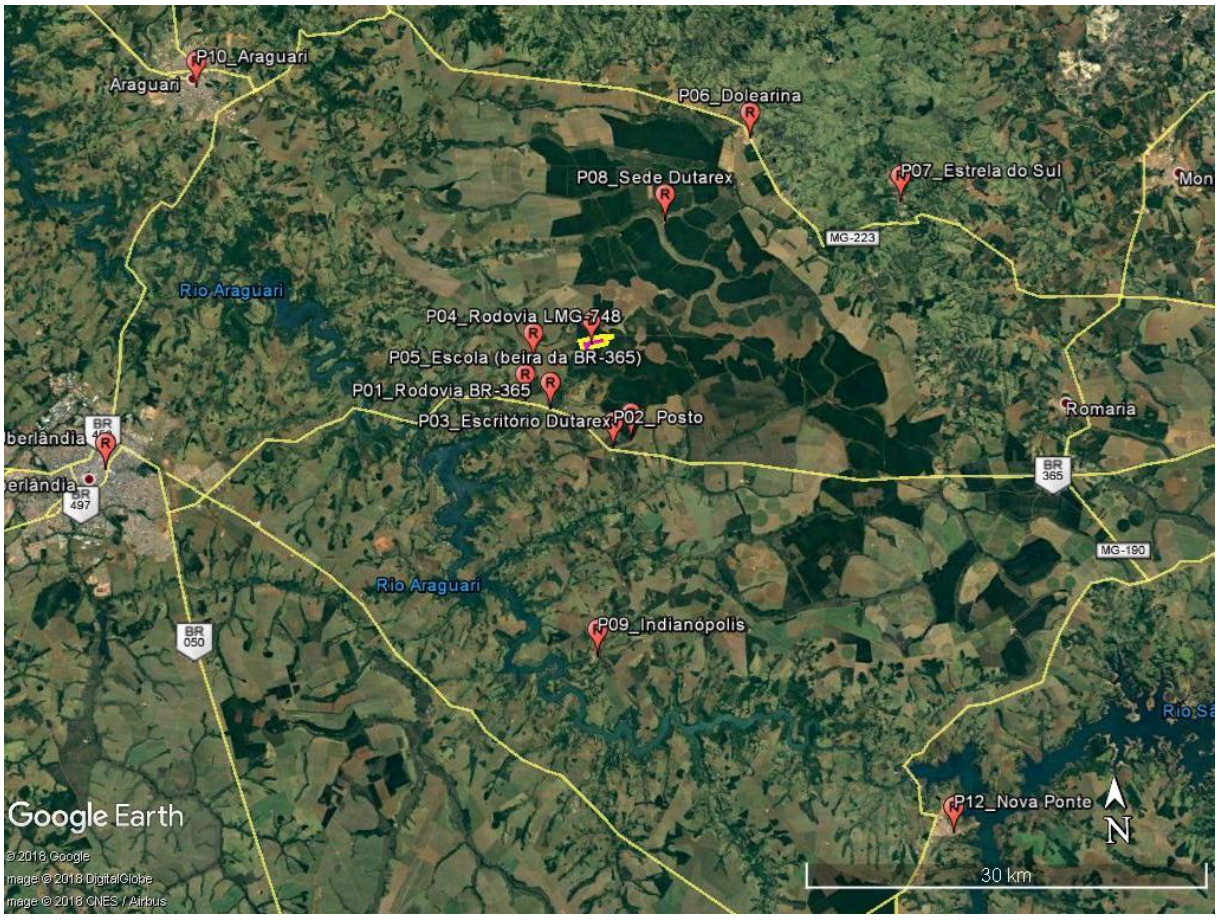

Figure 8: Discrete receivers placed in critical locations and in air quality monitoring stations.

Source: Google Earth.

In addition to the discrete receivers, the air quality is evaluated in this study of atmospheric dispersion from the concentrations calculated in a network of Cartesian receivers of high resolution, distributed in two square and regular Cartesian meshes centered in Apollo Mine, the first one with 40 km of side and a uniform resolution of 500 m and the second with 10 km of side and spatial resolution of 250 m, both of which are intercalated to present spatial resolution of less than 250 m in areas of maximum interest (Figure 9).

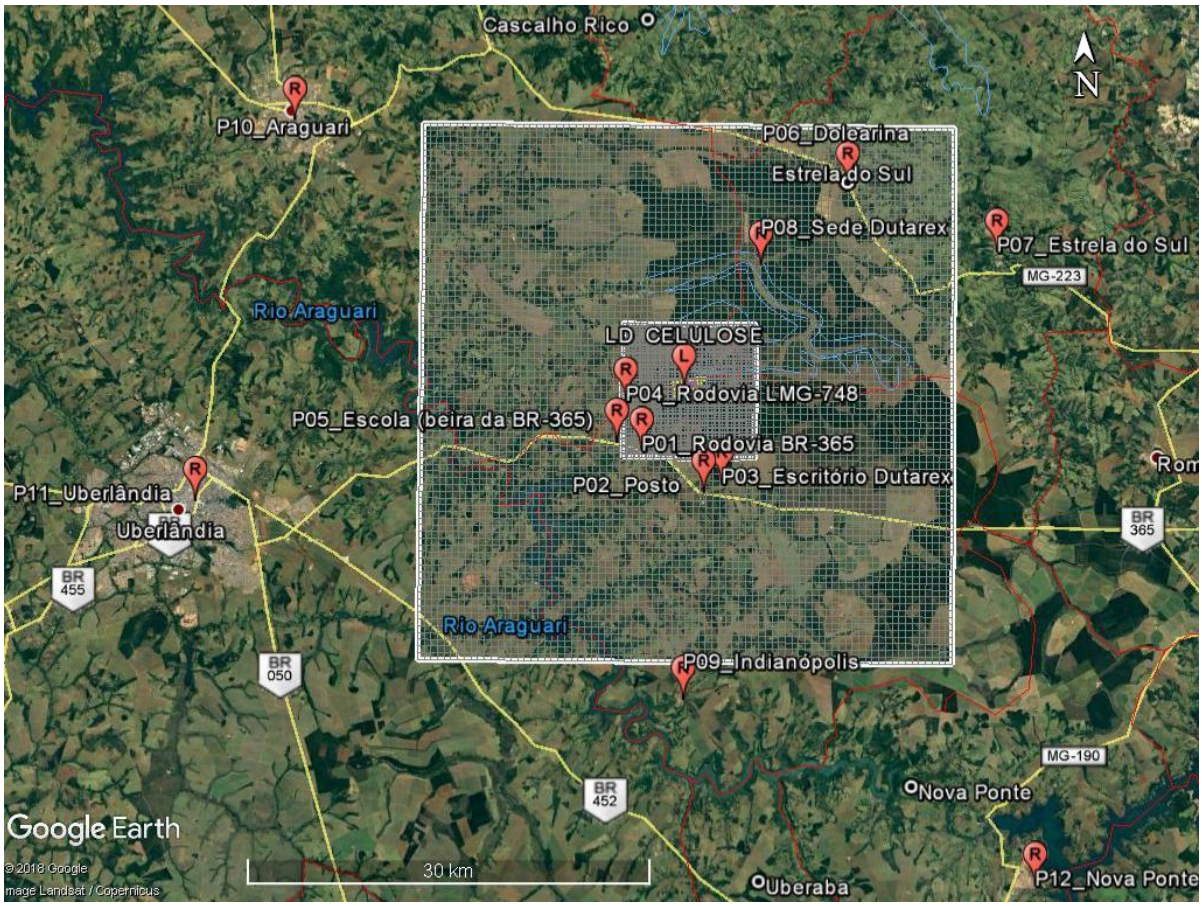

Figure 9: Simulated cartesian meshes, centered on the source

Source: Google Earth.

4.2 Terrain and Land use

In consultation with the National Register of Conservation Units (CNUC), through the page http://www.mma.gov.br/areas-protegidas/cadastro-nacional-de-ucs, no federal conservation units (UC) of complete protection in the study region (gray grid), the only UC found is located about 125 km from the proposed project (Figure 10).

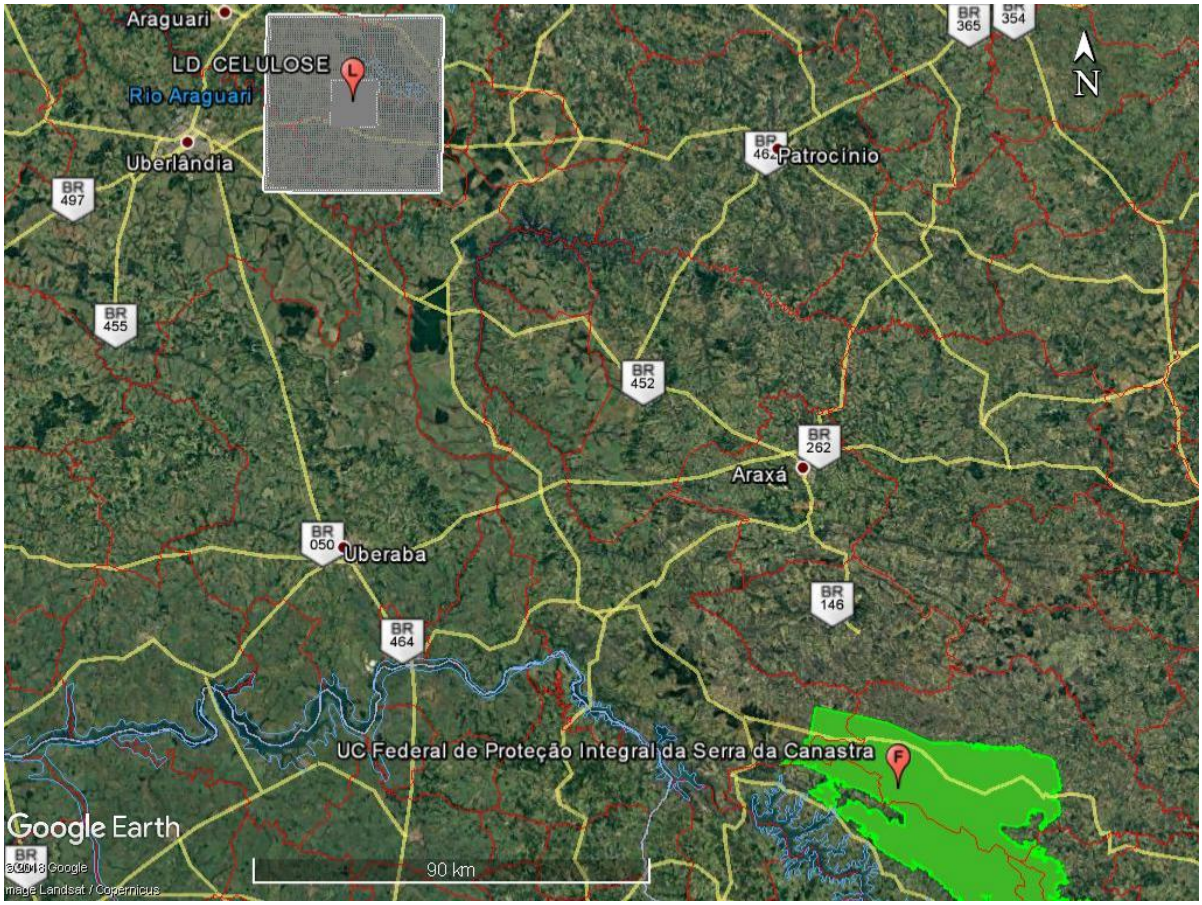

Figure 10: Mill Location Map and study domain outside the territorial boundaries of the conservation unit marked in green.

Source: CNUC, 2015.

The land use map shown in Figure 11 shows that the region studied has small areas of urban land use, marked in red, and rural predominance is evident.

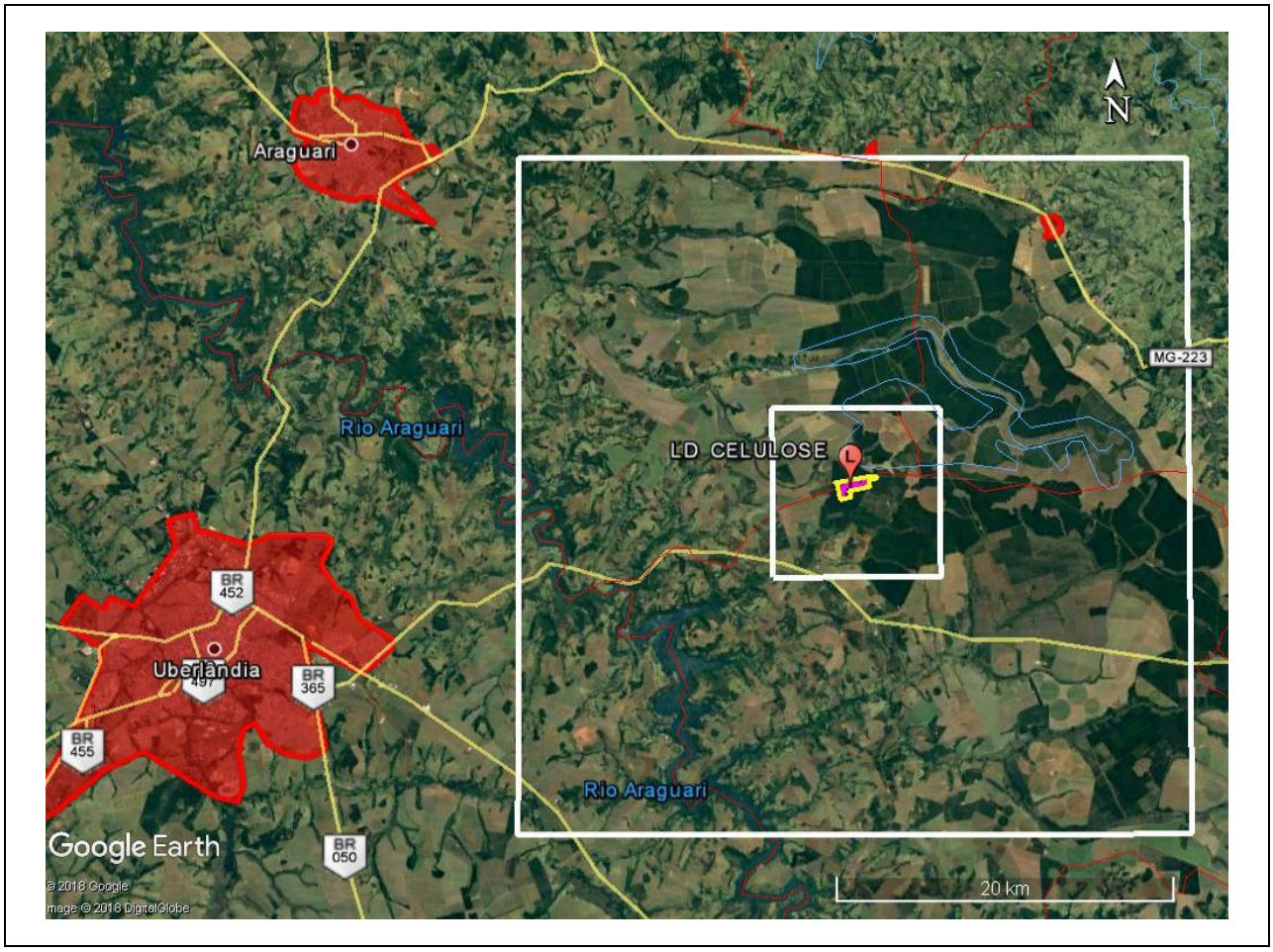

Figure 11: Land Use Map, urban areas in red.

Source: Google Earth

Soil terrain and land use for the turbulence parameters calculation were obtained by overlaying Google Earth images with relief data from the Shuttle Radar Topography Mission, conducted by NGI and NASA. The SRTM occurred on February 11, 2000, performing a global sampling with a precision of 3 "(seconds of degree), that is, a grid point every 90 meters approximately (Figure 12).

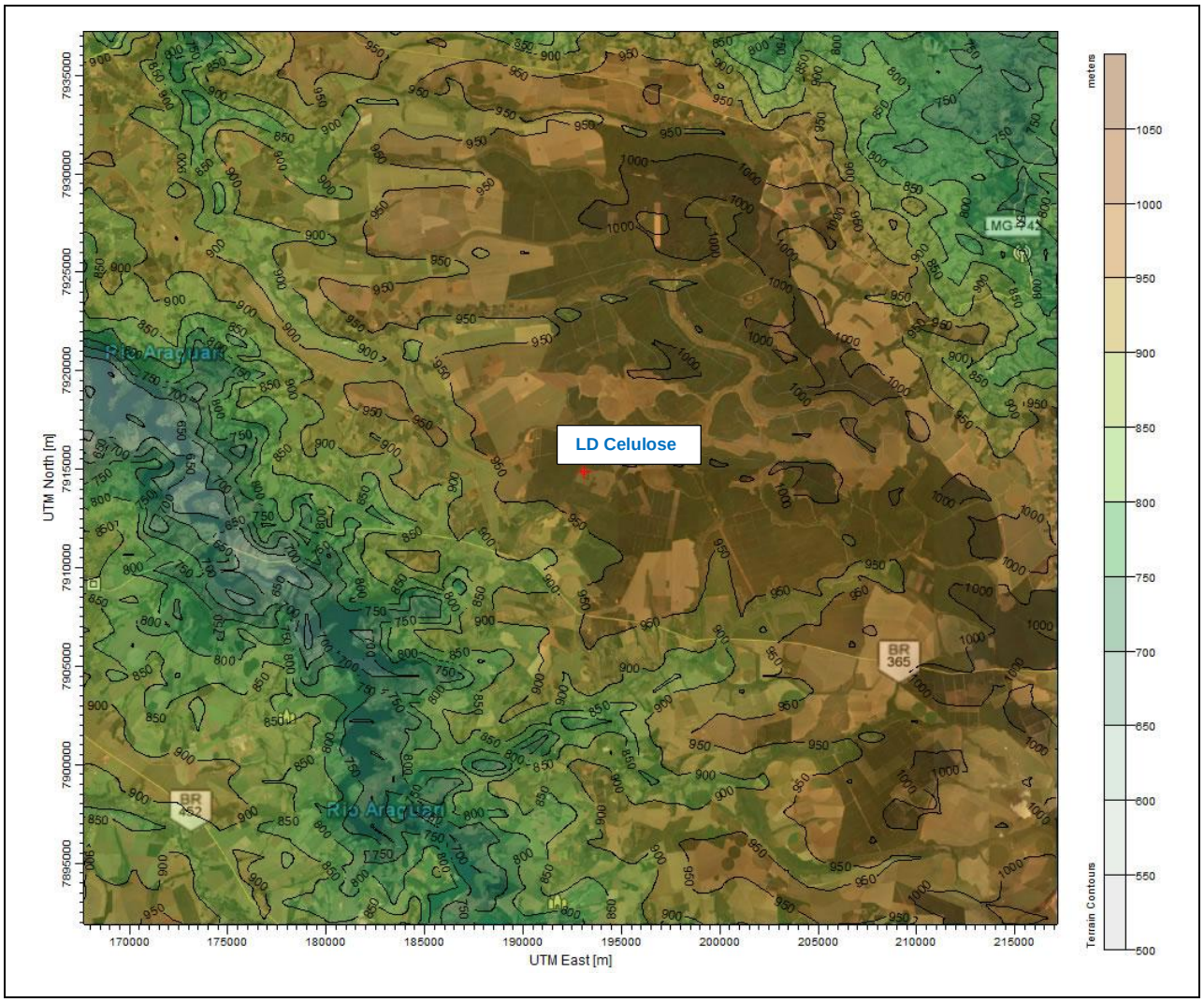

Figure 12: Level Curves (m) of the region highlighted for the development to the center.

Source dos dados originais: Shuttle Radar Topography Mission (2000).

4.3 Meteorological Data Analysis

The altitude and surface meteorological data used in this dispersion study were obtained by simulating the WRF (WEATHER RESEARCH AND FORECASTING) model, recommended by the EPA (Environmental Protection Agency), and reprocessed for simulations with the AERMOD model, referring to the center of the project studied for the years 2013 to 2017. The boundary conditions used were the output data from the Global GFS (Global Forecast System) model obtained from the *National Center for Environmental Prediction* (NCEP).

4.3.1 Weather Research and Forecasting – WRF

WRF model (*Weather Research and Forecast Model*) was developed through a collaboration between several agencies, including NCAR (National Center for Atmospheric Research), NOAA (National Oceanic and Atmospheric Administration), NCEP (National Center for Environmental Prediction), FSL (Forecast Systems Laboratory) , the AFWA (Air Force Weather Agency), the Naval Research Laboratory, Oklahoma University and the Federal Aviation Administration (FAA).

The ARW (Advanced Research WRF) is currently in version 3.9.1.1, available since August 2017. The version of the WRF used in this study was 3.6.1 released in 2014. The updates that have had since then do not cover changes in the parametrization algorithms required for proper use in the study area, and then this version (3.6.1) is fully capable of meeting all required requirements.

The WRF was born as a natural evolution of the MM5 model, which has been widely used over the years around the world, and is now built to be portable and applicable to the most diverse numbers of possible situations (NCAR, 2011).

The WRF model is in the public domain and recommended by the EPA for simulations of atmospheric conditions. Developed to be the best tool for atmospheric, flexible and efficient simulation on a variety of computing platforms, a data assimilation system and a software architecture that allows computational parallelism and system extensibility. The WRF is suitable for use on a wide range of scales ranging from meters to thousands of kilometers. The model follows the local terrain and admits the vertical

coordinate as hydrostatic pressure, with the top of the model to a constant pressure surface.

The pre-processing of input data required by the WRF needs to be done for each location the model will simulate. This pre-processing consists in the use of meteorological and geographic data taken from the global bases for each region of interest to be simulated.

The meteorological data simulation used three nested grids with 64 x 64 grid elements, the first one with a spatial resolution of 27 km, the second with a resolution of 9 km and the third with a resolution of 3 km.

WRF model used the usual configurations for the region: the use of input data from the Global Meteorological Model (GFS) with 0.5º spatial resolution, three levels of grid nesting (27, 9, 3 km) , used the Yonsei University to parameterize Atmospheric Limit Layer Turbulence, Betts-Miller-Janjic for the convection parameterization and formation of Cumulus, the WSM 3-class scheme to parameterize the Cloud microphysics, the RRTM scheme to parameterize the Radiation And the Similarity Theory of Monin-Obukhov (MM5 MRF PBL) to parameterize surface turbulence.

The survey period of the meteorological data and the simulation with the model AERMOD was from 01/01/2013 to 12/31/2017.

The complementary meteorological data used in this EDA were obtained from the meteorological network of airports (redemet), referring to the station of the Tancredo Neves International Airport (Belo Horizonte - Confins), located in the municipality of Confins, coordinates 23k, 608500 m E and 7828500 m S , distant about 450 km from the unit analyzed in this simulation.

4.3.2 Configuring the AERMOD Meteorological Preprocessor (AERMET)

The meteorological data obtained from the WRF simulation were used as input data from the AERMET meteorological preprocessor. The time series was extracted from the center of the 3 km grid, more precisely at the grid point closest to LD Cellulose. These data were placed in SAMSON format and used in the standard AERMET surface conFiguretions (Figure 13).

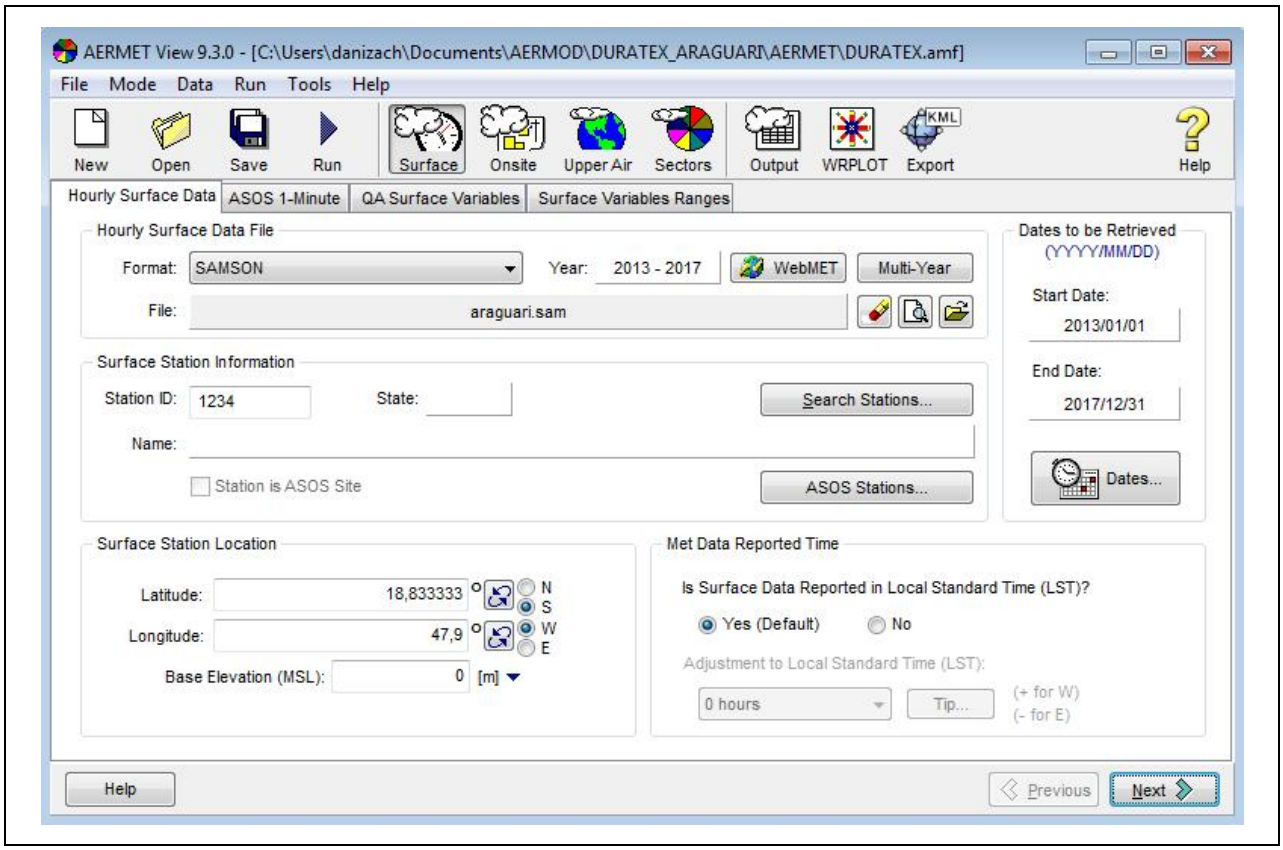

Figure 13: Surface station time data settings (AERMET).

In this study, local time (Onsite) time data were not included, and therefore, all data entered in the AERMET from the Surface Station and Upper Air Estimator tabs.

Soil coverage and land use data were obtained from the Global Land Cover Characterization (GLCC) remote sensing program, which consists of a large set of surface characterization data based primarily on the Advanced Very High Resolution Radiometer (AVHRR) and the NDVI (Normalized Difference Vegetation Index) in 10 day composition (Figure 14).

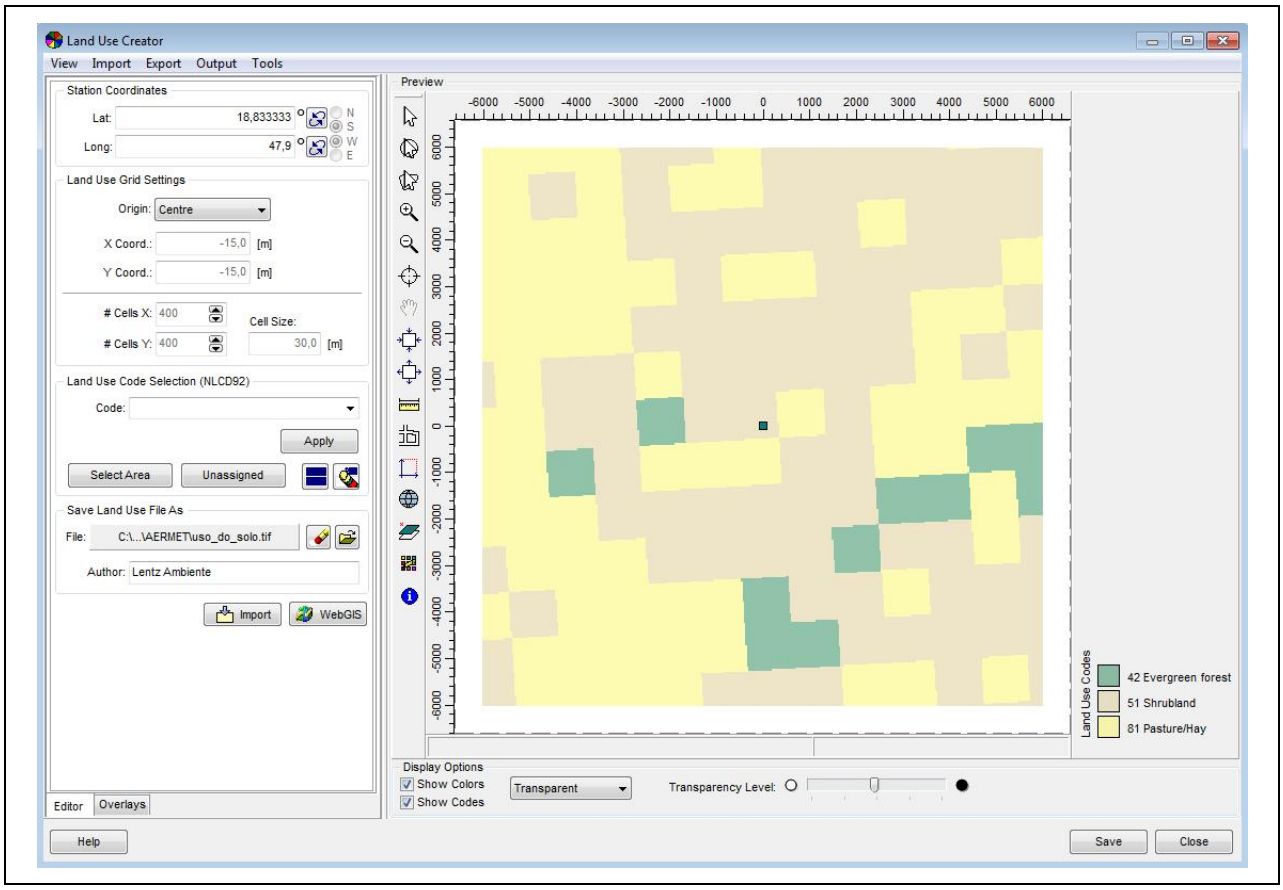

Figure 14: Land Use Creator settings including GLCC land-use categories at the project site.

From the GEOTIFF created by the Land Use Creator to the center point of the project, it was possible to import the surface data from the Land Use Viewer into the AERMET, thus defining the parameters of roughness, albedo and Bowen ratio in high resolution, using the maximum range of 5 km (Figure 15), for each of the twelve sectors (Figure 16).

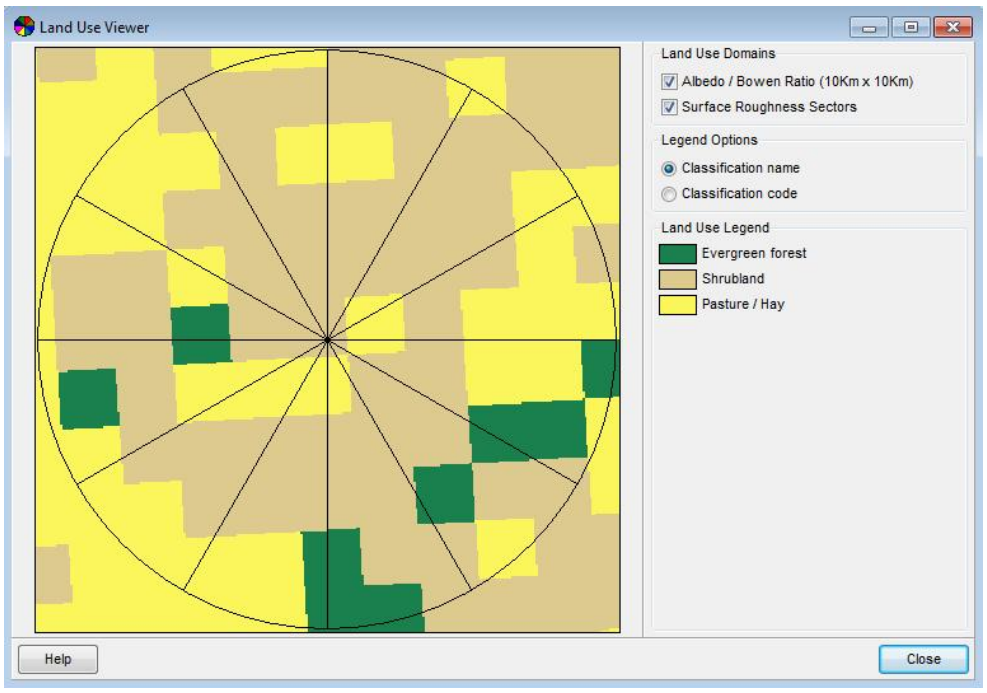

Figure 15: Land Use Viewer configuration with land use classification.

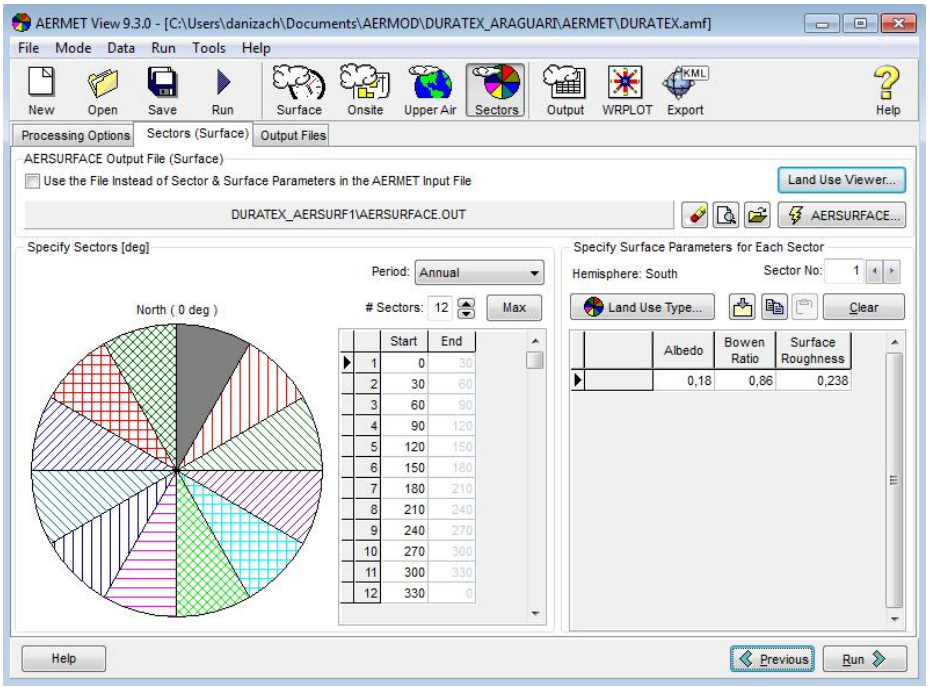

Figure 16: Configuration of surface parameters by wind direction.

4.3.3 Importance of Direction and Speed of Winds

The wind speed is a very important meteorological data in the calculation of the concentrations of pollutants through the model AERMOD, because it is in the denominator of the equation. Thus, by changing the wind speed from 1 m/s to 2 m/s, for example, the concentration of pollutants would be reduced by half. Other variables of the atmospheric boundary layer are also used to calculate the dispersion of atmospheric pollutants, but the influence of these variables on the final result is proportionally smaller and therefore will not be analyzed in this item.

The wind direction determines, every hour, which numeric receivers will be more or less impacted by the emission pen of each chimney. The greater the sampling period of the analyzed pollutant, the greater the importance of the wind direction predominance in the calculation of this concentration, since in these cases the number of hours used in the calculation of this concentration will be higher.

4.3.4 Directional Wind Histogram (WRF model data)

Figure 17 and Figure 18 show the directional wind histograms of the surface data of the weather station and the radiosonde, which obtained the same result.

Figure 17 shows the predominance of the winds in the NNE direction. This predominance is consistent with other databases in the region and is in accordance with the synoptic systems that influence the circulation of air masses in the region, specifically the cold fronts systems. There is a secondary predominance in the other directions of the wind, which refers only to the weaker winds. The lull index (winds below 1.0 m/s) is practically zero, due to the local conditions and undesired consequence of the simulation of meteorological data by models.

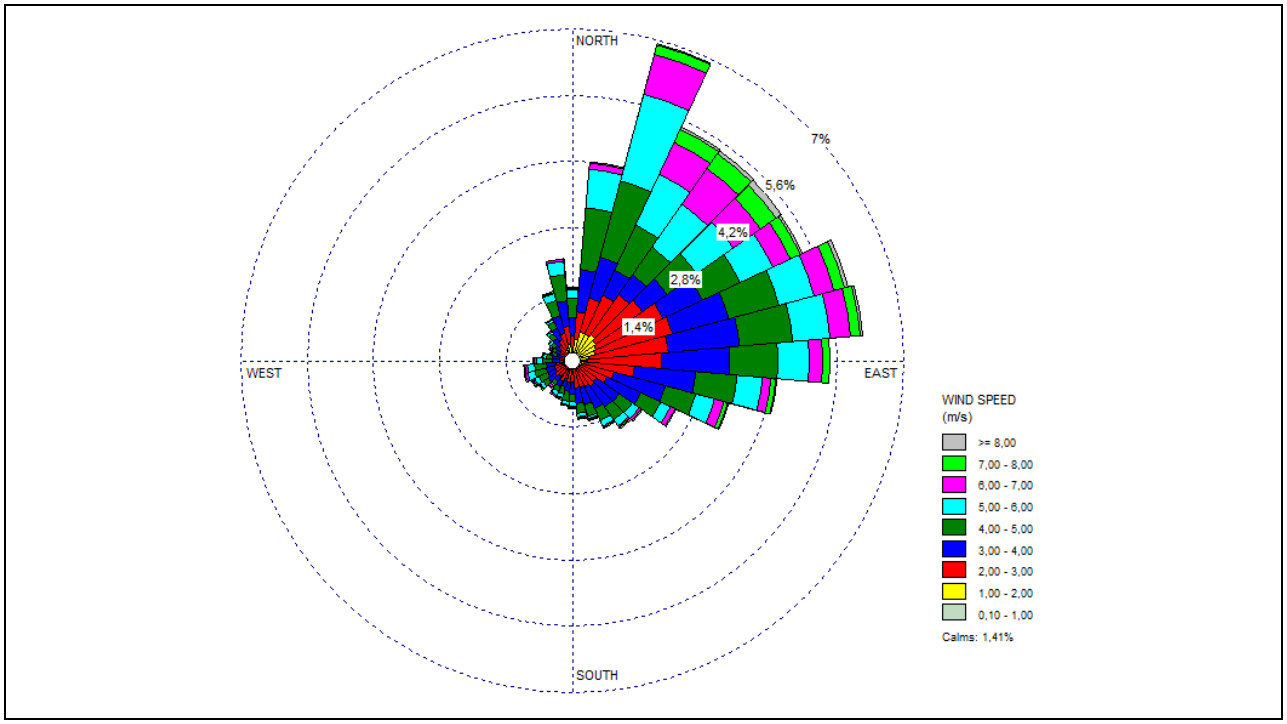

Figure 17: Wind rose with the classification of speed, direction and limit, in percentage, of the occurrence of calm winds.

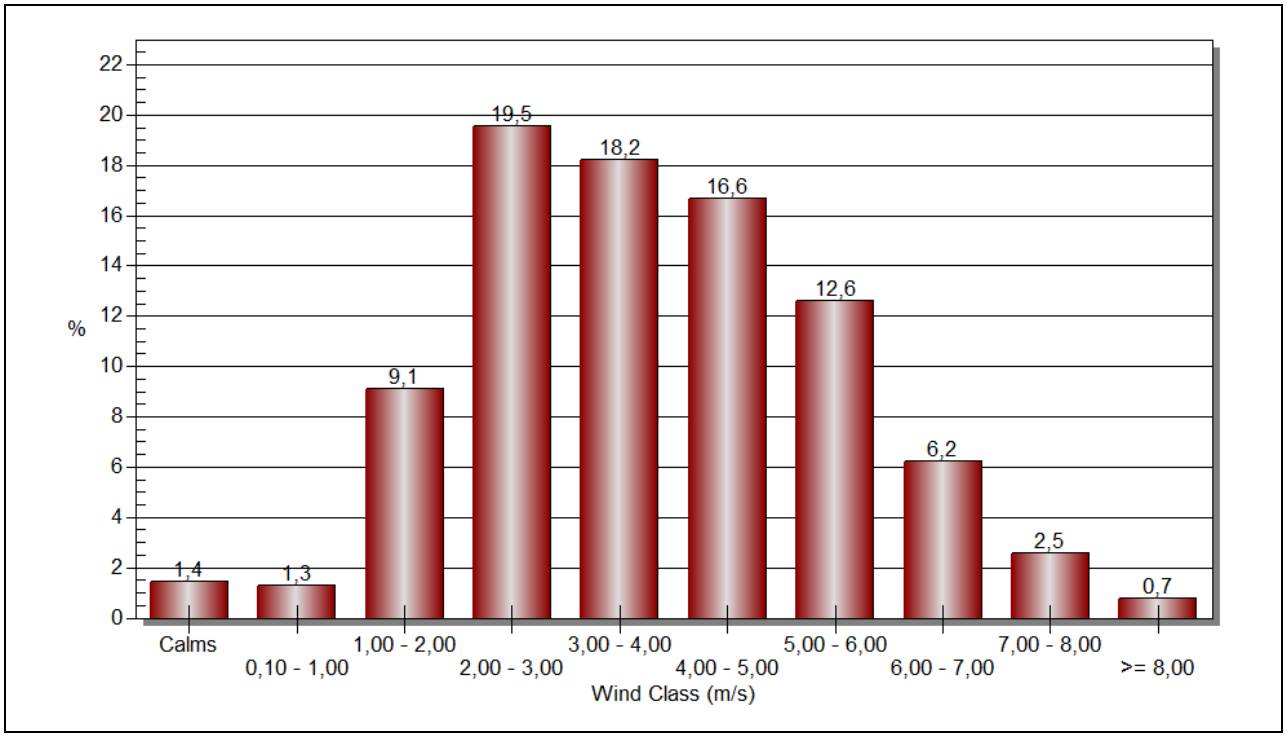

Figure 18: Histogram of classification of the frequency of wind distribution.

4.3.5 Surface Weather Data (WRF model data)

Figure 19 shows the results of the data processing by the AERMET, it is verified the availability of 88.11% of the meteorological data, which shows that they are sufficient to meet the criterion of minimum statistical representativeness, 2/3, or 66.7%.

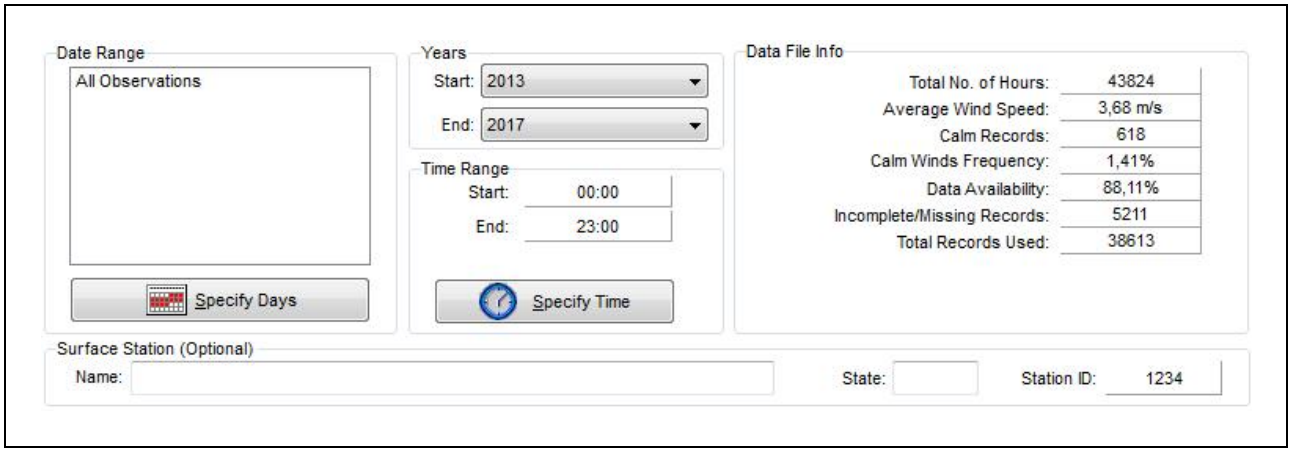

Figure 19: Data statistics used.

The absent hours were 5211 in total and the hours with recording of calms were 618, totaling 1.41% of the data.

The time series of air temperature (Figure 20) showed very small interannual variability during the simulated period, with seasonal characteristics adequate to that described by climatology (Figure 21).

The first half of 2014 data for air temperature (Figure 20) presented an unusual oscillation for the period, this difference in temperature coincides with the period of change of the model (and data supply) of the soil in the GFS files of 0.5 °. As data assimilation by sites by the model (WRFDA) was not used, this temperature variation became a little more evident in the period, but did not affect the final quality of the modeled data.

This variation was restricted to the temperature data, not being observed in the other meteorological variables.

The INMET climatological norm used to verify the initial quality of the data (Figure 20) shows a gradual but continuous warming of the monthly average of the air temperature, with special emphasis on the temperature increases observed in August, end of winter (Figure 21).

With the climatic elevation of the temperature, the immediate effect is the increase of the evaporation and consequently the increase of the values of humidity in the atmosphere. The relative humidity obtained by the simulation with the WRF (Figure 22) adequately represents the expected conditions over a three year period, according to the most current climatology (Figure 23).

The atmospheric pressure data generated by the WRF did not significantly reflect the change in the soil temperature model that generated the 0.5 ° GFS simulation files (Figure 24). The simulated data did not show significant interannual variation and the seasonal oscillations were within the expected by the climatology (Figure 25).

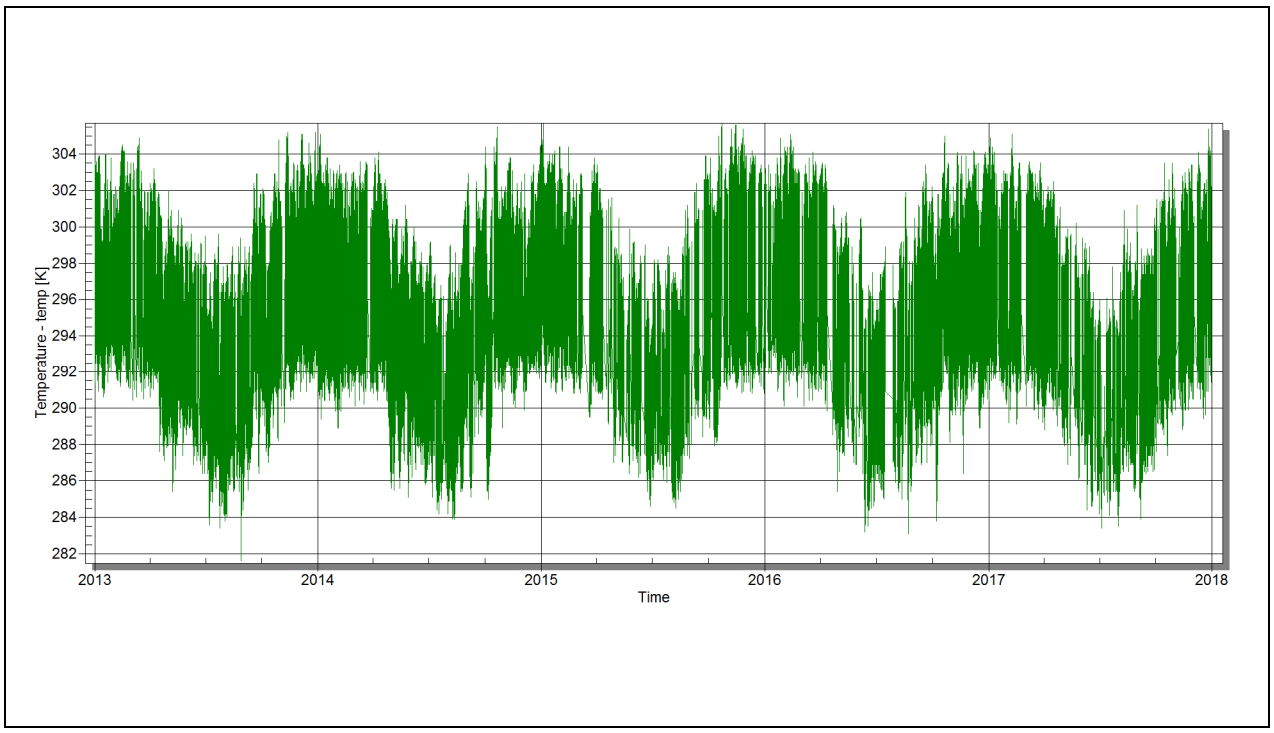

Figure 20: Time series of the air temperature (K) simulated with the WRF

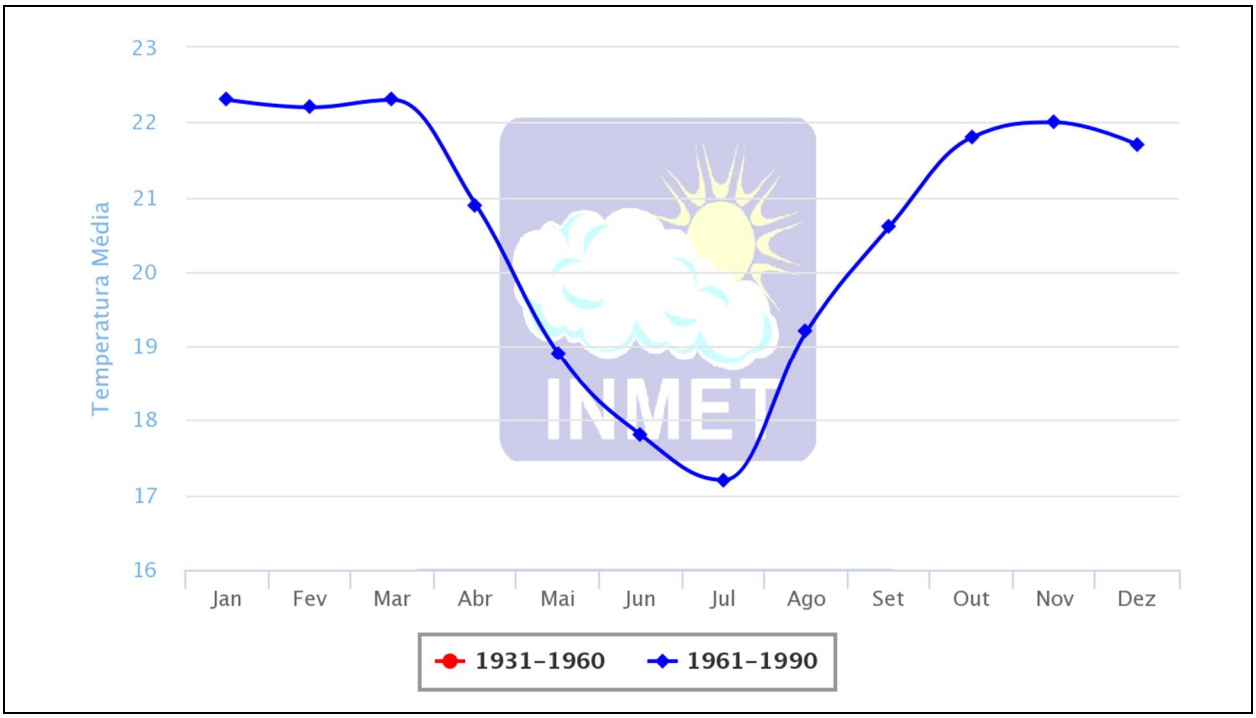

Figure 21: Graph of the climatic normal of air temperature (ºC) of the nearest reference station, located in the municipality of Patrocínio - MG

Source: Instituto Nacional Meteorologia (INMET).

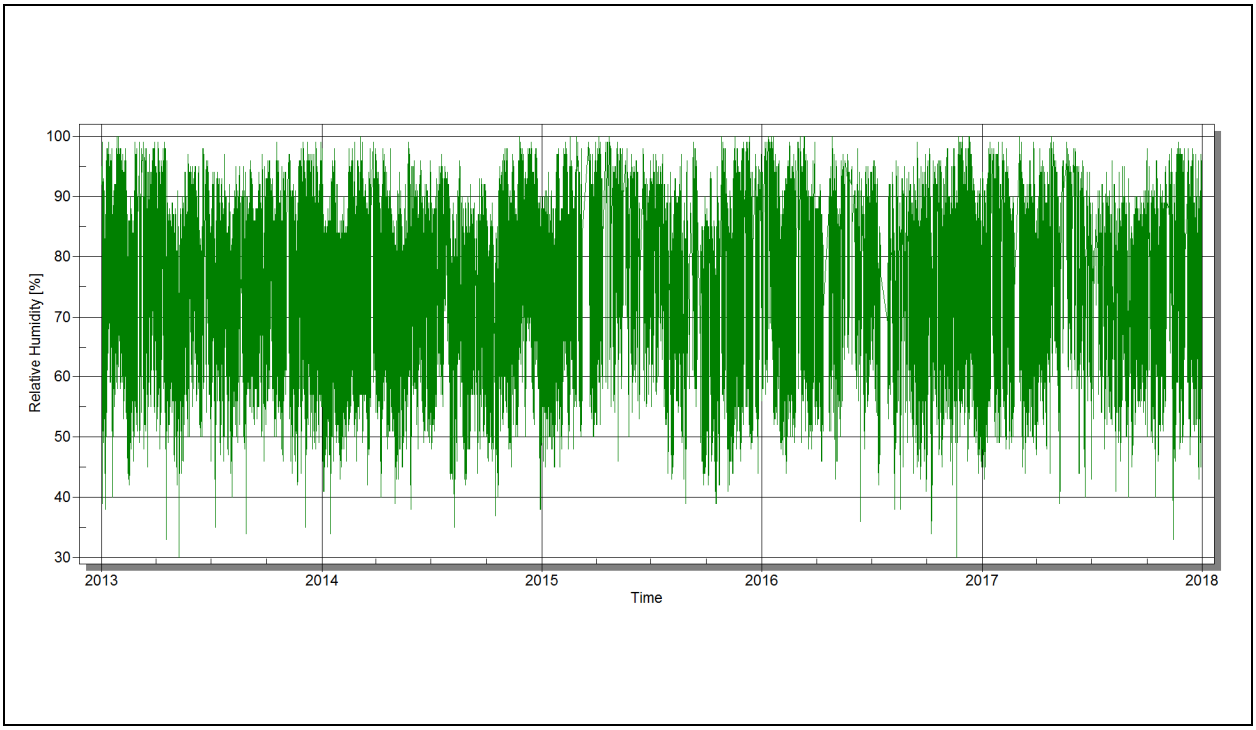

Figure 22: Time series of relative moisture (%) simulated with the WRF.

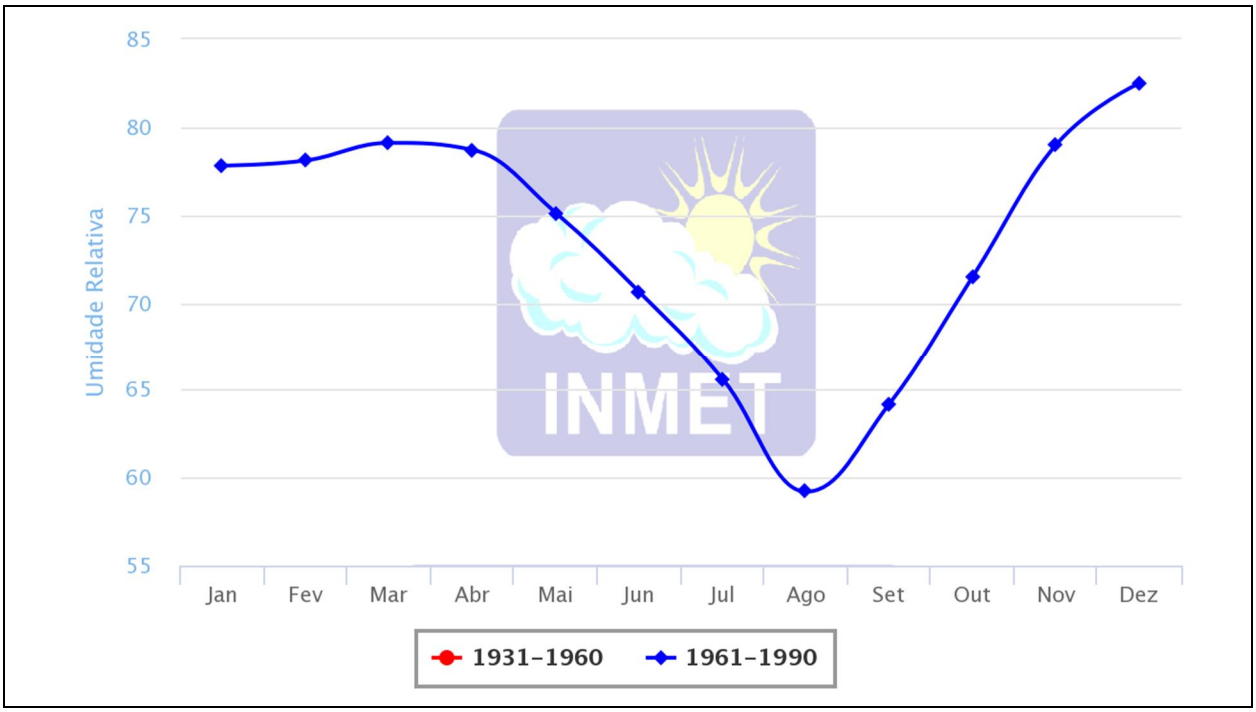

Figure 23: Graph of the climatological normal of the relative air moisture (%) of the nearest reference station, located in the municipality of Patrocínio - MG.

Source: Instituto Nacional Meteorologia (INMET).

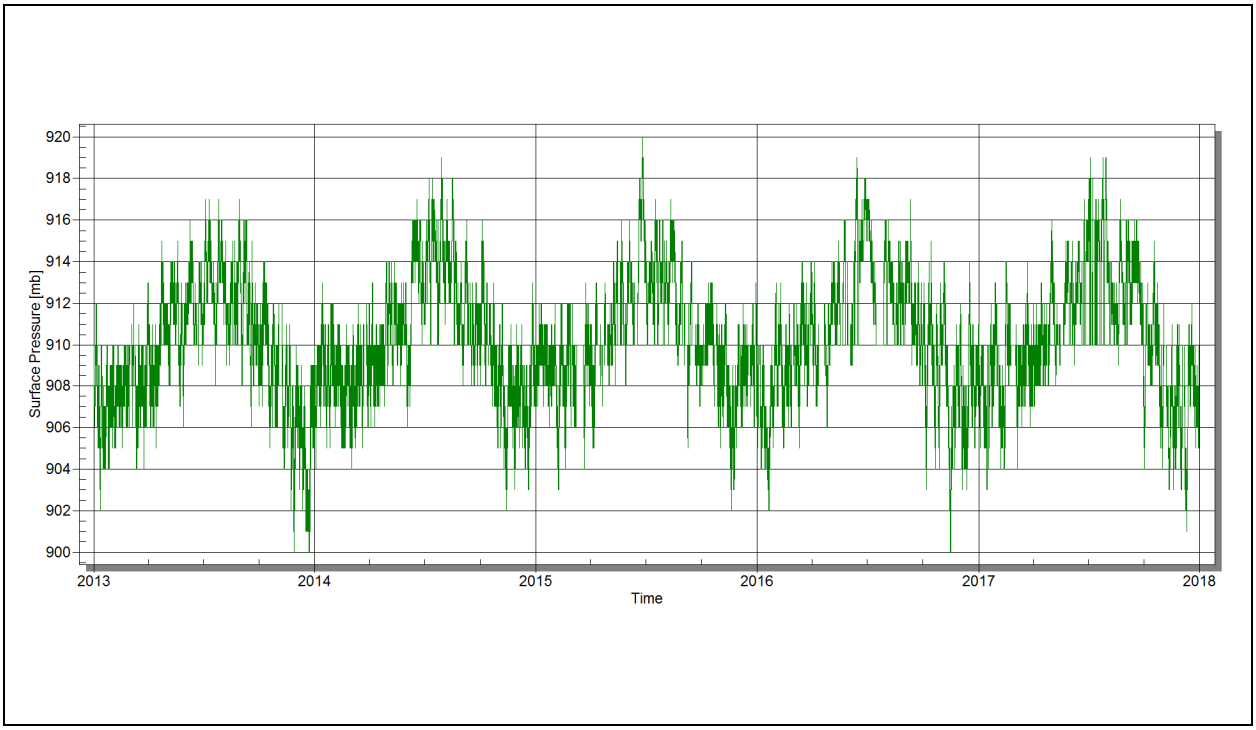

Figure 24: Time series of atmospheric pressure (hPa) simulated with the WRF.

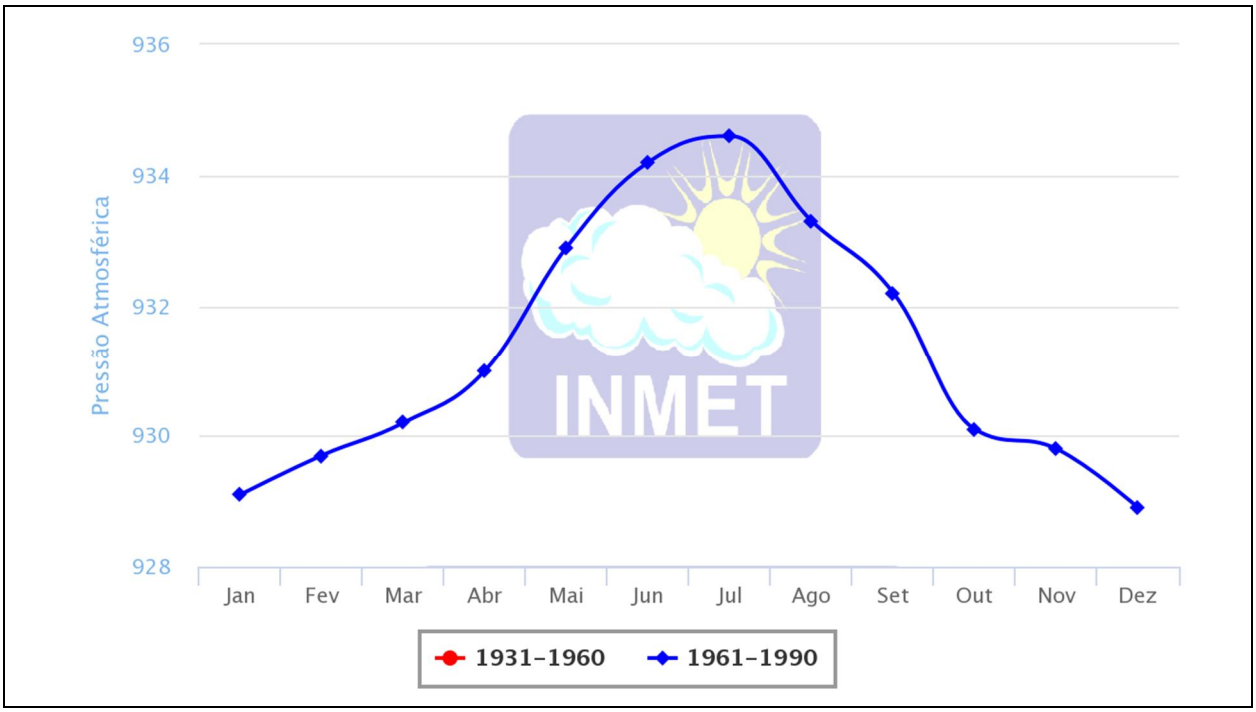

Figure 25: Graph of atmospheric pressure climatological normal (hPa) of the nearest reference station, located in the municipality of Patrocínio - MG.

Source: Instituto Nacional Meteorologia (INMET).

In the rainfall regime shown in Figure 26, the dry season is concentrated in the months of May to August and in the beginning of September, typically the winter months in SE Brazil and in the transition phases of the fall and spring seasons.

The months from May to August are critical for air quality, especially in the case of particulate matter emission, as low precipitation and high atmospheric pressure make it difficult to remove these pollutants from the atmosphere.

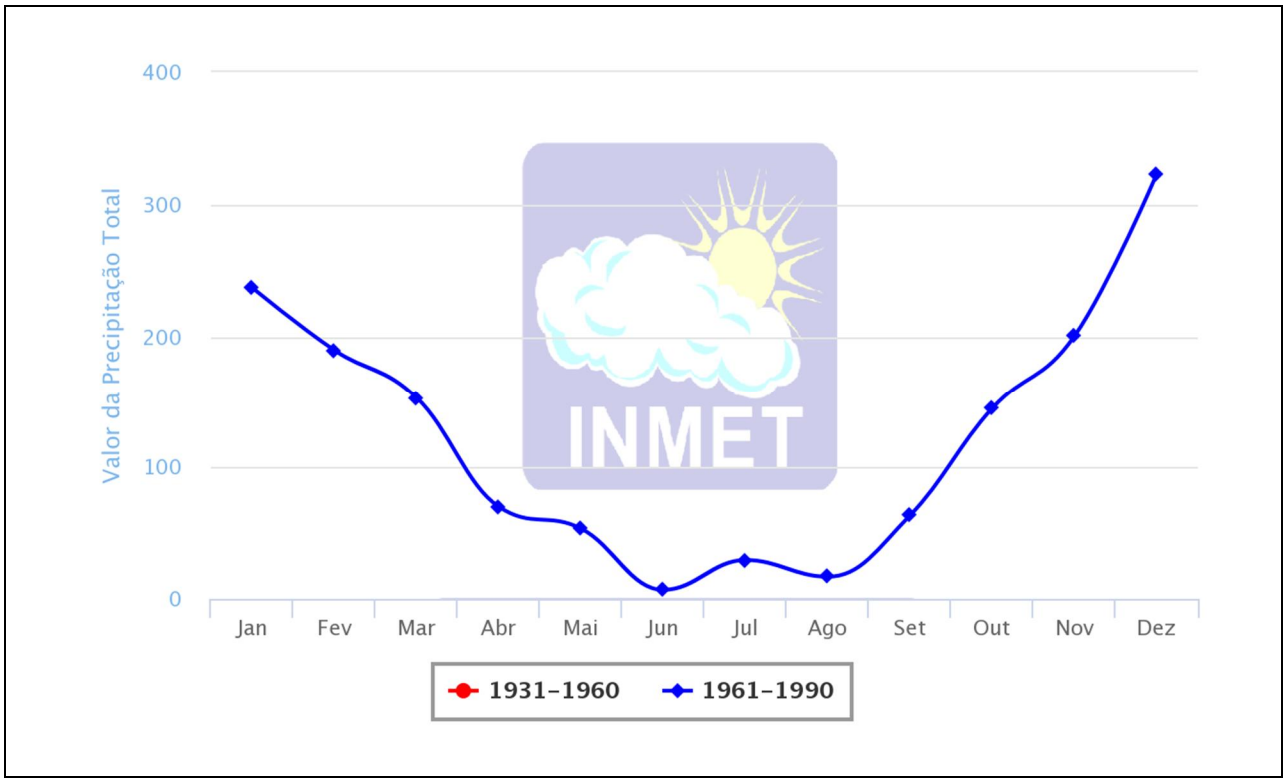

Figure 26: Monthly cumulative rainfall (rainfall in mm / month) of the nearest reference station, located in the municipality of Patrocínio - MG.

4.3.6 Statistics Tests and Model Validation

The validation of the elaborated models and algorithms followed the methodology described by Chang (CHANG and HANNA, 2004) to evaluate the performance of environmental and atmospheric models.

The trend indicates that the results simulated by the models exceeded the observed

values (reference values). A negative bias indicates that the results of the models are lower than the values of the observations.

Normalized bias can become very large when a minimum concentration limit is not used, so Fractional Bias is a useful indicator because it has the advantage of equally distributing the weight of the positive and negative estimates (CHANG and HANNA, 2004). The acceptance criterion of fractional bias for this study is: - 0.25 <FB <+0.25 (equation 1).

$$FB = \frac{\left(\overline{C_{mod}} - \overline{C_{ref}}\right)}{0{,}5\left(\overline{C_{mod}} + \overline{C_{ref}}\right)} \quad (1)$$

The geometric average of the bias calculates the residual average of the time-paired model, measured by the logarithm, being a useful indicator because it has the advantage of explaining the smaller deviations (CHANG and HANNA, 2004). The criterion of acceptance of Geometric Mean Bias (MG) for this study is: 0.75 <MG <1.25 (equation 2).

$$MG = \exp\left(\overline{\ln C_{mod}} - \overline{\ln C_{ref}}\right) \quad (2)$$

The average square error of normalized error (NMSE) is obtained by calculating the average of the absolute difference squared, normalized. In this test, the closer to zero, the better the result. The acceptance criterion for the Normalized Mean Square Error (NMSE) for this study is: 0.0 <NMSE <0.5 (equation 3).

$$NMSE = \frac{\overline{\left(C_{mod} - C_{ref}\right)^2}}{\overline{C_{mod}} \times \overline{C_{ref}}} \quad (3)$$

The geometric variance (VG) is obtained by averaging the logarithmic differences

between the dummy and the reference. The criterion of acceptance of Geometric Variance (VG = Geometric Variance) for this study is: 1.0 <VG <2.5 (equation 4).

$$VG = \exp\overline{\left(\ln C_{mod} - \ln C_{ref}\right)^2} \quad (4)$$

The correlation coefficient (R) shows the intensity of the linear relationship between two variables, one predicted and the other observed (equation 5). A positive correlation indicates that both variables grow together and a negative correlation indicates that when one variable grows, the other one decreases and the closer to 1.0 the better its correlation. The acceptance criterion of the linear correlation coefficient (R), for this study, is: 0.75 <R.

$$R = \frac{\overline{\left(C_{mod} - \bar{C}_{mod}\right)\left(C_{ref} - \bar{C}_{ref}\right)}}{\sigma c_{mod}\ \sigma c_{ref}} \quad (5)$$

The fraction of predictions that is within factor two (FAC2) demonstrates the amount of the results that are in acceptable levels of values, aligned in time (equation 6). The Fraction Data Acceptance criterion for this study is: 0.75 <FAC2.

$$FAC2 = Fração\ de\ dados\ que\ satisfaz: \qquad 0{,}5 \leq \frac{C_{mod}}{C_{ref}} \leq 2{,}0 \quad (6)$$

The results of the simulation with the WRF model were validated from previously described statistical tests, using METAR data from Ten Airport. Cel. Aviator César Bombonato - Uberlância.

The simulated meteorological variables have their own characteristics, so that different statistical tests are necessary to compose an accurate set of results and base the simulation quality evaluation.

The results of Table 2 show that wind speed and relative humidity adequately met four

of the statistical tests carried out, within the proposed criteria, with a reasonable level of reliability.

The direction of the wind is the most difficult variable to be represented, but even so, there was acceptance of the simulation in at least three of the statistical tests carried out, and not all the statistical tests can evaluate, a variable like this due to the segmentation of values (from 360 to 0º) in the North direction.

Air temperature and atmospheric pressure are the most representative variables, attending five and six statistical tests, respectively (Table 2).

Tabela 2: Results of the statistical tests of the simulation with the WRF

	Wind speed	Wind direction	Temperature	Relative humidity	Atm pressure	Evaluation criteria
FB	-0,089	-0,083	-0,033	-0,008	0,014	- 0,25 ~ 0,25
MG	0,898	1,140	0,990	1,120	1,000	0,75 ~1,25
NMSE	0,375	1,074	0,217	0,196	0,097	0,0 ~ 0,5
VG	1,549	11,654	1,649	1,396	2,394	1,0 ~ 2,5
R	0,502	0,363	0,825	0,221	0,107	~ 1
FAC2	0,481	0,399	0,570	0,569	0,627	~ 1

4.4 Regulatory Conformance of Simulations

The model was simulated using only the conformations determined as regulatory, disabling non-default options and disabling dry deposition and wet deposition (Figure 27).

The setup used as shown in Figure 27 maximizes the resulting concentrations of the model, thus avoiding questioning about underestimated results (conservative approach), and therefore, the configuration is generally considered ideal by environmental agencies.

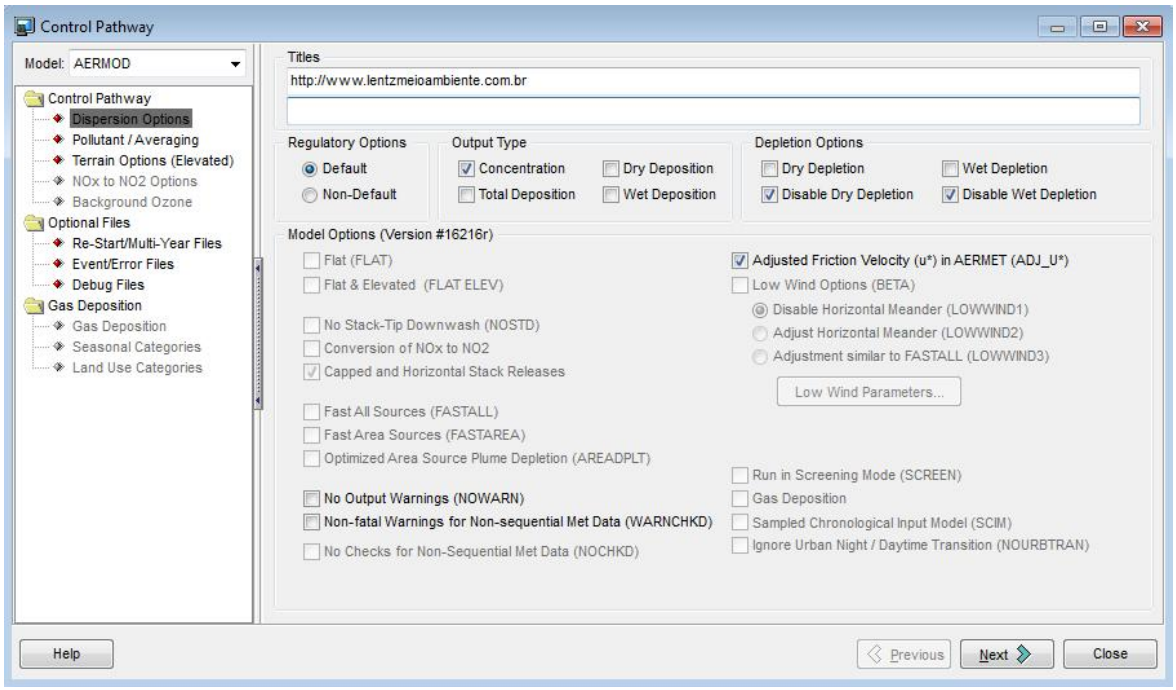

Figure 27: DEFAULT settings for the simulation of particulates emitted into the atmosphere.

4.5 Simulated scenarios

In this Air Dispersion Study (EDA), the emission rates used were provided by the contractor, and the pollutants analyzed were: Carbon Monoxide (CO), Total Reduced Sulfur (TRS), Nitrogen Oxides (NOx expressed as NO_2), Total Suspended Particles and Sulfur Oxides (SO_X expressed as SO_2).

In this study, a scenario of the current condition was not simulated due to the lack of an on-site project, so the simulated scenario corresponds to the future project condition (Figure 28).

Tabela 3: Simulated Scenarios in the Atmospheric Dispersion Study

Scenario	DESCRIÇÃO
CURRENT	No on-site ventures, no emissions to simulate. NOT SIMULATED SCENARIO
FUTURE	Emissions from the operation of the project.

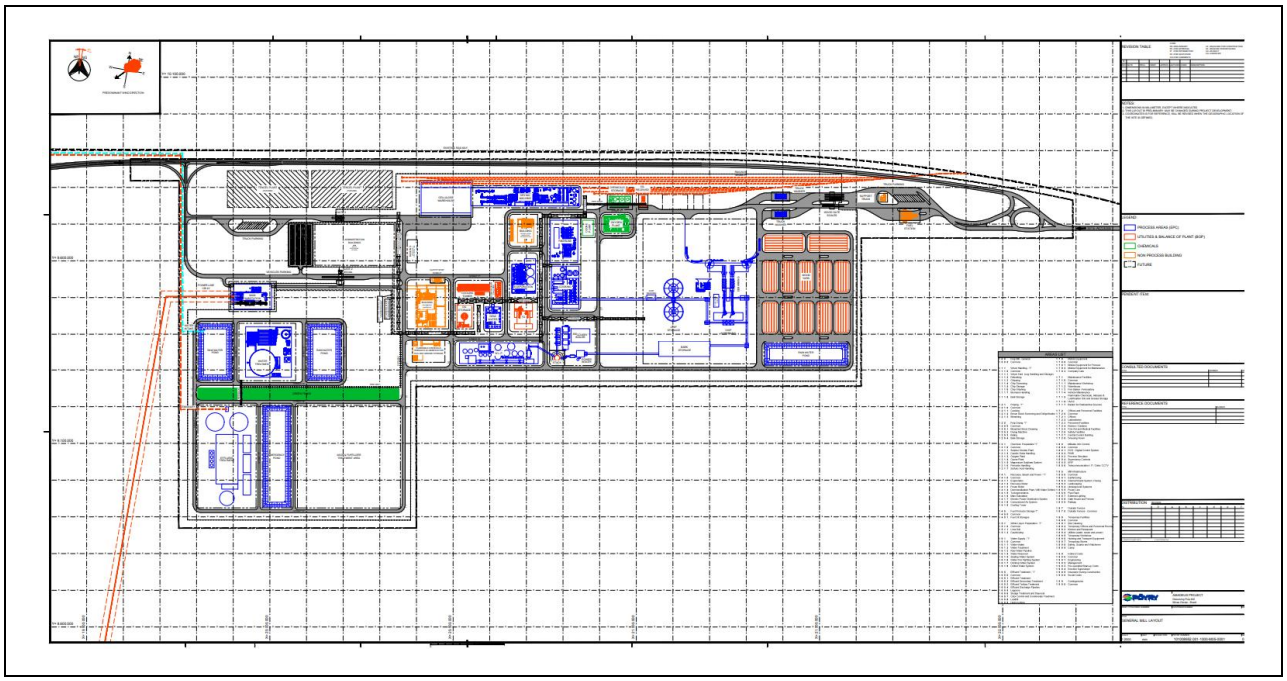

Figure 28: Projected Unit Design Layout.

4.6 Downwash effect

Buildings or other barriers near sources of emission may cause high concentrations of pollutants due to the formation of a vortex to leeward of the obstacle and the formation of a turbulent flow. This effect is known as downwash. These vortices carry part of the

plume to the surface by raising concentrations in their areas of influence. The AERMOD incorporates the Plume Rise Model Enhancements (PRIME) algorithms to estimate the accelerated growth and restraint of the plume rise due to the leeward formed vortices of the buildings.

Figure 29 presents a mock-up representative of the downwash effect on buildings caused by a low chimney (a), the respective computational simulation of that effect (b), and an example of a suitable chimney height source (c).

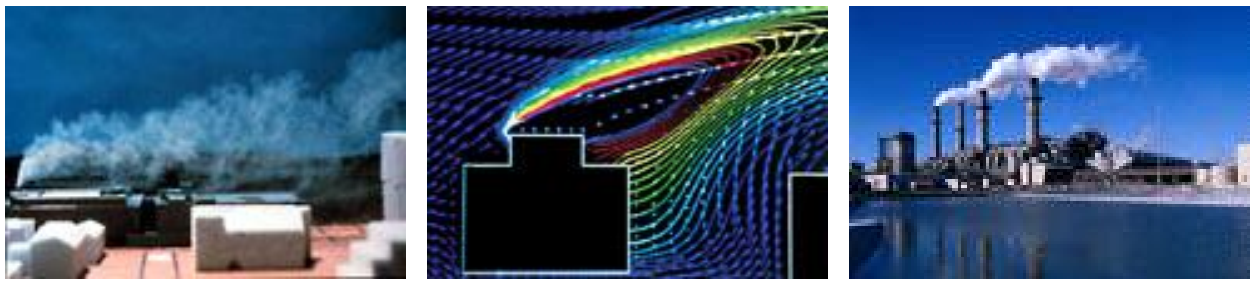

(a) (b) (c)

Figure 29: (a) simulation of the downwash effect in a model, (b) simulation of the downwash effect in a computational modeling, and c) displacement of the plume without downwash effect.

PRIME divides the mass of the boom between the region of the vortex and the region of the boom. The vortex dispersion is based on the geometry of the building and the vertical is assumed to be uniform. At the border of the vortex region part of the mass is emitted into the turbulent region. This mass is combined with the mass of the plume that has not been captured by the vortex and therefore dispersed with a propagation rate based on the source location, launch height and geometry of the building. A probability density function model and a vortex diffusion model are used to analyze the turbulent flow near and far, respectively.

The rise of the boom for buildings-influenced fountains is estimated by a model that includes deflection of the current line near the building, vertical shear of wind speed, increase of dilution from turbulent flow and loss of velocity. In general these effects induced by buildings act in a way to restrict the rise that the pen would have in the absence of the building.

The total concentration is given by a weighted sum of the concentrations obtained by the AERMOD (without considering the influence of the buildings) and PRIME (considering the influence of the buildings):

$$C_{Total} = \gamma\, C_{Prime} + (1-\gamma)\, C_{AERMOD}$$

The weight factor (γ) is obtained so that the PRIME contribution decreases exponentially as the boom moves away from the building (lateral and vertically), following the wind. The weight factor is calculated as:

$$\gamma = \exp\left(\frac{-(x-\sigma_{xg})^2}{2\sigma_{xg}^2}\right) \exp\left(\frac{-(y-\sigma_{yg})^2}{2\sigma_{yg}^2}\right) \exp\left(\frac{-(z-\sigma_{zg})^2}{2\sigma_{zg}^2}\right)$$

Where x is the distance dimension of the plume following the direction of the wind, y is the perpendicular dimension to the wind and z is the height of the receiver with respect to the ground.

The downwash effect was considered in this study due to the existence of buildings of significant dimensions and sufficiently close to the simulated sources that have potential influence in the formation of turbulent vortices to leeward. Data from nearby buildings for downwash processing were provided by the contractor.

In Figure 30 we have the schematic diagram with the locations of the buildings (in blue) and emission sources (in red) of the simulated scenario. Table 5 shows the coordinates of the buildings considered.

Table 4: Buildings description.

Building	Description
BLD_1	Biomass silo
BLD_2	Biomass silo
BLD_3	Fiber line
BLD_4	Evaporation
BLD_5	Caustizing

Building	Description
BLD_6	Turbogenerators
BLD_7	Water treatment plant
BLD_8	Effluent treatmente plant
BLD_9	Cooling tower
BLD_10	Office and control room
BLD_11	Warehouse

Tabela 5: Buildings used to calculate the downwash.

BUILDING	ELEVATION (m)	HIGHT (m)	UTM E (m)	UTM N (m)	X (m)	Y (m)
BLD_1	14,73	36,0	386464	7805908	31,0	97,0
BLD_2	15,97	27,0	386469	7805826	100,0	47,0
BLD_3	14,02	22,0	386525	7805629	34,0	114,0
BLD_4	14,95	16,0	386486	7805672	19,0	54,0
BLD_5	15,07	20,0	386480	7805575	21,0	78,0
BLD_6	23,26	78,0	386592	7805819	30,0	50,0
BLD_7	24,37	78,0	386630	7805808	35,0	70,0
BLD_8	26,58	78,0	386676	7805808	30,0	65,0
BLD_9	29,81	40,0	386758	7805843	18,0	33,0
BLD_10	28,81	40,0	386759	7805803	33,0	36,0
BLD_11	15,33	6,0	386617	7805659	40,0	10,0

Figure 30: Schematic diagram of the location of nearby buildings (in blue) and emission sources (in red).

Source: Google Earth.

4.7 Emission rate

The dispersion study considered all sources proposed in the project (Figure 28) provided by the contractor and presented in the environmental licensing process (Table 6). Table 7 shows the location of the source, height, diameter, temperature and emission velocity of simulated point sources in the FUTURE scenario. Table 8 presents the emission rates for the FUTURE scenario and, as Table 9 presents the same emission rates per unit volume.

Tabela 6: Data input sources simulated areas.

SOURCE	REFERÊNCE
BIO_01	Biomass Boiler
REC_01	Recovery Boiler
CAL_01	Lime Kiln

Tabela 7: Input data from simulated area sources in the FUTURE scenario.

SOURCE	Coordinators			Hight (m)	Temperature (K)	Velocity (m/s)	Diameter (m)
	UTMX (m)	UTMY (m)	ELEVATION (m)				
BIO_01	193118	7914917	989,00	90,0	443,0	20,0	2,37
REC_01	193115	7914921	989,00	90,0	473,0	20,0	5,67
CAL_01	193114	7914916	989,00	90,0	573,0	20,0	2,14

Tabela 8: Emission rates by simulated sources in the FUTURE scenario.

	Emission rates (g/s)				
	CO	MP	NOX	SOX	ERT
BIO_01	-	4,00	20,00	12,50	-
REC_01	105,00	21,00	120,00	24,00	3,40
CAL_01	-	2,80	14,00	7,00	0,80

Tabela 9: Emission rates per unit volume in the FUTURE scenario.

	Emission rates (mg/Nm^3)				
	CO	MP	NOX	SOX	ERT
BIO_01	-	80,00	400,00	250,00	-
REC_01	350,00	70,00	400,00	80,00	11,30
CAL_01	-	80,00	400,00	200,00	22,60

5 RESULTS

Air Quality Monitoring in the State of Minas Gerais

In advance of the results presentation, it is reported that, in order to monitor air quality in the state of Minas Gerais, FEAM operates a network consisting of 10 automatic stations located in the RMBH, as well as 19 other automatic stations installed in 6 other municipalities . Automatic monitoring area includes the following municipalities: Belo Horizonte, Betim, Contagem, Ibirité, Ipatinga, Itabira, Paracatu, São José da Lapa, Timóteo. These stations are very distant from the area focused in this work, not being representative of the quality. For this reason, this data was not used work. The air quality diagnosis in the area of the mill was carried out by means of self-monitoring, and primary data were generated during two distinct campaigns, each lasting seven consecutive days.

Applicable Air Quality Standards

The simulations results are analyzed for the purpose of determining the environmental compliance of the ambient concentrations resulting from the simulated units atmospheric emissions. The ambient air quality assessment was carried out in accordance with the criteria established in accordance with CONAMA Resolution 03/1990, once the State of Minas Gerais established it through COPAM NORMATIVE RESOLUTION No. 187 of 09/19/2013 (transcribed partially to follow).

"Air quality monitoring is performed to determine the concentration level of a universally recognized pollutants group as indicators, selected because of their increased frequency of occurrence in the atmosphere and the adverse effects they cause to the environment. They are: particulate matter (dust), sulfur dioxide (SO_2), carbon monoxide (CO), oxides of nitrogen (NOx), hydrocarbons (HC) and ozone (O_3).

For each of these substances, air quality standards have been defined, ie maximum concentration limits which, when exceeded, can affect the health, safety and well-being of the population, as well as causing damage to the environment in general . In Brazil, air quality standards were set by the National Environment Council (CONAMA), through Resolution CONAMA 03/90, and they were also adopted in Minas Gerais[1]."

As stated in CONAMA Resolution No. 3/1990, the differentiated application of primary and secondary standards requires that the national territory be divided into classes I, II and III according to the intended use. The same resolution also provides that as long as the classification of areas is not established, the applicable standards will be the primary[2].

Therefore, taking into account the FEAM and the Ministry of Cities considerations, in this work, the primary air quality standards defined by res. CONAMA 03/1990.

[1] http://www.feam.br/noticias/1/1329-qualidade-do-ar, (acesso 7/6/2018)
[2] http://www.mma.gov.br/cidades-sustentaveis/qualidade-do-ar/padroes-de-qualidade-do-ar (acesso 7/6/2018)

The simulations results of the 5 maximum concentrations of each of the parameters evaluated in distinct (independent) receivers are presented from Table 10 to Table 14. In Annex A, we present the concentration isolates of the simulations performed, to determine the location of the simulated maximum concentrations. In Annex B, the tables are presented with the 50 maximum short-term concentrations and the 10 maximum long-term (annual) concentrations.

Table 10:. Maximum concentrations (μg/m^3) at different receptors for CO in the FUTURE scenario

Period		Maximum concentration			CONAMA 03/90	
		UTMX	UTMY	Concentration	Primary Standard	Secudary Standard
01 h	1ª Máx	193375	7914375	78,3564	40 000 (μg/m^3)	40 000 (μg/m^3)
	2ª Máx	193375	7915375	76,2697		
	3ª Máx	193375	7915625	73,7879		
	4ª Máx	192625	7914375	71,5329		
	5ª Máx	192875	7914375	70,8502		
08 h	1ª Máx	193375	7915625	45,1198	10 000 (μg/m^3)	10 000 (μg/m^3)
	2ª Máx	192625	7914375	43,7238		
	3ª Máx	192375	7914125	37,5749		
	4ª Máx	192625	7913875	37,2239		
	5ª Máx	192625	7914125	35,7880		

Table 11: Maximum concentrations (μg/m^3) at different receptors for NO_X in the FUTURE scenario.

Period		Maximum concentration			CONAMA 03/90	
		UTMX	UTMY	Concentration	Primary Standard	Secudary Standard
01 h	1ª Máx	193375	7914375	136,6148	320 (μg/m^3)	190 (μg/m^3)
	2ª Máx	192625	7914375	116,8077		
	3ª Máx	193500	7915500	115,1345		
	4ª Máx	193375	7915375	112,7259		
	5ª Máx	193625	7915875	106,5896		
Anual	1ª Máx	192625	7914125	8,1550	100 (μg/m^3)	100 (μg/m^3)
	2ª Máx	192875	7914375	8,1405		
	3ª Máx	192875	7914125	7,5925		
	4ª Máx	192500	7914000	7,4946		
	5ª Máx	192625	7914375	7,4469		

Table 12: Maximum concentrations (μg/m^3) at different receptors for PTS in the FUTURE scenario.

Scenario	24 h	Maximum concentration			CONAMA 03/90	
		UTMX	UTMY	Concentration	Primary Standard	Secudary Standard
24 h	1ª Máx	192375	7914375	7,5171	240 (μg/m^3)	150 (μg/m^3)
	2ª Máx	192375	7915125	7,1099		
	3ª Máx	192625	7914125	7,0823		
	4ª Máx	192625	7914375	6,9328		
	5ª Máx	192500	7914500	6,8361		
Anual	1ª Máx	192875	7914375	1,5347	80 (μg/m^3)	60 (μg/m^3)
	2ª Máx	192625	7914125	1,5316		
	3ª Máx	192625	7914375	1,4162		
	4ª Máx	192875	7914125	1,4128		
	5ª Máx	192500	7914000	1,4068		

Table 13: Maximum concentrations (μg/m^3) at different receptors for SOx in the FUTURE scenario.

Scenario	24h	Maximum concentration			CONAMA 03/90	
		UTMX	UTMY	Concentration	Primary Standard	Secudary Standard
24 h	1ª Máx	192375	7914375	15,9987	365 (μg/m^3)	100 (μg/m^3)
	2ª Máx	192375	7915125	15,4757		
	3ª Máx	192500	7914500	15,2555		
	4ª Máx	192625	7914375	15,0559		
	5ª Máx	192625	7914125	14,6217		
Anual	1ª Máx	192875	7914375	3,2798	80 (μg/m^3)	40 (μg/m^3)
	2ª Máx	192625	7914125	3,1975		
	3ª Máx	192625	7914375	3,1819		
	4ª Máx	192500	7914000	2,9258		
	5ª Máx	192875	7914125	2,7816		

The Total Reduced Sulfur (TRS) is a gas that does not have an air quality standard defined by the CONAMA 03/90 resolution, so the LPO (Odor Perception Limit) provided by CETESB's chemical registration card was used. TRS concentrations were below the established value for LPO (Table 14).

Table 14: Maximum concentrations (μg/m^3) at different receptors for TRS in the FUTURE scenario.

1h	Maximum concentration			Odor Perception Limit
	UTMX	UTMY	Concentration	CETESB[3]
1ª Máx	193375	7914375	3,6136	6,55 (0,0047 ppm)
2ª Máx	192625	7914375	3,1556	
3ª Máx	193500	7915500	3,0772	
4ª Máx	192625	7915375	3,0332	
5ª Máx	193625	7915875	2,8192	

[3] Material Safety Data SheetFicha de Informação of CETESB, obtained on web site: http://sistemasinter.cetesb.sp.gov.br/produtos/ficha_completa1.asp?consulta=SULFETO%20DE%20HIDROG%CANIO

5.1 Discrete Receivers Results

The simulations results are analyzed for the purpose of determining the ambient concentrations environmental compliance resulting from the atmospheric emissions of the simulated units.

The results of the parameter-separated simulations in discrete receivers are shown below:

Table 15: Maximum concentrations (μg / m^3) in discrete receivers placed at the critical points for CO in the FUTURE scenario.

Duration		Maximum concentration			CONAMA 03/90	
		UTMX	UTMY	Concentration	Primary Standard	Secudary Standard
01 h	RECP_01	189623	7910157	15,1400	40 000 (μg/m^3)	40 000 (μg/m^3)
	RECP_02	194298	7907130	11,9414		
	RECP_03	195643	7907779	12,5158		
	RECP_04	188397	7913871	17,5899		
	RECP_05	187749	7910803	13,3895		
	RECP_06	204960	7930177	8,8148		
	RECP_07	216219	7925259	5,9940		
	RECP_08	198458	7924119	10,4454		
	RECP_09	192887	7891741	4,5171		
	RECP_10	162359	7935846	4,9518		
	RECP_11	154938	7907156	4,6535		
	RECP_12	219301	7878211	4,7817		
08 h	RECP_01	189623	7910157	3,6723	10 000 (μg/m^3)	10 000 (μg/m^3)
	RECP_02	194298	7907130	3,0600		
	RECP_03	195643	7907779	2,7533		
	RECP_04	188397	7913871	5,9513		
	RECP_05	187749	7910803	4,8865		
	RECP_06	204960	7930177	2,0212		
	RECP_07	216219	7925259	1,3099		
	RECP_08	198458	7924119	1,9235		
	RECP_09	192887	7891741	1,5360		
	RECP_10	162359	7935846	1,2857		
	RECP_11	154938	7907156	1,6742		
	RECP_12	219301	7878211	1,2945		

Table 16: Maximum concentrations (μg / m^3) in discrete receivers placed at the critical points for NOx in the FUTURE scenario.

Duration		Maximum concentration			Padrão CONAMA 03/90	
		UTMX	UTMY	Concentration	Primary Standard	Secudary Standard
01 h	RECP_01	189623	7910157	25,0213	320 (μg/m^3)	190 (μg/m^3)
	RECP_02	194298	7907130	19,2153		
	RECP_03	195643	7907779	20,4886		
	RECP_04	188397	7913871	28,7666		
	RECP_05	187749	7910803	22,3178		
	RECP_06	204960	7930177	15,4520		
	RECP_07	216219	7925259	10,2593		
	RECP_08	198458	7924119	19,2709		
	RECP_09	192887	7891741	7,2701		
	RECP_10	162359	7935846	8,4056		
	RECP_11	154938	7907156	8,0335		
	RECP_12	219301	7878211	8,0534		
Anual	RECP_01	189623	7910157	0,8024	100 (μg/m^3)	100 (μg/m^3)
	RECP_02	194298	7907130	0,2654		
	RECP_03	195643	7907779	0,2354		
	RECP_04	188397	7913871	0,5287		
	RECP_05	187749	7910803	0,5855		
	RECP_06	204960	7930177	0,0650		
	RECP_07	216219	7925259	0,0599		
	RECP_08	198458	7924119	0,0997		
	RECP_09	192887	7891741	0,1171		
	RECP_10	162359	7935846	0,1091		
	RECP_11	154938	7907156	0,2194		
	RECP_12	219301	7878211	0,0425		

Table 17: Maximum concentrations (μg / m^3) in discrete receivers placed at the critical points for PTS in the FUTURE scenario.

Scenario	24 h	Maximum concentration			CONAMA 03/90	
		UTMX	UTMY	Concentration	Primary Standard	Secudary Standard
24 h	RECP_01	189623	7910157	0,6693	240 (μg/m^3)	150 (μg/m^3)
	RECP_02	194298	7907130	0,4687		
	RECP_03	195643	7907779	0,3752		
	RECP_04	188397	7913871	1,2340		
	RECP_05	187749	7910803	0,8131		
	RECP_06	204960	7930177	0,2401		
	RECP_07	216219	7925259	0,1306		
	RECP_08	198458	7924119	0,3777		
	RECP_09	192887	7891741	0,2600		
	RECP_10	162359	7935846	0,1970		
	RECP_11	154938	7907156	0,2078		
	RECP_12	219301	7878211	0,1550		
Anual	RECP_01	189623	7910157	0,1476	80 (μg/m^3)	60 (μg/m^3)
	RECP_02	194298	7907130	0,0483		
	RECP_03	195643	7907779	0,0430		
	RECP_04	188397	7913871	0,0985		
	RECP_05	187749	7910803	0,1085		
	RECP_06	204960	7930177	0,0119		
	RECP_07	216219	7925259	0,0109		
	RECP_08	198458	7924119	0,0182		
	RECP_09	192887	7891741	0,0213		
	RECP_10	162359	7935846	0,0200		
	RECP_11	154938	7907156	0,0405		
	RECP_12	219301	7878211	0,0078		

Table 18: Maximum concentrations (μg / m^3) in discrete receivers placed at the critical points for SOx in the FUTURE scenario.

Scenario	24h	Maximum concentration			CONAMA 03/90	
		UTMX	UTMY	Concentration	Primary Standard	Secudary Standard
24 h	RECP_01	189623	7910157	1,3193	365 (μg/m^3)	100 (μg/m^3)
	RECP_02	194298	7907130	1,0339		
	RECP_03	195643	7907779	0,9854		
	RECP_04	188397	7913871	2,2944		
	RECP_05	187749	7910803	1,4852		
	RECP_06	204960	7930177	0,4128		
	RECP_07	216219	7925259	0,2442		
	RECP_08	198458	7924119	0,8092		
	RECP_09	192887	7891741	0,4426		
	RECP_10	162359	7935846	0,3401		
	RECP_11	154938	7907156	0,4181		
	RECP_12	219301	7878211	0,2685		
Anual	RECP_01	189623	7910157	0,2676	80 (μg/m^3)	40 (μg/m^3)
	RECP_02	194298	7907130	0,0816		
	RECP_03	195643	7907779	0,0737		
	RECP_04	188397	7913871	0,1960		
	RECP_05	187749	7910803	0,2071		
	RECP_06	204960	7930177	0,0202		
	RECP_07	216219	7925259	0,0182		
	RECP_08	198458	7924119	0,0314		
	RECP_09	192887	7891741	0,0353		
	RECP_10	162359	7935846	0,0356		
	RECP_11	154938	7907156	0,0759		
	RECP_12	219301	7878211	0,0133		

Table 19: Maximum concentrations (μg / m^3) in discrete receivers placed at the critical points for TRS in the FUTURE scenario

Scenario	1h	Maximum concentration			LPO[4]
		UTMX	UTMY	Concentration	Ficha CETESB[5]
1h	RECP_01	189623	7910157	0,66769	6,55 (0,0047 ppm)
	RECP_02	194298	7907130	0,51579	
	RECP_03	195643	7907779	0,54683	
	RECP_04	188397	7913871	0,76903	
	RECP_05	187749	7910803	0,59256	
	RECP_06	204960	7930177	0,40796	
	RECP_07	216219	7925259	0,27230	
	RECP_08	198458	7924119	0,49197	
	RECP_09	192887	7891741	0,19505	
	RECP_10	162359	7935846	0,22099	
	RECP_11	154938	7907156	0,21162	
	RECP_12	219301	7878211	0,21417	

[4] LPO: Limite de Percepção de Odor
[5] Ficha de Informação de Produto Químico da CETESB, obtida no site: http://sistemasinter.cetesb.sp.gov.br/produtos/ficha_completa1.asp?consulta=SULFETO%20DE%20HIDROG%CANIO

6 CONCLUSION

The simulations results presented concentrations within the limits established by the (more restrictive) secondary standard of the CONAMA 03/90 resolution for all the simulated pollutants (CO, PTS, SO_2 and NO_2), being therefore in environmental compliance with the COPAM 187 of 19/09/2013.

In the case of the TRS, there is no standard defined by national legislation. However, it is known that H_2S, a gas that falls within the category of TRS, has an odor perception threshold of 6.55 µg/m^3. As can be seen above in item 5, the maximum concentration is on the order of 50% of this limit.

7 TECHNICAL TEAM

George Lentz César Fruehauf

Bacharel em Matemática	IM/UFRJ
Mestrado em Meteorologia	SJSU/USA
Doutorado em Geografia	FFLCH/USP
Engenharia Ambiental	USM/SP
CREA-SP: 5062008073	REGISTRO IBAMA: 573856

Daniel Constantino Zacharias

Bacharel em Meteorologia	IAG/USP
Mestrado em Meteorologia	IAG/USP
Doutorado em Meteorologia	IAG/USP
CREA-SP: 5063075757	REGISTRO IBAMA: 638533

BIBLIOGRAPHIC REFERENCES

CONAMA 03/1990 – Resolução do Conselho Nacional de Meio Ambiente

LAKES Environmental Software (2007).User's Guide ISC-AERMod View.

US EPA (1987).Environmental Protection Agency, 1987.On-Site Meteorological Program Guidance for Regulatory Modeling Applications, EPA - 450/4-87-013.

US EPA (2007).AERMOD Modeling System (acesso 19/06/2007)

http://www.epa.gov/scram001/dispersion_prefrec.htm#aermod.

ANNEX A: SPACE DISTRIBUTION OF POLLUTANT CONCENTRATIONS

Figure 31: Spatial distribution of the average 1h of the CO concentration in the image 40 km x 40 km, with the maximum concentration highlighted and the unit boundaries in red, white relief isolines, in the FUTURO scenario.

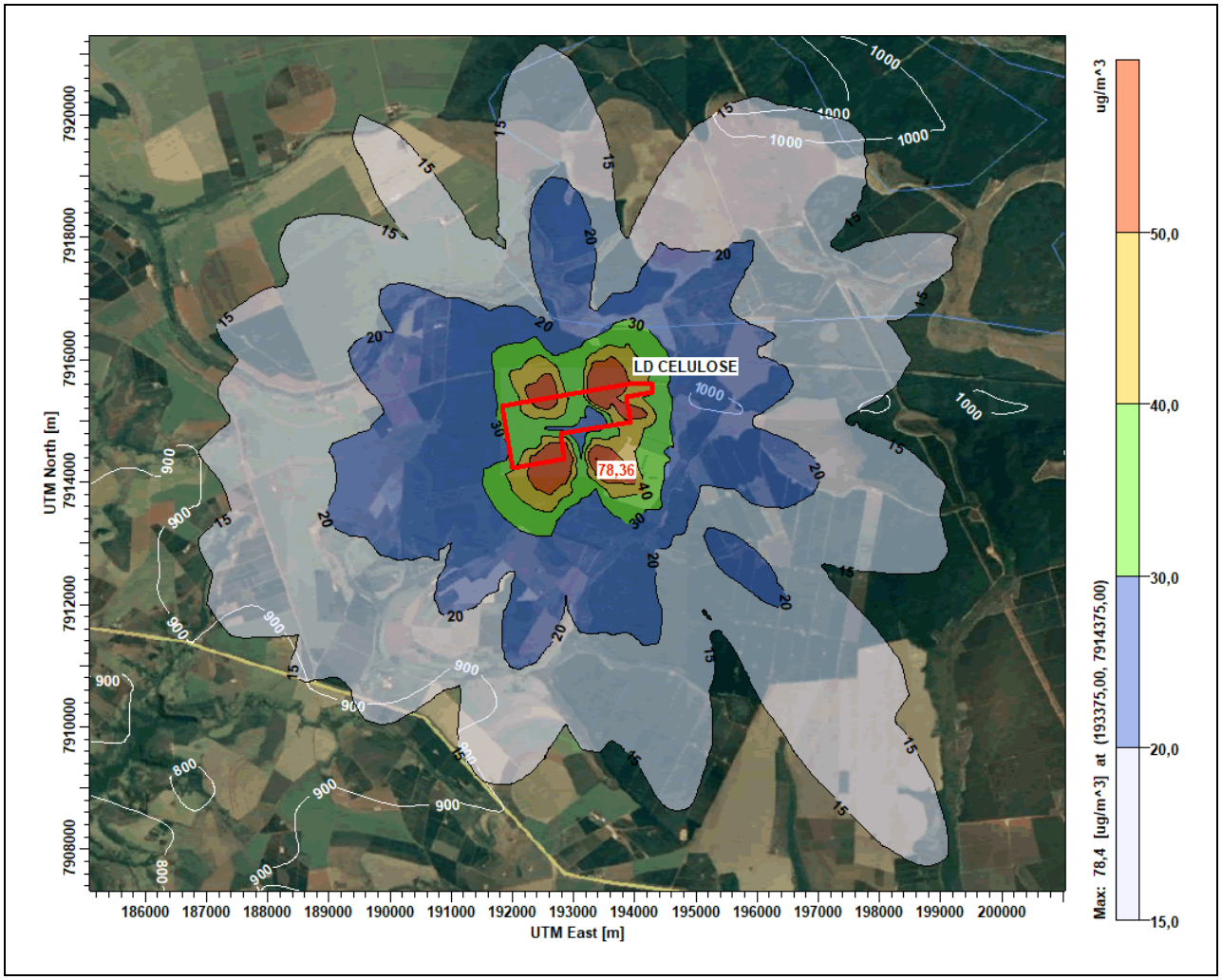

Figure 32: Spatial distribution of the average 1h of the CO concentration in the image 10 km x 10 km, with the maximum concentration highlighted and the unit boundaries in red, white relief isolines, in the FUTURO scenario.

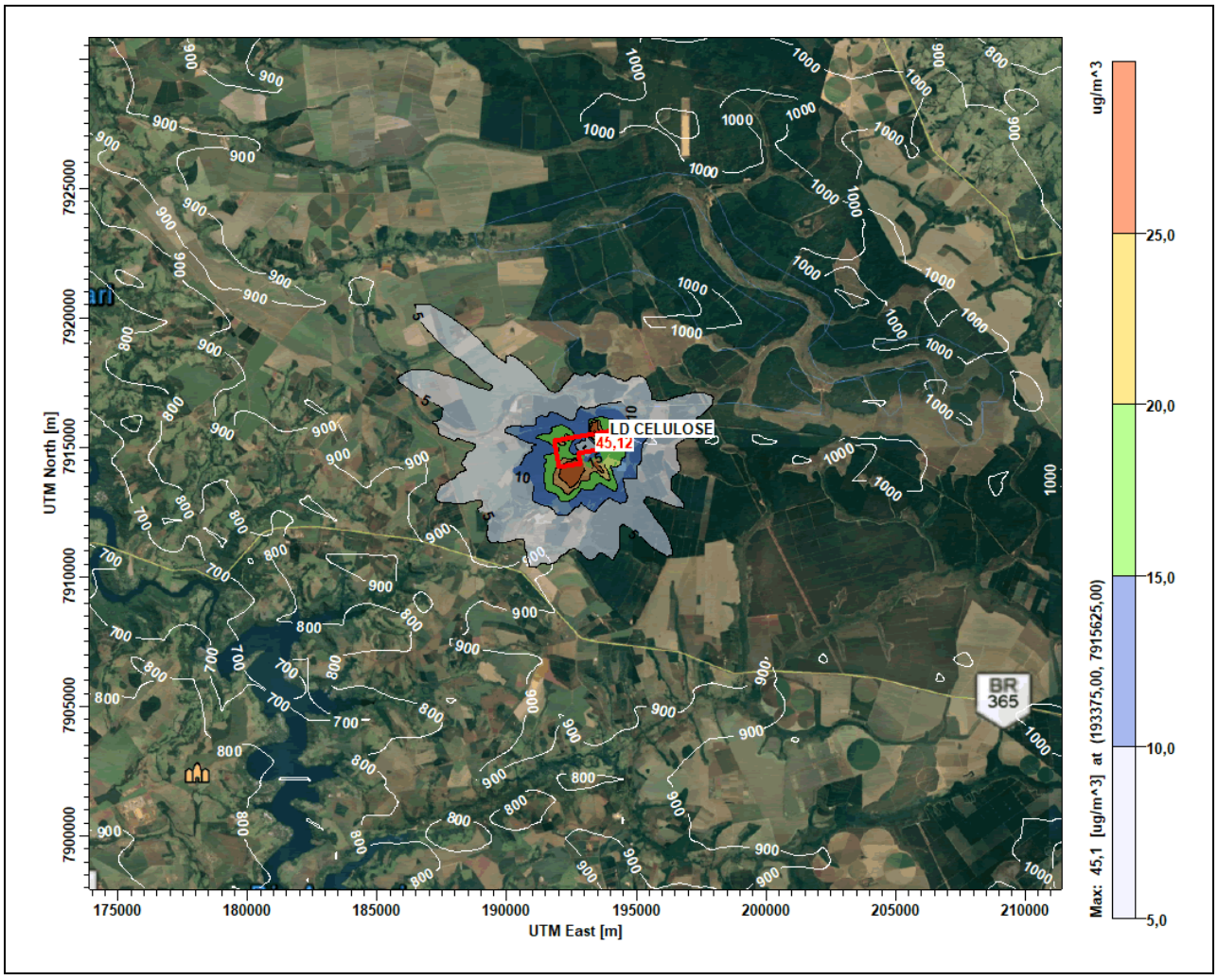

Figure 33: Spatial distribution of the average 8h of the CO concentration in the image 40 km x 40 km, with the maximum concentration highlighted and the unit boundaries in red, white relief isolines, in the FUTURO scenario

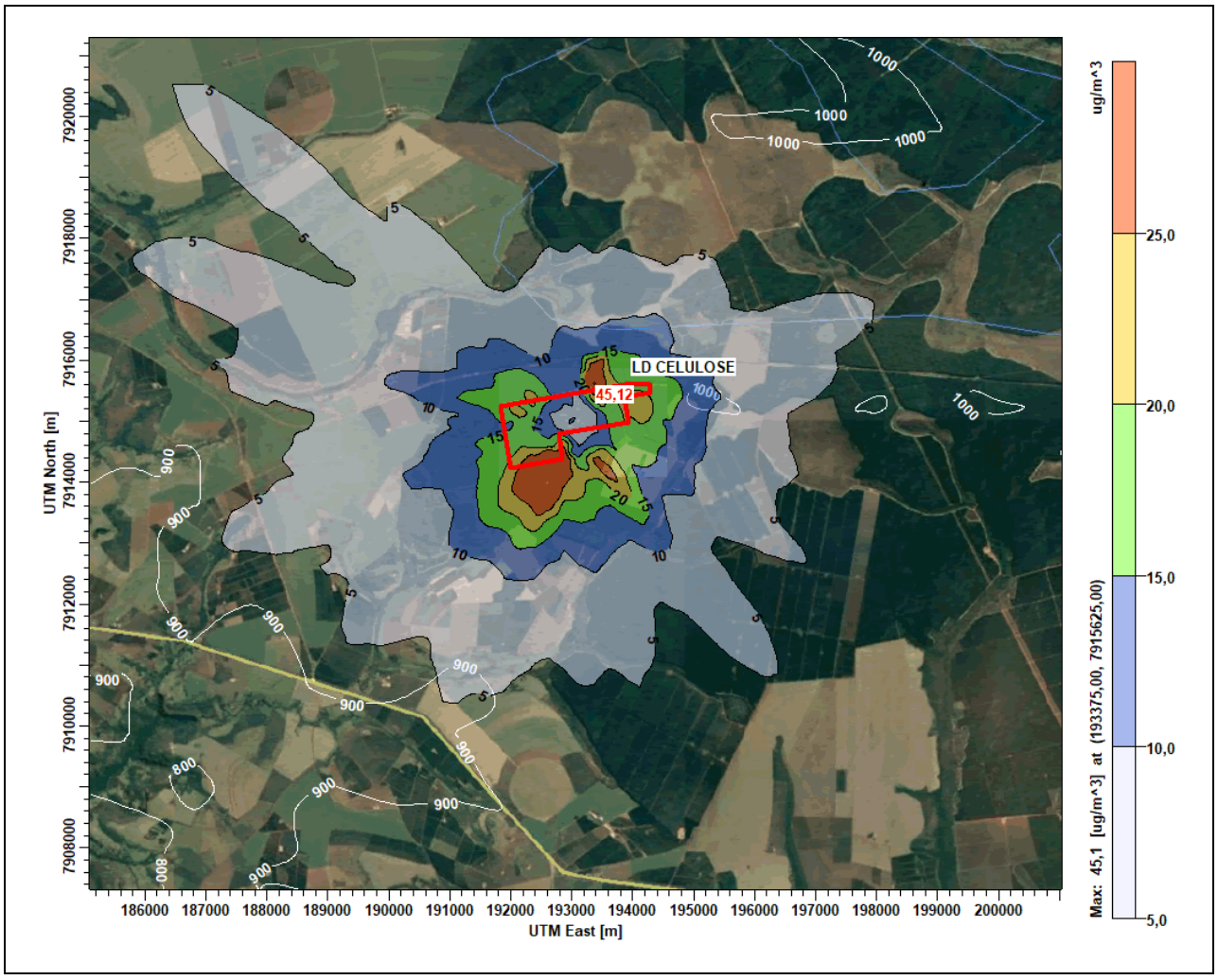

Figure 34: Spatial distribution of the average 8h of the CO concentration in the image 10 km x 10 km, with the maximum concentration highlighted and the unit boundaries in red, white relief isolines, in the FUTURO scenario

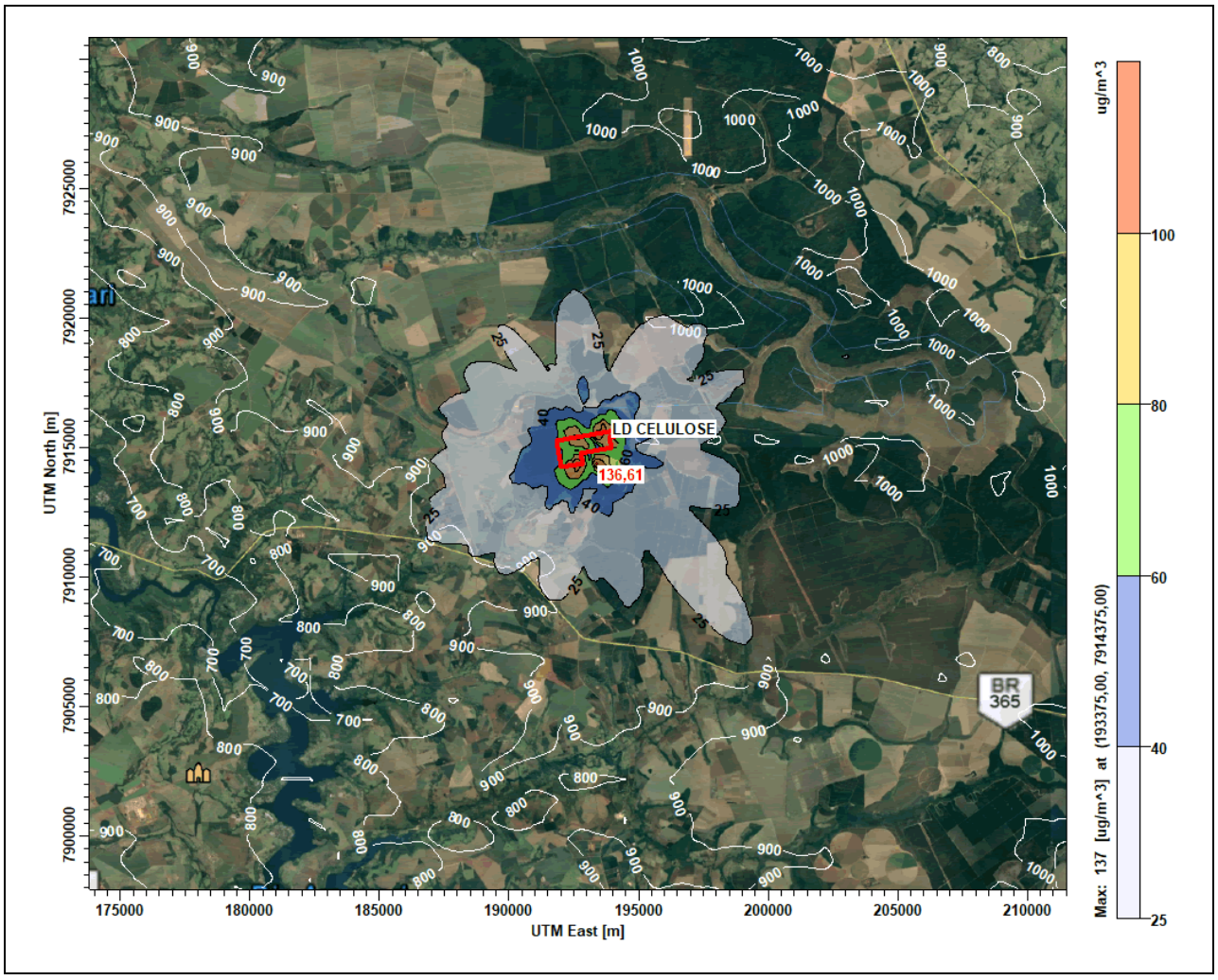

Figure 35: Spatial distribution of the average 1h of the NOx concentration in the image 40 km x 40 km, with the maximum concentration highlighted and the unit boundaries in red, white relief isolines, in the FUTURO scenario

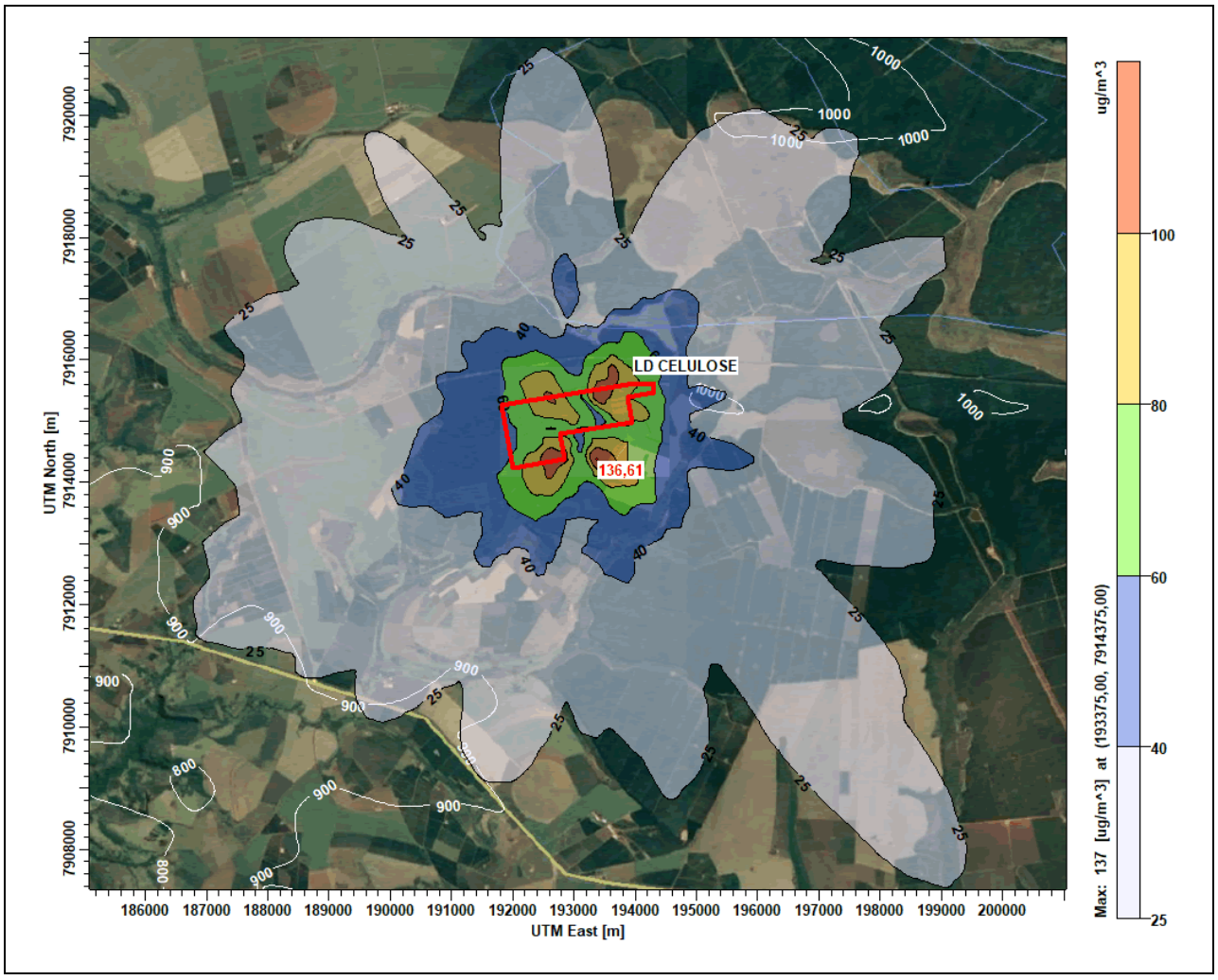

Figure 36: Spatial distribution of the average 1h of the NOx concentration in the image 10 km x 10 km, with the maximum concentration highlighted and the unit boundaries in red, white relief isolines, in the FUTURO scenario.

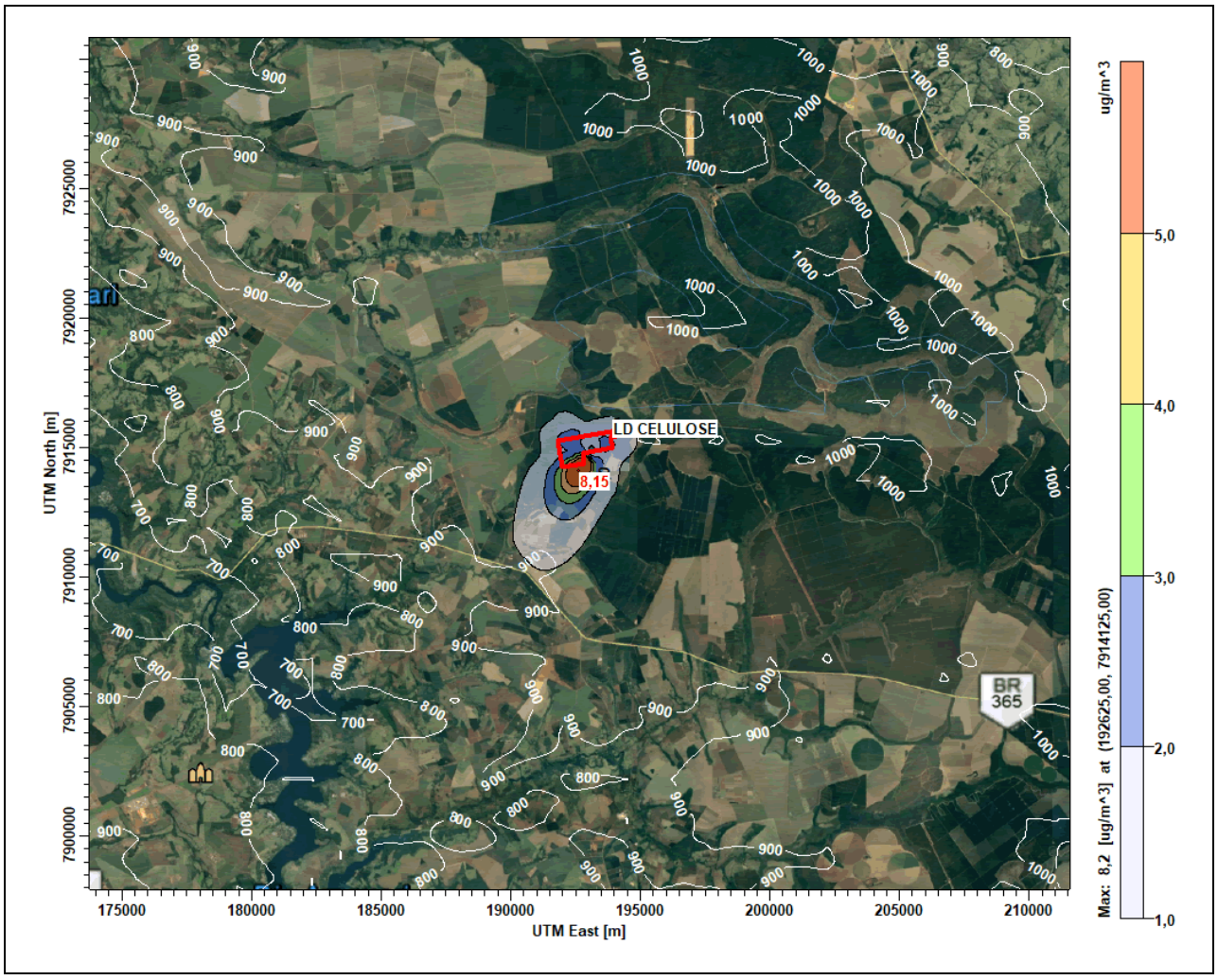

Figure 37: Spatial distribution of the annual average of the NOx concentration in the image 40 km x 40 km, with the maximum concentration highlighted and the unit boundaries in red, white relief isolines, in the FUTURO scenario

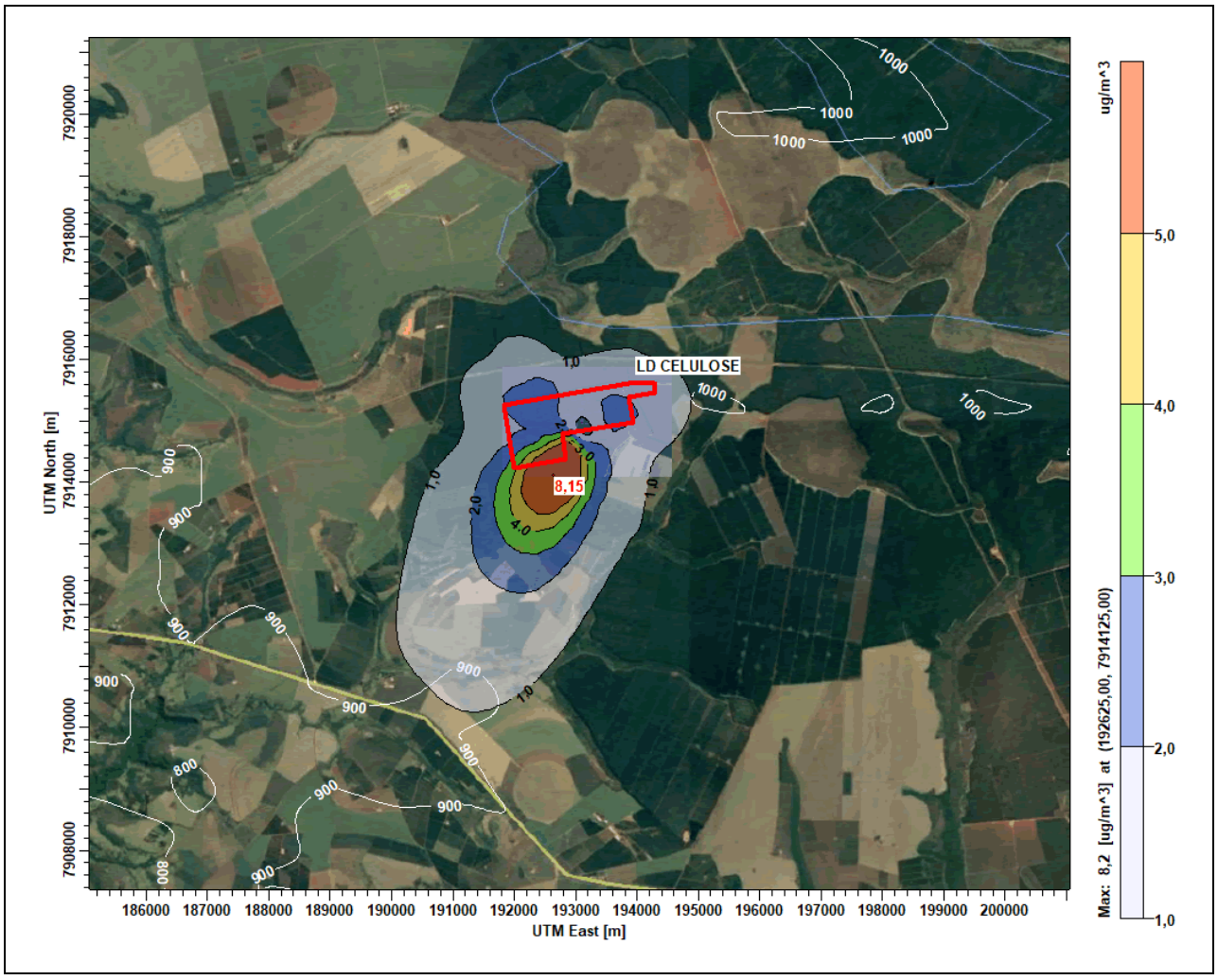

Figure 38: Spatial distribution of the annual average of the NOx concentration in the image 10 km x 10 km, with the maximum concentration highlighted and the unit boundaries in red, white relief isolines, in the FUTURO scenario

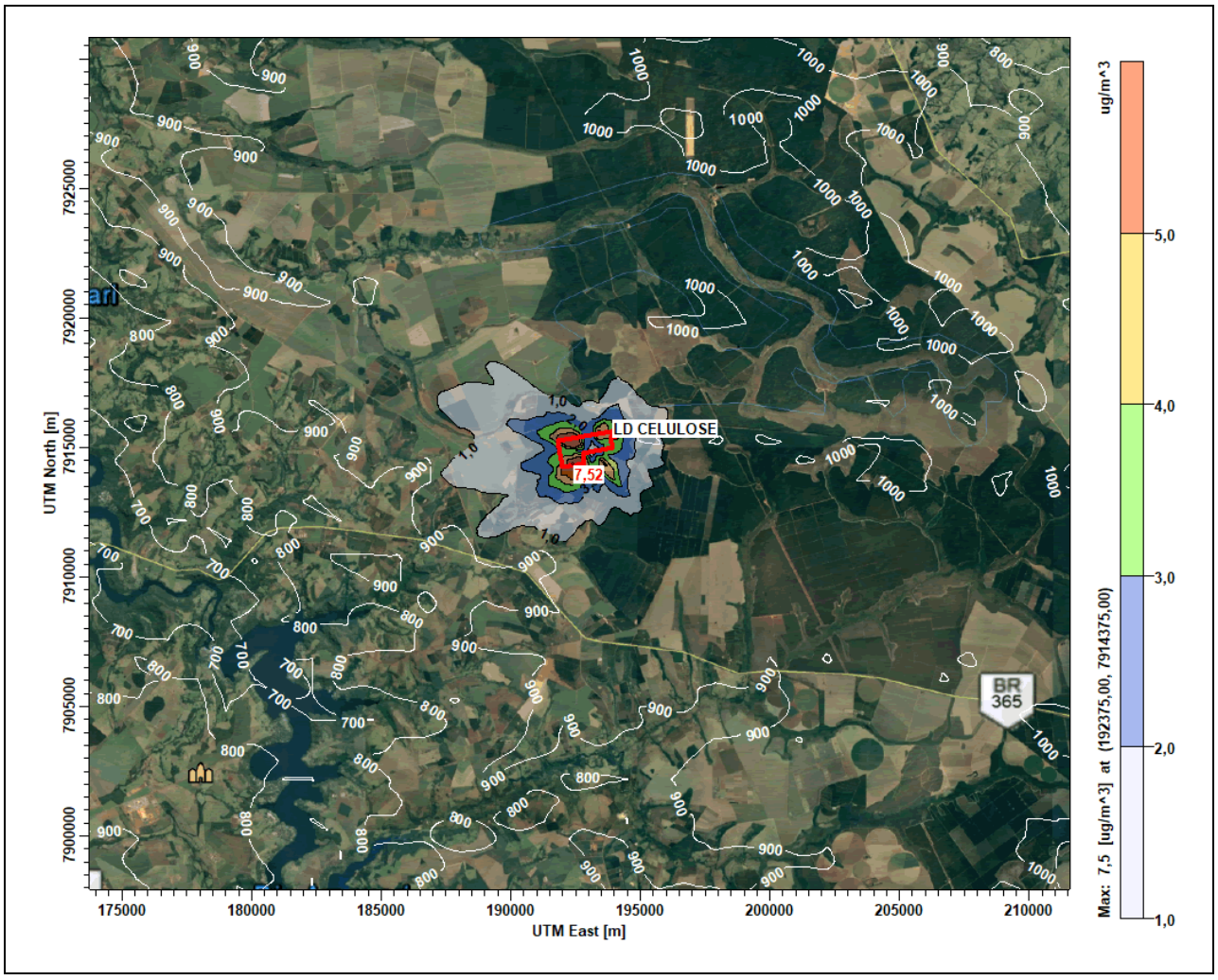

Figure 39: Spatial distribution of the average 24h of the PTS concentration in the image 40 km x 40 km, with the maximum concentration highlighted and the unit boundaries in red, white relief isolines, in the FUTURO scenario

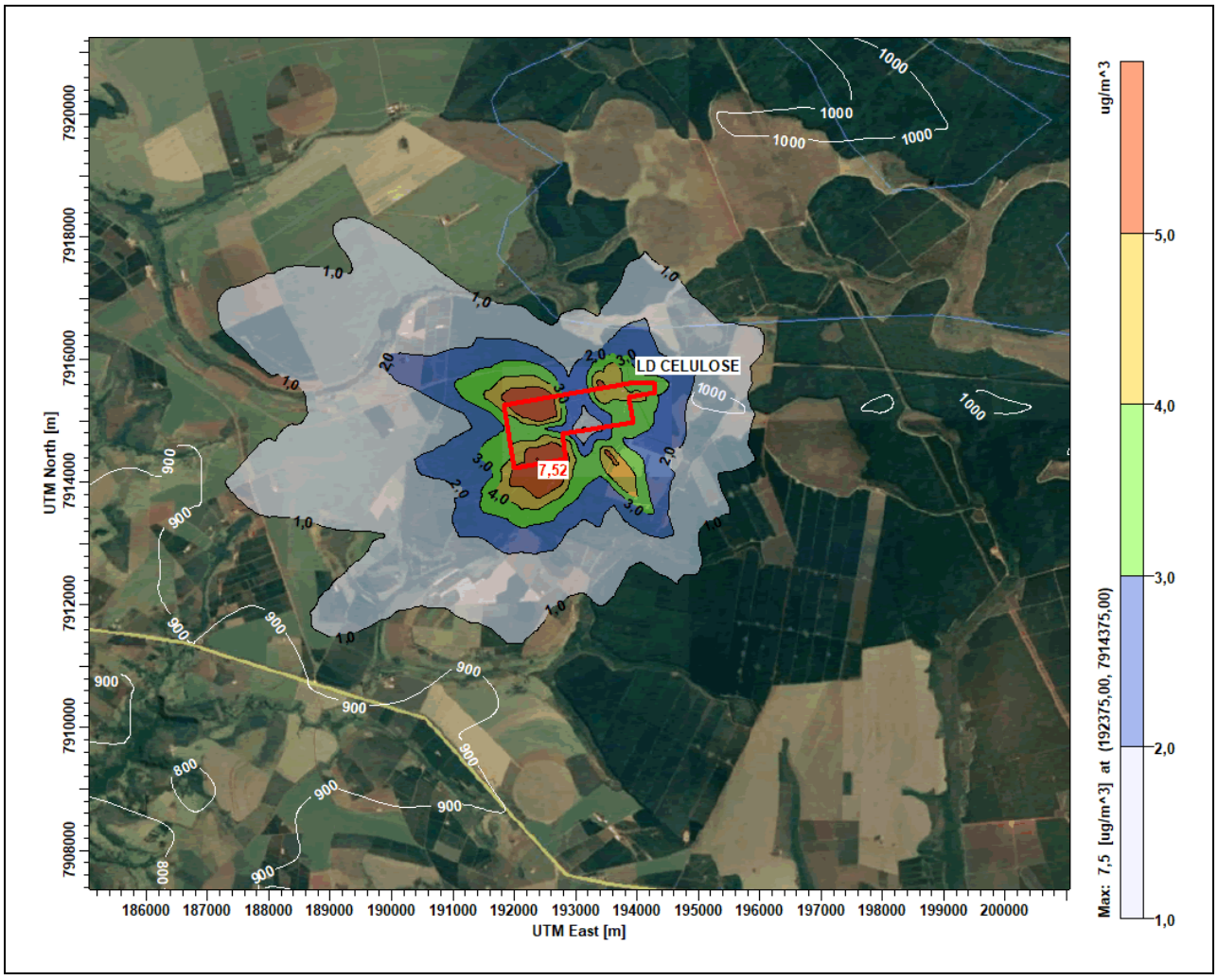

Figure 40: Spatial distribution of the average 24h of the PTS concentration in the image 10 km x 10 km, with the maximum concentration highlighted and the unit boundaries in red, white relief isolines, in the FUTURO scenario

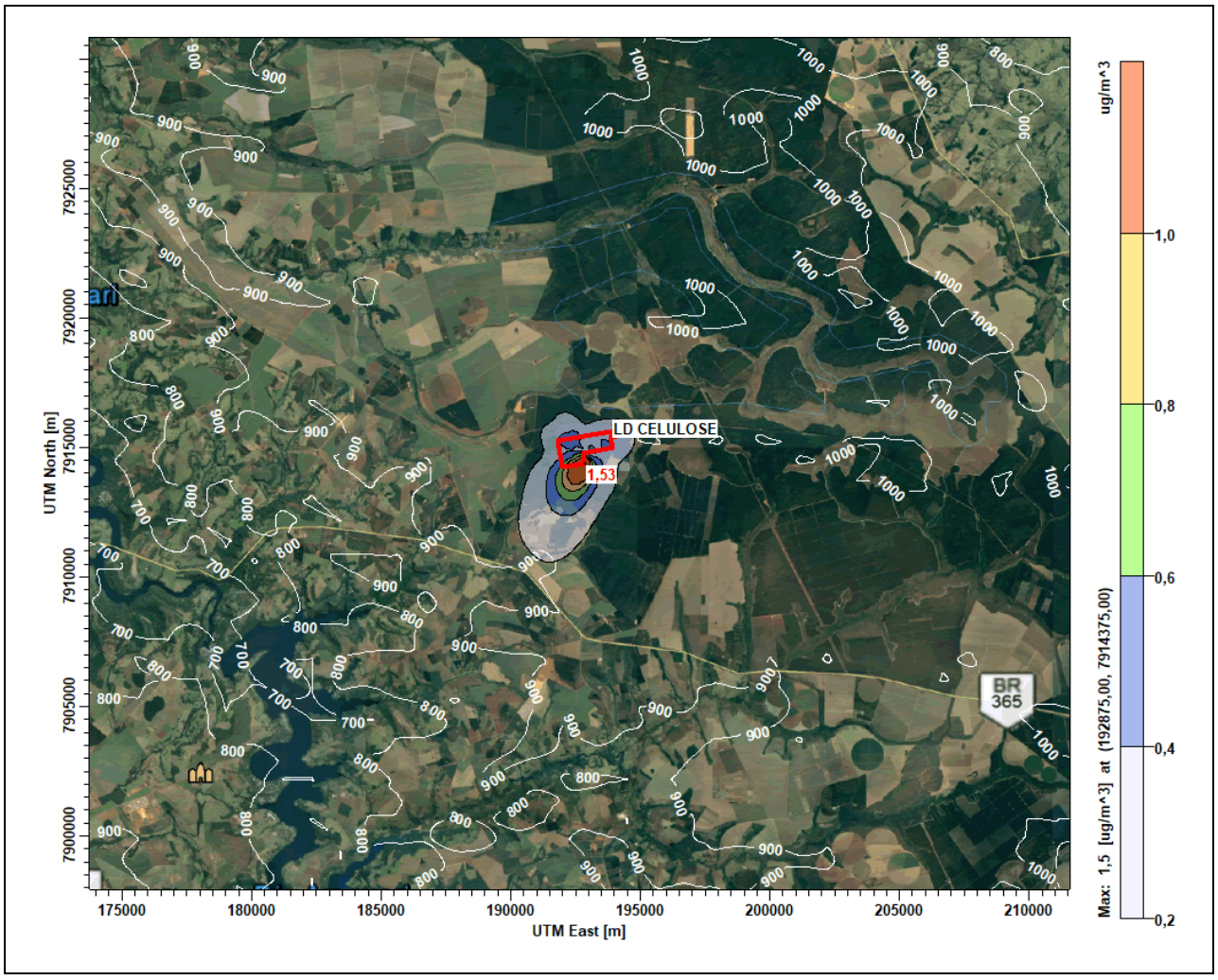

Figure 41: Spatial distribution of the annual average of the PTS concentration in the image 40 km x 40 km, with the maximum concentration highlighted and the unit boundaries in red, white relief isolines, in the FUTURO scenario

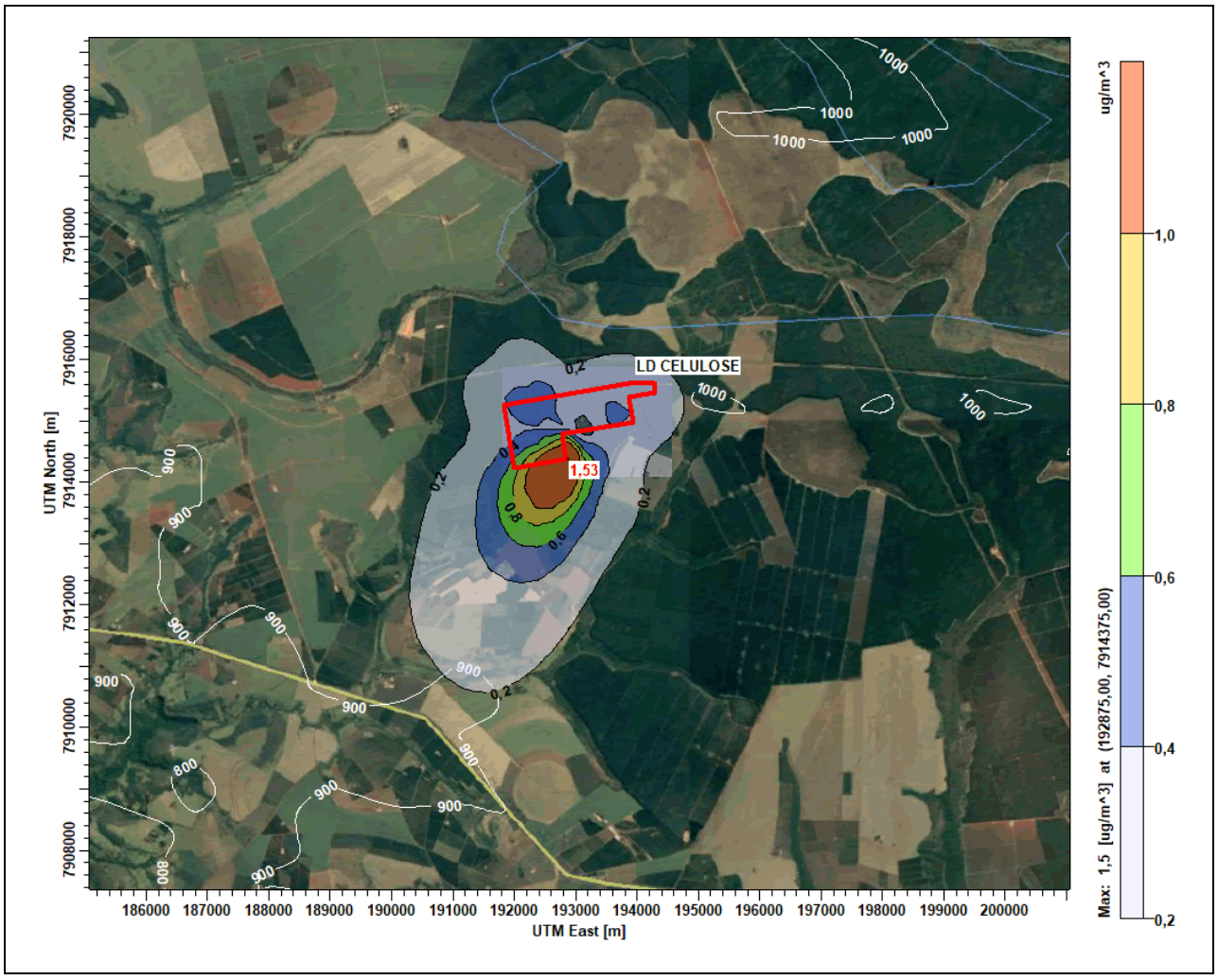

Figure 42: Spatial distribution of the annual average of the PTS concentration in the image 10 km x 10 km, with the maximum concentration highlighted and the unit boundaries in red, white relief isolines, in the FUTURO scenario

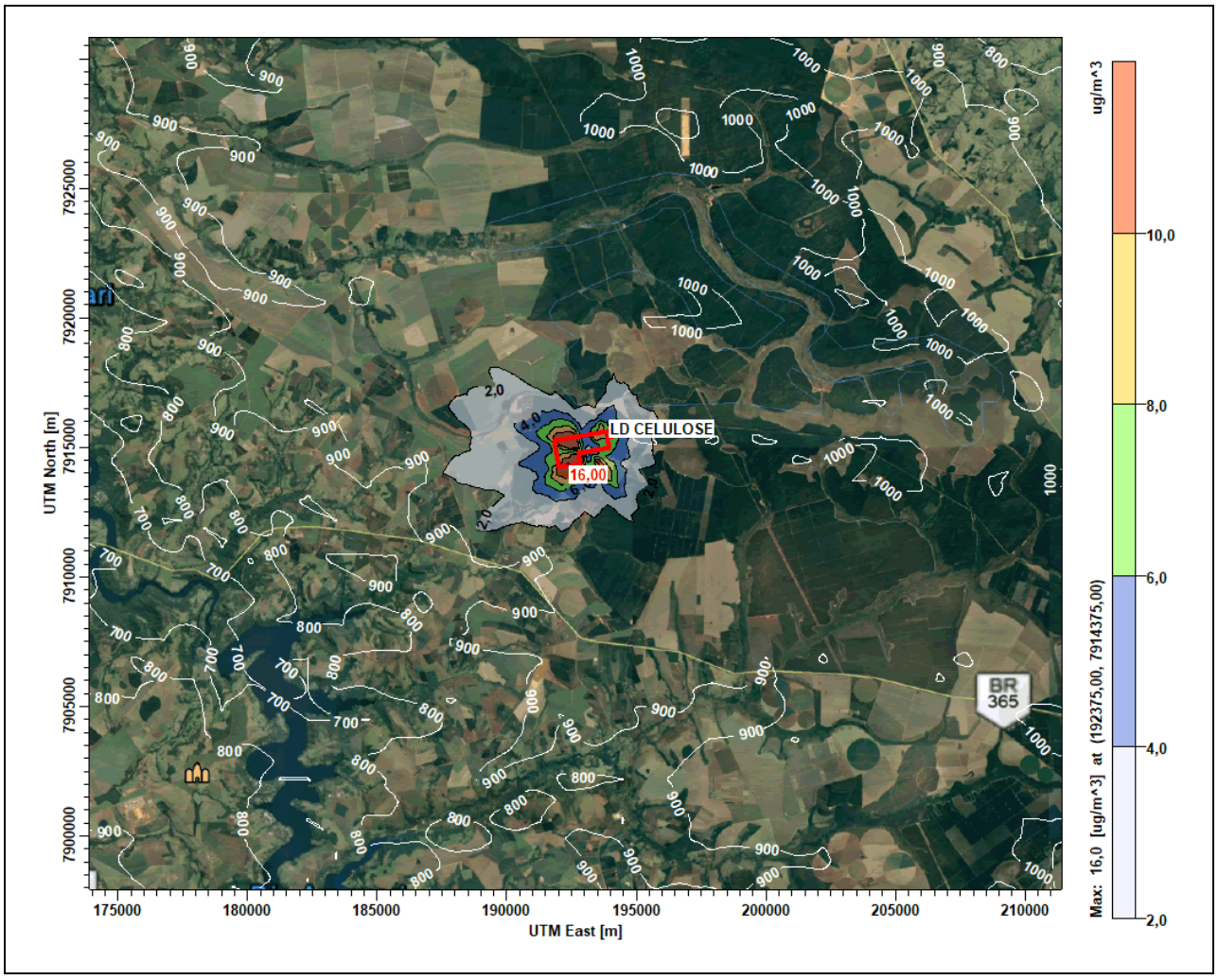

Figure 43: Spatial distribution of the average 24h of the SOx concentration in the image 40 km x 40 km, with the maximum concentration highlighted and the unit boundaries in red, white relief isolines, in the FUTURO scenario

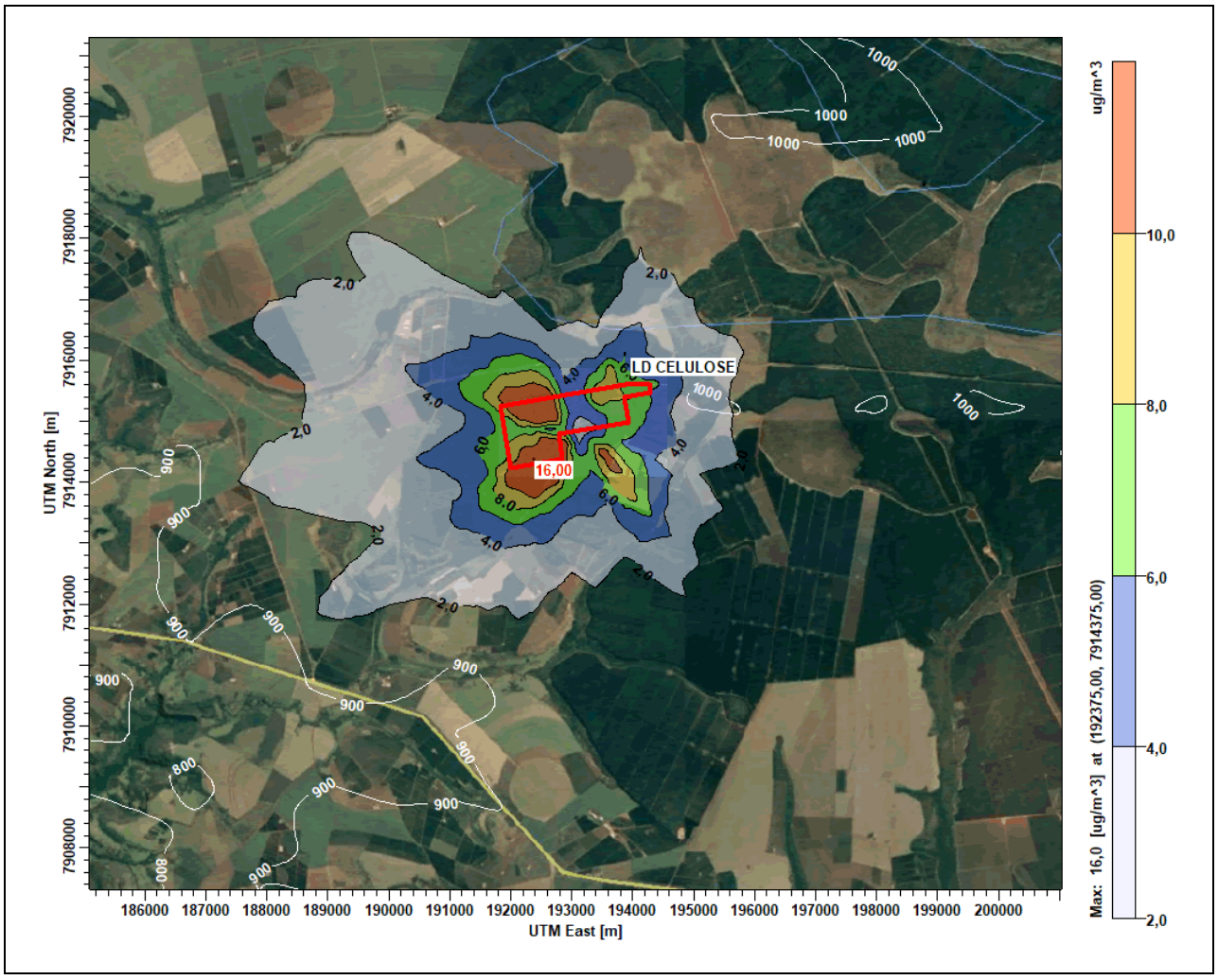

Figure 44: Spatial distribution of the average 24h of the SOx concentration in the image 10 km x 10 km, with the maximum concentration highlighted and the unit boundaries in red, white relief isolines, in the FUTURO scenario

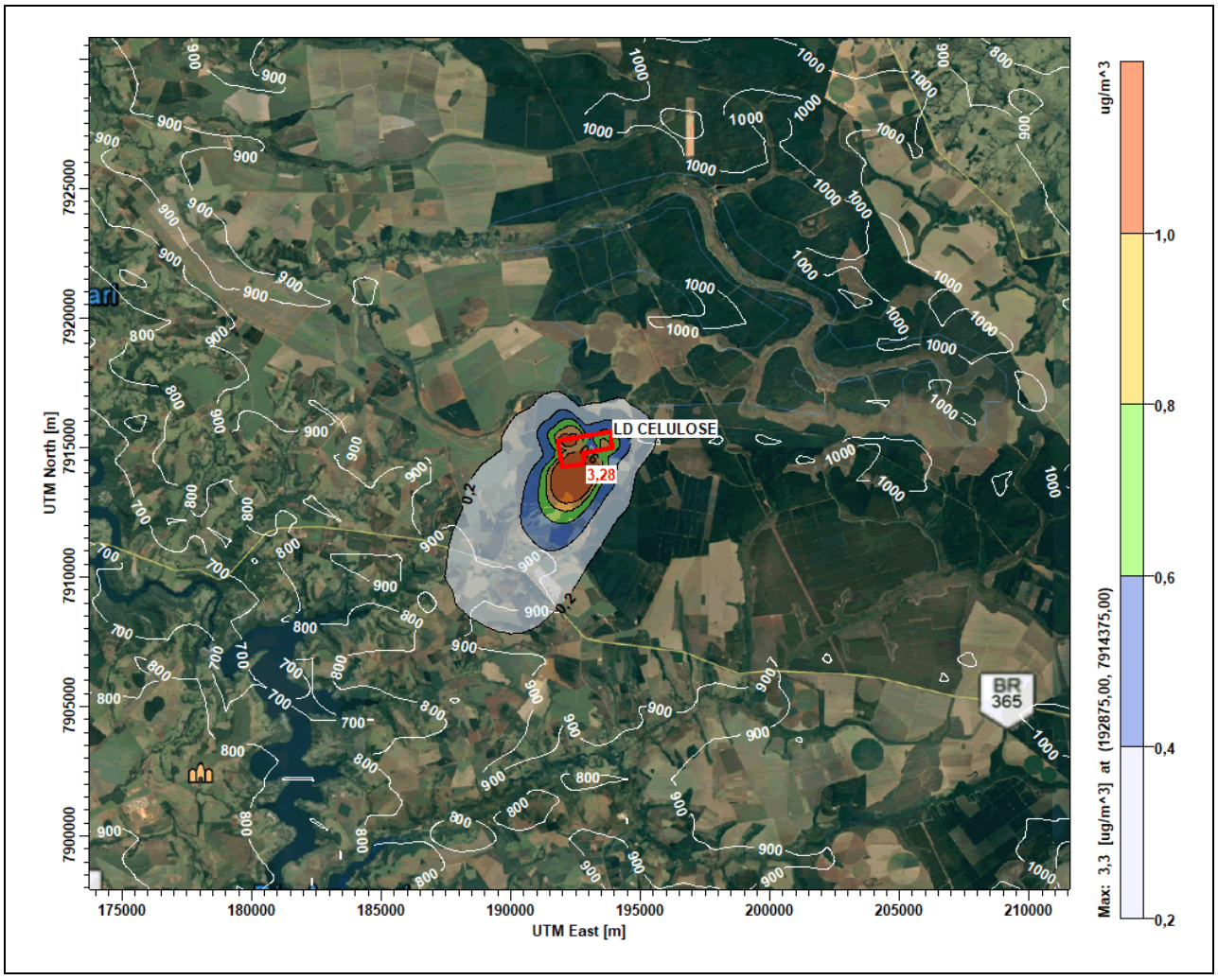

Figure 45: Spatial distribution of the annual average of the SOx concentration in the image 40 km x 40 km, with the maximum concentration highlighted and the unit boundaries in red, white relief isolines, in the FUTURO scenario

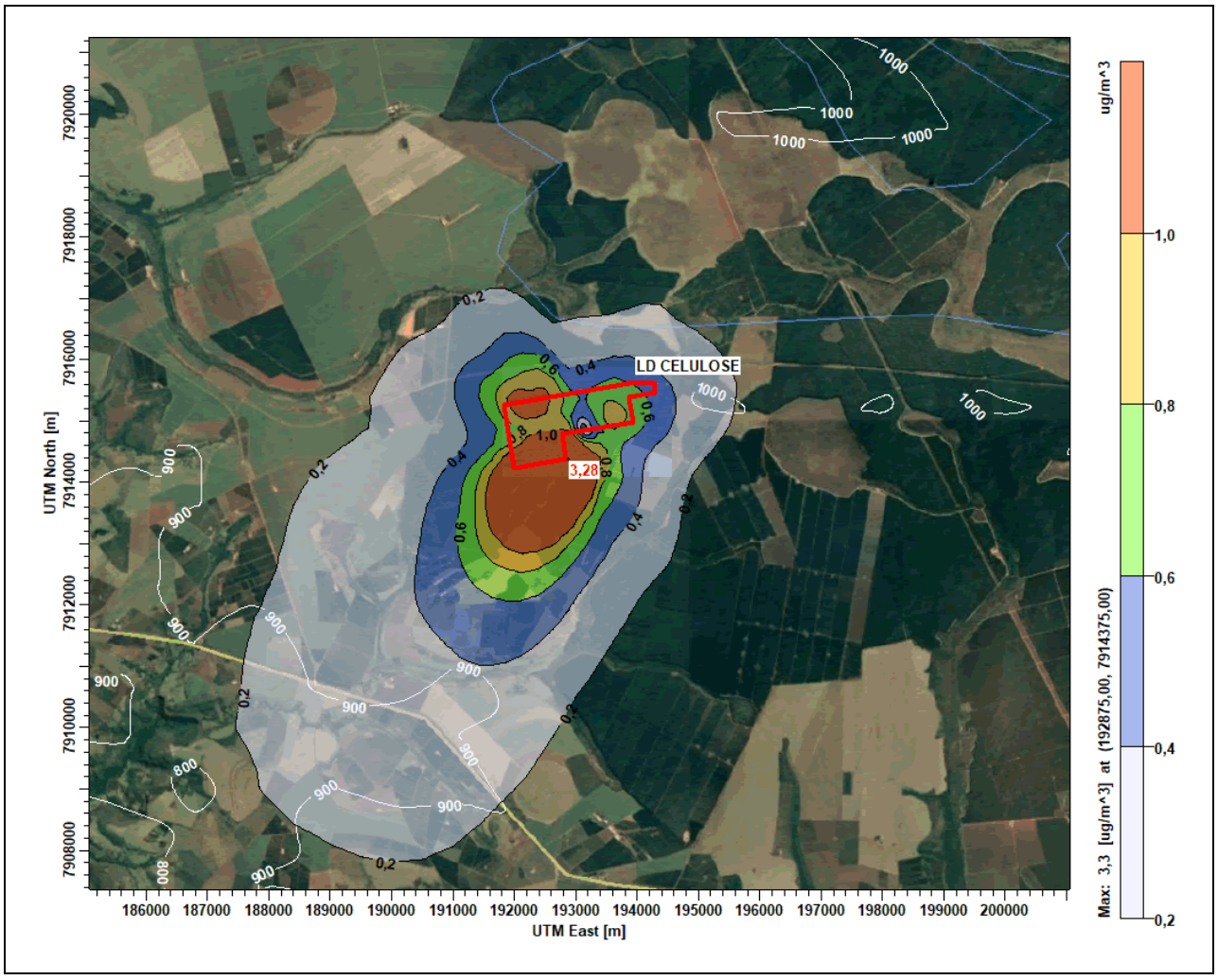

Figure 46: Spatial distribution of the annual average of the SOx concentration in the image 10 km x 10 km, with the maximum concentration highlighted and the unit boundaries in red, white relief isolines, in the FUTURO scenario

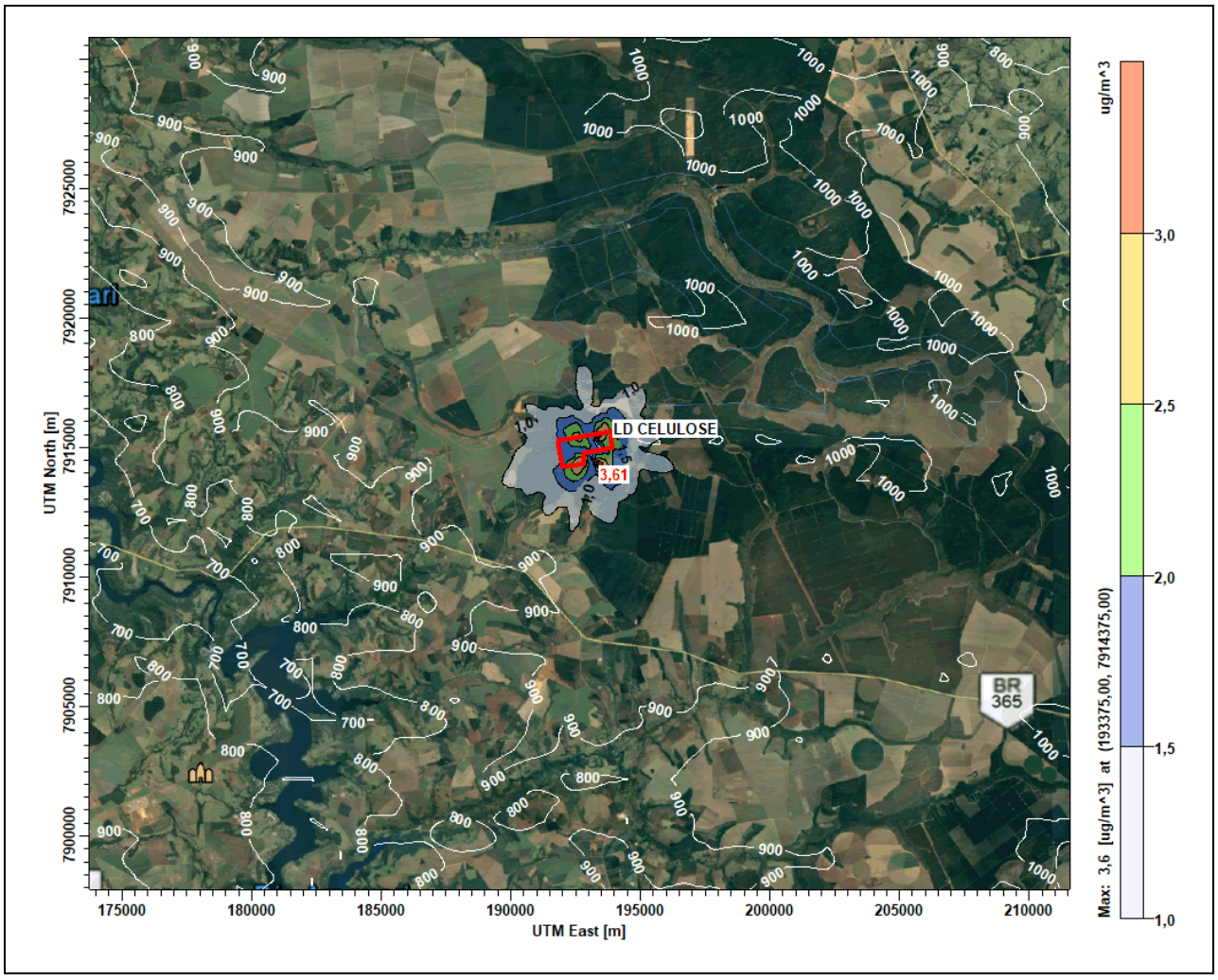

Figure 47: Spatial distribution of the average 1h of the TRS concentration in the image 40 km x 40 km, with the maximum concentration highlighted and the unit boundaries in red, white relief isolines, in the FUTURO scenario

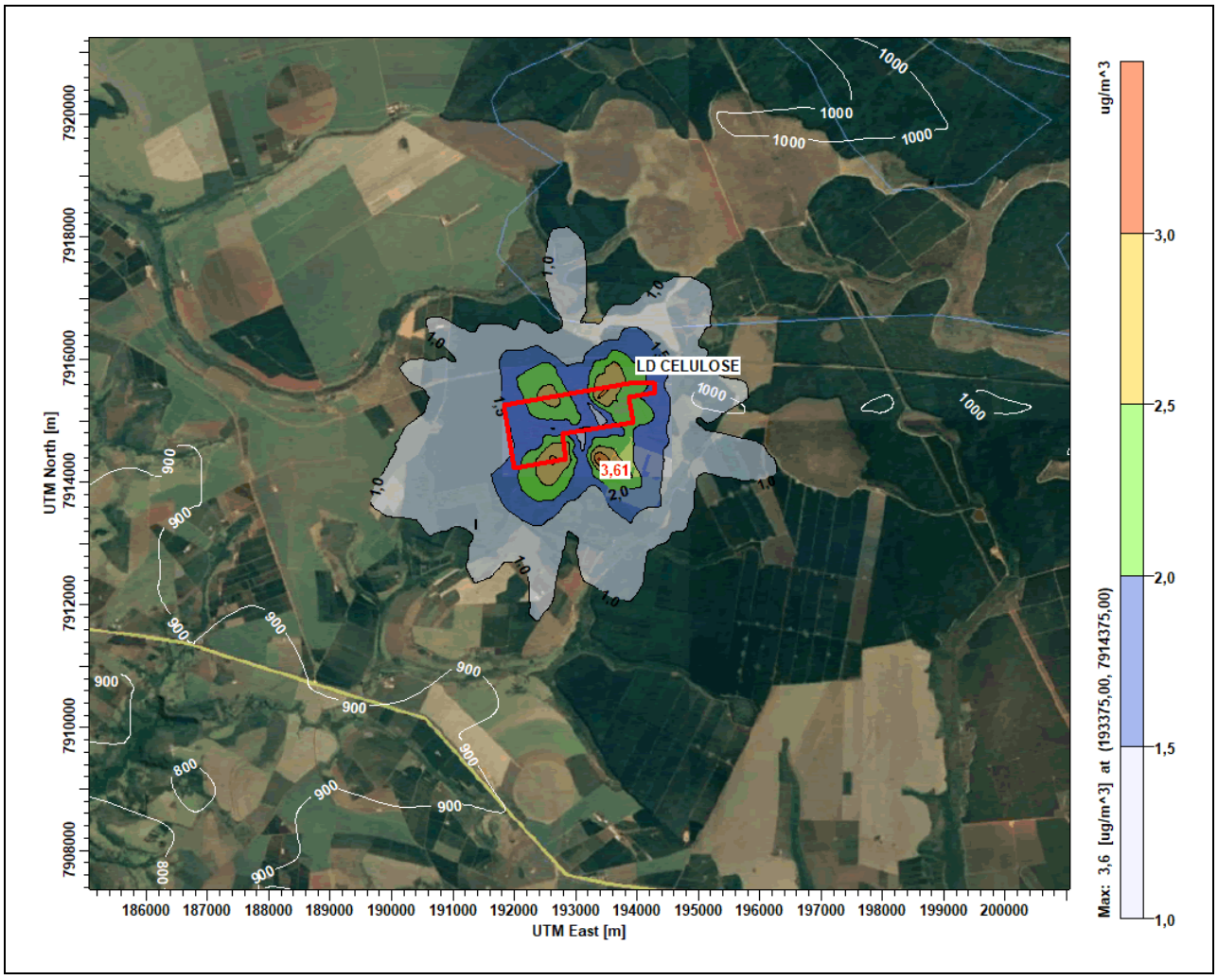

Figure 48: Spatial distribution of the average 1h of the TRS concentration in the image 10 km x 10 km, with the maximum concentration highlighted and the unit boundaries in red, white relief isolines, in the FUTURO scenario

ANNEX B: FIFTY (50) HIGHER SHORT-TERM CONCENTRATIONS

Tabela 20: Fifty higher short-term (1 h) CO concentrations in the FUTURE scenario (µg/m^3)

RANK	CONC (YYMMDDHH) AT	RECEPTOR (XR,YR) OF TYPE	RANK	CONC (YYMMDDHH) AT	RECEPTOR (XR,YR) OF TYPE
1.	78.35644 (13092213) AT	(193375.00, 7914375.00) GC	26.	62.23745 (13041916) AT	(193375.00, 7915625.00) GC
2.	76.26968 (15090915) AT	(193375.00, 7915375.00) GC	27.	62.02593 (15121118) AT	(193500.00, 7915500.00) GC
3.	75.77526 (15050614) AT	(193375.00, 7914375.00) GC	28.	62.00519 (13111316) AT	(193375.00, 7915625.00) GC
4.	75.51864 (14030913) AT	(193375.00, 7914375.00) GC	29.	61.95605 (13100412) AT	(193625.00, 7914375.00) GC
5.	73.78785 (17061002) AT	(193375.00, 7915625.00) GC	30.	61.73597 (16052319) AT	(193500.00, 7915500.00) GC
6.	71.53293 (17021210) AT	(192625.00, 7914375.00) GC	31.	60.70498 (15020219) AT	(193375.00, 7915625.00) GC
7.	70.97778 (15100419) AT	(193375.00, 7915625.00) GC	32.	60.67584 (13100412) AT	(193875.00, 7914125.00) GC
8.	70.85019 (14122023) AT	(192875.00, 7914375.00) GC	33.	60.50828 (13122415) AT	(193375.00, 7914375.00) GC
9.	70.70919 (15020218) AT	(193500.00, 7915500.00) GC	34.	60.20845 (13121012) AT	(193875.00, 7914125.00) GC
10.	69.04212 (16011914) AT	(193375.00, 7914375.00) GC	35.	59.40172 (15011517) AT	(193375.00, 7915375.00) GC
11.	68.25719 (14092119) AT	(193375.00, 7915625.00) GC	36.	58.96909 (16082010) AT	(192625.00, 7914125.00) GC
12.	67.84655 (17102317) AT	(193375.00, 7915625.00) GC	37.	58.87341 (13120614) AT	(192375.00, 7915375.00) GC
13.	67.03301 (15011517) AT	(193375.00, 7915625.00) GC	38.	58.78938 (16021815) AT	(193375.00, 7915625.00) GC
14.	65.81329 (15013020) AT	(193375.00, 7915625.00) GC	39.	58.20019 (14122115) AT	(193375.00, 7914375.00) GC
15.	65.71821 (15090915) AT	(193375.00, 7915625.00) GC	40.	57.66866 (17011722) AT	(192875.00, 7914125.00) GC
16.	64.61525 (16052319) AT	(193625.00, 7915625.00) GC	41.	57.65172 (16040322) AT	(192625.00, 7915375.00) GC
17.	64.58615 (15020218) AT	(193375.00, 7915375.00) GC	42.	57.63693 (17112317) AT	(193375.00, 7915625.00) GC
18.	64.13276 (13050617) AT	(193375.00, 7915625.00) GC	43.	57.63561 (14122116) AT	(193375.00, 7914375.00) GC
19.	63.93333 (14042418) AT	(193375.00, 7915625.00) GC	44.	57.50995 (15100419) AT	(193375.00, 7915875.00) GC
20.	63.35993 (13050617) AT	(193375.00, 7915375.00) GC	45.	57.47999 (17040510) AT	(192625.00, 7914125.00) GC
21.	63.25528 (13122611) AT	(193625.00, 7915875.00) GC	46.	57.29023 (15121118) AT	(193625.00, 7915625.00) GC
22.	62.53813 (15020218) AT	(193625.00, 7915625.00) GC	47.	57.21746 (17021210) AT	(192375.00, 7914125.00) GC
23.	62.49582 (16011317) AT	(193375.00, 7914375.00) GC	48.	57.13042 (14120815) AT	(192875.00, 7914375.00) GC
24.	62.34811 (13121815) AT	(193375.00, 7915625.00) GC	49.	57.09899 (14060215) AT	(193875.00, 7915125.00) GC
25.	62.28908 (13121012) AT	(193625.00, 7914375.00) GC	50.	57.09410 (17021211) AT	(192500.00, 7914500.00) GC

Tabela 21: Fifty higher short-term (8h) CO concentrations in the FUTURE scenario (µg/m^3)

RANK	CONC (YYMMDDHH) AT	RECEPTOR (XR,YR) OF TYPE	RANK	CONC (YYMMDDHH) AT	RECEPTOR (XR,YR) OF TYPE
1.	45.11980 (13092508)	AT (193375.00, 7915625.00) GC	26.	30.31024 (17092216)	AT (192500.00, 7914000.00) GC
2.	43.72381 (17021216)	AT (192625.00, 7914375.00) GC	27.	29.91613 (17110816)	AT (192500.00, 7914000.00) GC
3.	37.57485 (17021216)	AT (192375.00, 7914125.00) GC	28.	29.79416 (14120216)	AT (192625.00, 7914375.00) GC
4.	37.22394 (16082016)	AT (192625.00, 7913875.00) GC	29.	29.35017 (15102616)	AT (192625.00, 7914125.00) GC
5.	35.78795 (17111016)	AT (192625.00, 7914125.00) GC	30.	29.21534 (16013016)	AT (192500.00, 7914000.00) GC
6.	34.75421 (16101216)	AT (192625.00, 7913875.00) GC	31.	29.09399 (16082016)	AT (192875.00, 7914125.00) GC
7.	32.48141 (17111016)	AT (192500.00, 7914000.00) GC	32.	28.87132 (14110416)	AT (192625.00, 7913875.00) GC
8.	32.38442 (16082016)	AT (192875.00, 7914375.00) GC	33.	28.67688 (16012916)	AT (192625.00, 7914125.00) GC
9.	32.22272 (16013016)	AT (192625.00, 7914125.00) GC	34.	28.65927 (17110916)	AT (192625.00, 7914375.00) GC
10.	32.21092 (17110916)	AT (192375.00, 7914125.00) GC	35.	28.57310 (15100816)	AT (192625.00, 7913875.00) GC
11.	31.63619 (17110816)	AT (192625.00, 7914125.00) GC	36.	28.51713 (14110416)	AT (192625.00, 7914125.00) GC
12.	31.37696 (16082016)	AT (192625.00, 7914125.00) GC	37.	28.23456 (17021216)	AT (192125.00, 7913875.00) GC
13.	31.37676 (17092216)	AT (192625.00, 7914125.00) GC	38.	28.19355 (13101416)	AT (192625.00, 7914125.00) GC
14.	31.29402 (17021316)	AT (192375.00, 7914125.00) GC	39.	28.17576 (14120216)	AT (192500.00, 7914000.00) GC
15.	31.16537 (17111016)	AT (192625.00, 7913875.00) GC	40.	28.16157 (13103016)	AT (192625.00, 7914125.00) GC
16.	31.01110 (14120216)	AT (192375.00, 7914125.00) GC	41.	28.14261 (15122316)	AT (192875.00, 7914125.00) GC
17.	31.00652 (17021316)	AT (192625.00, 7914375.00) GC	42.	28.04305 (16121916)	AT (192875.00, 7914125.00) GC
18.	30.99651 (13092508)	AT (193375.00, 7915875.00) GC	43.	27.98681 (16100316)	AT (192875.00, 7914375.00) GC
19.	30.97989c(17040516)	AT (192500.00, 7914000.00) GC	44.	27.95047 (16101216)	AT (192625.00, 7914125.00) GC
20.	30.84537c(17040516)	AT (192625.00, 7914125.00) GC	45.	27.94912 (16013016)	AT (192625.00, 7913875.00) GC
21.	30.73726 (15010516)	AT (192625.00, 7914125.00) GC	46.	27.78956 (17101716)	AT (192375.00, 7914375.00) GC
22.	30.66768 (15010516)	AT (192625.00, 7913875.00) GC	47.	27.78522 (14090916)	AT (192375.00, 7914125.00) GC
23.	30.61960 (16101216)	AT (192875.00, 7914125.00) GC	48.	27.76015 (16082016)	AT (192625.00, 7913625.00) GC
24.	30.56748 (16101216)	AT (192875.00, 7914375.00) GC	49.	27.74826 (16012916)	AT (192625.00, 7913875.00) GC
25.	30.33758 (16100316)	AT (192625.00, 7913875.00) GC	50.	27.52267 (15102616)	AT (192500.00, 7914000.00) GC

Tabela 22: Fifty higher short-term (1h) concentrations of NOX in the FUTURE scenario (µg/m^3)

RANK	CONC (YYMMDDHH) AT	RECEPTOR (XR,YR) OF TYPE	RANK	CONC (YYMMDDHH) AT	RECEPTOR (XR,YR) OF TYPE
1.	136.61475 (13092213) AT	(193375.00, 7914375.00) GC	26.	102.59894 (15121118) AT	(193500.00, 7915500.00) GC
2.	132.69736 (14030913) AT	(193375.00, 7914375.00) GC	27.	102.31467 (13040717) AT	(193375.00, 7915375.00) GC
3.	130.67146 (15050614) AT	(193375.00, 7914375.00) GC	28.	101.69678 (13122712) AT	(193625.00, 7915875.00) GC
4.	122.91052 (16011914) AT	(193375.00, 7914375.00) GC	29.	101.57032 (17093013) AT	(193375.00, 7914375.00) GC
5.	116.80768 (17021210) AT	(192625.00, 7914375.00) GC	30.	101.48987 (16022310) AT	(192625.00, 7914125.00) GC
6.	115.13447 (15020218) AT	(193500.00, 7915500.00) GC	31.	101.46781 (15100419) AT	(193375.00, 7915625.00) GC
7.	112.72591 (15020218) AT	(193375.00, 7915375.00) GC	32.	101.44194 (17040510) AT	(192625.00, 7914125.00) GC
8.	112.06784 (15090915) AT	(193375.00, 7915375.00) GC	33.	100.57202 (17102317) AT	(193375.00, 7915625.00) GC
9.	108.36514 (13122415) AT	(193375.00, 7914375.00) GC	34.	100.41074 (15090915) AT	(193375.00, 7915625.00) GC
10.	108.02545 (14122115) AT	(193375.00, 7914375.00) GC	35.	100.33421 (17021311) AT	(192625.00, 7914375.00) GC
11.	106.83311 (16011317) AT	(193375.00, 7914375.00) GC	36.	100.24897 (13121813) AT	(193625.00, 7915625.00) GC
12.	106.58959 (13122611) AT	(193625.00, 7915875.00) GC	37.	99.91894 (16120112) AT	(192625.00, 7914375.00) GC
13.	106.57923 (17111913) AT	(193375.00, 7914375.00) GC	38.	99.89774 (14011915) AT	(193375.00, 7915375.00) GC
14.	105.55930 (14122116) AT	(193375.00, 7914375.00) GC	39.	99.83646 (16012909) AT	(192625.00, 7914375.00) GC
15.	105.44147 (13121012) AT	(193625.00, 7914375.00) GC	40.	99.81903 (13121012) AT	(193500.00, 7914500.00) GC
16.	105.35508 (16040322) AT	(192625.00, 7915375.00) GC	41.	99.70953 (15020218) AT	(193625.00, 7915625.00) GC
17.	105.30507 (14122113) AT	(193375.00, 7914375.00) GC	42.	99.61781 (17021211) AT	(192500.00, 7914500.00) GC
18.	105.28774 (13100412) AT	(193625.00, 7914375.00) GC	43.	99.34065 (15112515) AT	(193500.00, 7915500.00) GC
19.	104.73286 (16052319) AT	(193625.00, 7915625.00) GC	44.	99.19755 (16040322) AT	(192500.00, 7915500.00) GC
20.	104.28373 (13120413) AT	(193375.00, 7914375.00) GC	45.	99.10046 (15012116) AT	(193375.00, 7915375.00) GC
21.	103.89263 (14120815) AT	(192875.00, 7914375.00) GC	46.	99.06815 (17091410) AT	(192625.00, 7914375.00) GC
22.	103.87326 (16082010) AT	(192625.00, 7914125.00) GC	47.	99.03944 (17110809) AT	(192625.00, 7914375.00) GC
23.	103.11777 (16052319) AT	(193500.00, 7915500.00) GC	48.	99.03685 (15011517) AT	(193375.00, 7915625.00) GC
24.	102.83619 (16032215) AT	(193500.00, 7914500.00) GC	49.	98.94432 (13111412) AT	(192625.00, 7914375.00) GC
25.	102.78160 (17100113) AT	(193375.00, 7914375.00) GC	50.	98.88323 (17032017) AT	(193375.00, 7915375.00) GC

Tabela 23: Fifty higher short-term (24h) PTS concentrations in the FUTURE scenario

RANK	CONC (YYMMDDHH) AT	RECEPTOR (XR,YR) OF TYPE	RANK	CONC (YYMMDDHH) AT	RECEPTOR (XR,YR) OF TYPE
1.	7.51711 (17021324) AT	(192375.00, 7914375.00) GC	26.	5.79389 (17110824) AT	(192375.00, 7914125.00) GC
2.	7.30564 (17110924) AT	(192375.00, 7914375.00) GC	27.	5.70162 (16121524) AT	(192125.00, 7915125.00) GC
3.	7.10991 (16121524) AT	(192375.00, 7915125.00) GC	28.	5.68322 (16121524) AT	(192625.00, 7915125.00) GC
4.	7.08230 (17111024) AT	(192625.00, 7914125.00) GC	29.	5.61187 (14120824) AT	(192625.00, 7914375.00) GC
5.	6.93284 (14120224) AT	(192625.00, 7914375.00) GC	30.	5.59740 (14120224) AT	(192625.00, 7914125.00) GC
6.	6.83611 (17021324) AT	(192500.00, 7914500.00) GC	31.	5.56522 (17111024) AT	(192375.00, 7914125.00) GC
7.	6.75028 (17111024) AT	(192500.00, 7914000.00) GC	32.	5.55975 (14120224) AT	(192500.00, 7914000.00) GC
8.	6.66315 (17110924) AT	(192500.00, 7914500.00) GC	33.	5.53983 (17021424) AT	(192500.00, 7914500.00) GC
9.	6.52356 (17021224) AT	(192375.00, 7914375.00) GC	34.	5.52670 (14120824) AT	(192375.00, 7914125.00) GC
10.	6.48564 (17110824) AT	(192625.00, 7914375.00) GC	35.	5.52369 (16101324) AT	(192625.00, 7914375.00) GC
11.	6.35440 (17021324) AT	(192125.00, 7914125.00) GC	36.	5.49486 (14120224) AT	(192375.00, 7914375.00) GC
12.	6.32467 (14100224) AT	(192375.00, 7915375.00) GC	37.	5.48586 (13011324) AT	(192375.00, 7914125.00) GC
13.	6.29140 (17021324) AT	(192625.00, 7914375.00) GC	38.	5.48580 (17021324) AT	(192000.00, 7914000.00) GC
14.	6.23953 (17021224) AT	(192500.00, 7914500.00) GC	39.	5.47146 (17110824) AT	(192500.00, 7914000.00) GC
15.	6.19274 (14120224) AT	(192375.00, 7914125.00) GC	40.	5.46021 (13011324) AT	(192625.00, 7914125.00) GC
16.	6.12468 (17111024) AT	(192625.00, 7914375.00) GC	41.	5.45884 (16121524) AT	(191875.00, 7915375.00) GC
17.	6.08048 (17110924) AT	(192125.00, 7914125.00) GC	42.	5.45853 (17111624) AT	(192625.00, 7914125.00) GC
18.	6.03099 (17021224) AT	(192625.00, 7914375.00) GC	43.	5.39542 (17110824) AT	(192625.00, 7914125.00) GC
19.	5.90883 (17021324) AT	(192375.00, 7914125.00) GC	44.	5.39080 (17021424) AT	(192375.00, 7914375.00) GC
20.	5.89577 (17111024) AT	(192375.00, 7913875.00) GC	45.	5.38805 (13122424) AT	(193500.00, 7914500.00) GC
21.	5.83722 (14100224) AT	(192125.00, 7915375.00) GC	46.	5.36913 (17110924) AT	(192625.00, 7914375.00) GC
22.	5.83698 (16082024) AT	(192625.00, 7914125.00) GC	47.	5.34800 (16121524) AT	(192125.00, 7915375.00) GC
23.	5.83228 (14100224) AT	(192625.00, 7915125.00) GC	48.	5.34474 (14090924) AT	(192625.00, 7914375.00) GC
24.	5.82319 (13011324) AT	(192625.00, 7914375.00) GC	49.	5.31470 (13092524) AT	(193375.00, 7915625.00) GC
25.	5.81758 (16012924) AT	(192625.00, 7914375.00) GC	50.	5.28766 (13011324) AT	(192500.00, 7914000.00) GC

www.lentzmeioambiente.com.br
Fone/Fax: (11) 3853-2138
lentz@lentzmeioambiente.com.br
Rua Álvaro Luís Roberto Assumpção, 431, São Paulo/SP – 04618-020

Tabela 24: Fifty higher short-term (24h) concentrations of SOX in the FUTURE scenario (µg/m^3)

RANK	CONC (YYMMDDHH) AT	RECEPTOR (XR,YR) OF TYPE	RANK	CONC (YYMMDDHH) AT	RECEPTOR (XR,YR) OF TYPE
1.	15.99874 (17021324)	AT (192375.00, 7914375.00) GC	26.	12.45559 (16012924)	AT (192625.00, 7914375.00) GC
2.	15.79240 (17110924)	AT (192375.00, 7914375.00) GC	27.	12.42550 (17110924)	AT (192125.00, 7914125.00) GC
3.	15.47566 (16121524)	AT (192375.00, 7915125.00) GC	28.	12.40075 (14120224)	AT (192375.00, 7914125.00) GC
4.	15.25547 (17110924)	AT (192500.00, 7914500.00) GC	29.	12.39715 (17111024)	AT (192375.00, 7914125.00) GC
5.	15.21817 (17021324)	AT (192500.00, 7914500.00) GC	30.	12.38879 (17021424)	AT (192500.00, 7914500.00) GC
6.	15.05593 (14120224)	AT (192625.00, 7914375.00) GC	31.	12.31133 (14120224)	AT (192375.00, 7914375.00) GC
7.	14.62167 (17111024)	AT (192625.00, 7914125.00) GC	32.	12.19527 (16111924)	AT (192625.00, 7915375.00) GC
8.	14.57070 (13011324)	AT (192625.00, 7914375.00) GC	33.	12.15639 (15071324)	AT (192375.00, 7914125.00) GC
9.	14.39829 (14100224)	AT (192625.00, 7915125.00) GC	34.	12.14060 (17111024)	AT (192375.00, 7913875.00) GC
10.	14.21093 (17111024)	AT (192625.00, 7914375.00) GC	35.	12.10390 (16101324)	AT (192625.00, 7914375.00) GC
11.	14.03602 (16121524)	AT (192625.00, 7915125.00) GC	36.	12.07658b(13112624)	AT (192625.00, 7914375.00) GC
12.	13.88268 (17111024)	AT (192500.00, 7914000.00) GC	37.	12.01287 (14120224)	AT (192875.00, 7914625.00) GC
13.	13.74450 (14100224)	AT (192375.00, 7915375.00) GC	38.	12.00775 (13011324)	AT (192625.00, 7914125.00) GC
14.	13.68639 (17110824)	AT (192625.00, 7914375.00) GC	39.	11.94279 (17111624)	AT (192625.00, 7914125.00) GC
15.	13.47928 (17021224)	AT (192375.00, 7914375.00) GC	40.	11.92818 (17021424)	AT (192625.00, 7914625.00) GC
16.	13.43809 (17021224)	AT (192500.00, 7914500.00) GC	41.	11.87411 (17021224)	AT (192625.00, 7914625.00) GC
17.	13.36125 (14120824)	AT (192625.00, 7914375.00) GC	42.	11.85949 (14072324)	AT (192625.00, 7914375.00) GC
18.	13.32608 (17021324)	AT (192625.00, 7914375.00) GC	43.	11.81445 (14072324)	AT (192375.00, 7914375.00) GC
19.	12.99225b(13112624)	AT (192375.00, 7914125.00) GC	44.	11.77124 (16121524)	AT (192125.00, 7915125.00) GC
20.	12.91827 (17021324)	AT (192125.00, 7914125.00) GC	45.	11.76030 (17111024)	AT (192875.00, 7914625.00) GC
21.	12.91510 (17110924)	AT (192625.00, 7914625.00) GC	46.	11.75959 (17021324)	AT (192375.00, 7914125.00) GC
22.	12.89271 (13011324)	AT (192375.00, 7914125.00) GC	47.	11.71781 (13122424)	AT (193500.00, 7914500.00) GC
23.	12.83900 (14120824)	AT (192375.00, 7914125.00) GC	48.	11.68023 (14120224)	AT (192625.00, 7914125.00) GC
24.	12.65057 (17021324)	AT (192625.00, 7914625.00) GC	49.	11.67839 (16082024)	AT (192625.00, 7914125.00) GC
25.	12.46413 (14100224)	AT (192125.00, 7915375.00) GC	50.	11.57844 (13011324)	AT (192500.00, 7914000.00) GC

Tabela 25: Fifty higher short-term (1 h) concentrations of TRS in the FUTURE scenario (µg/m^3)

RANK	CONC (YYMMDDHH) AT	RECEPTOR (XR,YR) OF TYPE	RANK	CONC (YYMMDDHH) AT	RECEPTOR (XR,YR) OF TYPE
1.	3.61360 (13092213) AT	(193375.00, 7914375.00) GC	26.	2.72438 (17102317) AT	(193375.00, 7915625.00) GC
2.	3.50643 (14030913) AT	(193375.00, 7914375.00) GC	27.	2.71137 (17040510) AT	(192625.00, 7914125.00) GC
3.	3.46666 (15050614) AT	(193375.00, 7914375.00) GC	28.	2.71129 (16022310) AT	(192625.00, 7914125.00) GC
4.	3.24991 (16011914) AT	(193375.00, 7914375.00) GC	29.	2.70762 (15090915) AT	(193375.00, 7915625.00) GC
5.	3.15564 (17021210) AT	(192625.00, 7914375.00) GC	30.	2.69765 (17100113) AT	(193375.00, 7914375.00) GC
6.	3.07723 (15020218) AT	(193500.00, 7915500.00) GC	31.	2.68507 (16032215) AT	(193500.00, 7914500.00) GC
7.	3.03318 (15090915) AT	(193375.00, 7915375.00) GC	32.	2.68448 (15011517) AT	(193375.00, 7915625.00) GC
8.	2.98302 (15020218) AT	(193375.00, 7915375.00) GC	33.	2.68100 (17021311) AT	(192625.00, 7914375.00) GC
9.	2.87326 (13122415) AT	(193375.00, 7914375.00) GC	34.	2.66711 (15020218) AT	(193625.00, 7915625.00) GC
10.	2.84730 (16011317) AT	(193375.00, 7914375.00) GC	35.	2.66600 (17021211) AT	(192500.00, 7914500.00) GC
11.	2.84599 (14122115) AT	(193375.00, 7914375.00) GC	36.	2.66248 (13122712) AT	(193625.00, 7915875.00) GC
12.	2.81917 (13122611) AT	(193625.00, 7915875.00) GC	37.	2.65791 (17110809) AT	(192625.00, 7914375.00) GC
13.	2.80094 (16040322) AT	(192625.00, 7915375.00) GC	38.	2.65472 (16012909) AT	(192625.00, 7914375.00) GC
14.	2.79028 (13121012) AT	(193625.00, 7914375.00) GC	39.	2.65402 (16120112) AT	(192625.00, 7914375.00) GC
15.	2.78804 (16052319) AT	(193625.00, 7915625.00) GC	40.	2.65022 (14092119) AT	(193375.00, 7915625.00) GC
16.	2.78538 (17111913) AT	(193375.00, 7914375.00) GC	41.	2.64811 (13121813) AT	(193625.00, 7915625.00) GC
17.	2.78417 (14122116) AT	(193375.00, 7914375.00) GC	42.	2.64744 (13050617) AT	(193375.00, 7915625.00) GC
18.	2.78302 (16082010) AT	(192625.00, 7914125.00) GC	43.	2.64680 (13040717) AT	(193375.00, 7915375.00) GC
19.	2.77899 (13100412) AT	(193625.00, 7914375.00) GC	44.	2.64371 (17093013) AT	(193375.00, 7914375.00) GC
20.	2.76860 (14120815) AT	(192875.00, 7914375.00) GC	45.	2.63928 (16040322) AT	(192500.00, 7915500.00) GC
21.	2.76121 (15100419) AT	(193375.00, 7915625.00) GC	46.	2.63899 (16013010) AT	(192625.00, 7914125.00) GC
22.	2.73980 (16052319) AT	(193500.00, 7915500.00) GC	47.	2.63456 (17091410) AT	(192625.00, 7914375.00) GC
23.	2.73839 (14122113) AT	(193375.00, 7914375.00) GC	48.	2.63415 (13100412) AT	(193875.00, 7914125.00) GC
24.	2.73455 (13120413) AT	(193375.00, 7914375.00) GC	49.	2.63327 (15112515) AT	(193500.00, 7915500.00) GC
25.	2.73452 (15121118) AT	(193500.00, 7915500.00) GC	50.	2.62908 (13111412) AT	(192625.00, 7914375.00) GC